The Curious Case of Offset Bars: Markers for a Baby Galaxy Disk or Signposts of an Interaction with Dark Matter Sub Halos ?

by

Marc Harris Yao Fortune

A thesis submitted in partial fulfillment for the degree of Magister Scientiae

in the

Faculty of Science
Department of Physics

UNIVERSITY *of the*
WESTERN CAPE

15 December 2016

Supervisor:

Dr Michelle Cluver, Dr Kartik Sheth

Declaration of Authorship

I, Marc Harris Yao Fortune, declare that this thesis titled, 'The Curious Case of Offset Bars: Markers for a Baby Galaxy Disk or Signposts of an Interaction with Dark Matter Sub Halos ?' and the work presented in it are my own. I confirm that:

- This work was done wholly or mainly while in candidature for a research degree at this University.
- Where any part of this thesis has previously been submitted for a degree or any other qualification at this University or any other institution, this has been clearly stated.
- Where I have consulted the published work of others, this is always clearly attributed.
- Where I have quoted from the work of others, the source is always given. With the exception of such quotations, this thesis is entirely my own work.
- I have acknowledged all main sources of help.
- Where the thesis is based on work done by myself jointly with others, I have made clear exactly what was done by others and what I have contributed myself.

Signed: _____

Date: _____

"The longest journey begins with a single step"

Lao Tzu

Contents

List of Figures

List of Tables

UNIVERSITY OF THE WESTERN CAPE

Abstract

Faculty of Science
Department of Physics

Masters

by Marc Harris Yao Fortune

We have used the *Spitzer* Survey of Stellar Structure in Galaxies (S^4G) as a representative sample of the local universe (total of 2352 galaxies in S^4G) to make a catalog of offset disk barred galaxies. Using the combined variation of the position angle and the ellipticity (provided by ellipse fit) and also through visual inspection, we have been able to identify all offset structures in S^4G. While primary bars are present in 2/3 of the disk galaxies in the visible universe, offset bars have a much lower fraction. Of the $\sim$ 1500 (3.6μm images) disk galaxies available in S^4G, we classified only 49 as offset barred disk galaxies. We have determined basic properties (bar to total luminosity ratio, bar length, disk scale-length and bars of offset bars shape) using GALFIT, a widely used galaxy decomposition software package. Our main conclusion is that all the offset bars are boxy, independent of their offset from the galaxy center, or the mass of the host galaxy. Additionally we find that, the early type offset bars seem to be more boxy than the late types. The comparison of our offset sample with two other samples, respectively, low mass and high mass normal barred galaxies ("normal" for bars located at the photometric center of the host galaxy), reveals them to be at an intermediate position between the two normal samples. The bar length, disk scale-length and bar to total luminosity ratio are on average larger than the low mass normal and smaller than high mass normal barred galaxies. We have found, overall, a tighter correlation between the disk and bar properties for offset bars in comparison to the two normal samples. Our explanation is that, although the offset has no visible impact on the global shape of the bars, the process responsible for these disturbances seems to affect the star formation rate such that their disk and bars are on average more active than the normal barred galaxies in the same mass range, but not enough to surpass normal barred galaxies with much higher mass.

Dedicated to my parents, all the persons who help me & God Almighty

Chapter 1

INTRODUCTION

Unlike strongly barred galaxies like NGC1097 or NGC1365, offset bars such as those in the Large Magellanic Cloud (LMC) or NGC3906 have an offset between the "disk" and the bar center. They are believed to be common structures in low mass, late type spiral galaxies and mostly found in Magellanic systems (de Vaucouleur & Freeman 1972; Odewahn 1996), but how they form is a mystery!

The leading possibility is that the offset formed via an interaction that pulled or pushed the bar aside from the center of the galaxy disk (Odewhan 1996). Numerical simulations reveal that barred galaxies become offset after an interaction of a small companion with the disk of the galaxy (Athanassoula 1996; Berentzen et al. 2003; Pardy et al. 2016). However many of these galaxies are extremely isolated, making the interaction hypothesis puzzling as there is no obvious interacting partner near many of these galaxies. In cases like NGC 3906 there is no obvious signature of a recent interaction - so could it be that these bars are young, inchoate structures that always form, perhaps offset at times, in newly formed galaxy disks? Or could it be that the isolated galaxy suffered an interaction with an unseen companion, perhaps a dark matter subhalo? This is a hypothesis proposed by Bekki (2009) to explain the offset bar in the Large Magellanic Cloud and discussed for NGC 3906 in de Swardt et al. (2015). Many studies have already analysed primary bars using one and two dimensional decomposition techniques (Sheth et al. 2000; 2002; 2008a; 2012; Menendez-Delmestre et al. 2007; Eskridge et al. 2000 ; Elmegreen and Elmegreen 1985; Ohta et al. 1986). In the same order of studies, Kim et al. (2014) interpret the change in the bar profile as an indication of bar evolution. According to them, as bars capture more star in their orbits, they evacuate the disk and the light profile along the bar changes from an exponential disk profile to a flat profile (see Figure 1.1). Properties of bars, specially offset bars, although these studies, still have to be investigated. The *Spitzer* Survey of Stellar Structure in Galaxies (S^4G, Sheth et al. 2010) gives us an opportunity to measure the bar light profile, it shape and the disk profile. S^4G is a survey of 2352 nearby galaxies using the Infrared Array Camera (IRAC, Fazio et al. 2004) at 3.6 and 4.5 μm. The light at this wavelength is relatively free from the effect of extinction due to dust. Additionally it better takes into account the contribution of the low mass stars which, due to their presence in large numbers, are true representation of the stellar mass of the galaxy.

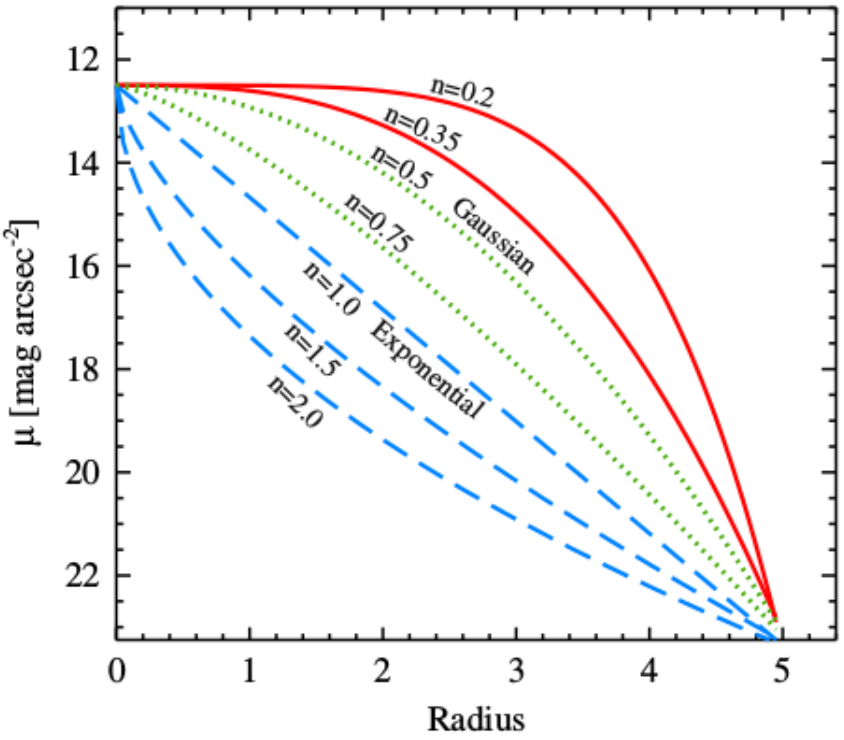

Figure 1.1: *Schematic plot of sersic profiles for different radial surface brightness profiles of bars. Radial profiles of n = 0.2 up to 2 are presented. Gaussian (n = 0.5) and exponential (n = 1.0) profiles are also shown. Flat profiles are in red, intermediate profiles are in green, and exponential steep profiles are in blue. Radius is in an arbitrary unit (Kim et al. 2015).*

1.1 Background

Bars are common structures in disk galaxies. About 2/3rd of these galaxies possess a bar (de Vaucouleurs 1963) whose contribution to the blue light is less than 30 percent of the total luminosity. The bar arises from a gravitational instability in a rotationally supported disk that is sufficiently massive and dynamically cold. In this case, the formation of the stellar bar is relatively fast (∼ hundred millions of years). But the bar formation is delayed either by an initially dominant dark matter (DM) halo or dynamically hot (dispersion-dominated) disk.

Simulations have shown that a dominant DM halo strongly impacts the time scale for bar formation (Athanassoula 2002) delaying the onset of bar instability. Bars that form in such a system are stronger than bars that form in the contrary, in non-DM dominated galaxy because the DM halo act as an efficient sink of angular momentum and energy of baryons, wich are redistributed to form the bar (Sheth et al. 2012-and references therein). Some barred galaxies have a second bar in addition to the primary one. The second bar is much smaller with a typical length of 1 kpc. It is believed that in the evolution of galaxies with two bars, the secondary bar can dissolve and transform into a triaxial bulge like a central body.

Within galaxies, the gas flow in the disk experiences a hydrodynamic shock that forms along the leading edge of the bar – the gas is driven inwards down the dust lanes which are the locii of these shocks (Athanassoula 1992a, 1992b). The bar luminosity along the major and minor axis can be modeled

respectively by an exponential and a Gaussian function. So the intensity distribution of the bar can be written as the following:

$$I(x,y) = I(0,0)e^{(-x/x_0)}e^{(-(y/y_0)^2)} \tag{1.1}$$

This formula was proposed by Blackman (1983) . The bar mass density is usually defined as an ellipsoid with density:

$$\rho = [\rho_0(1-(x/a)^2-(y/b)^2-(z/c)^2]^n \tag{1.2}$$

x, y and z are the tridimensional positions. a, b,c and n are parameter used by the model.
The bar shape is describe by Anthanassoula et al. (1990) using the following formula:

$$\left(\frac{|x|}{a}\right)^c + \left(\frac{|y|}{b}\right)^c = 1 \tag{1.3}$$

where x and y are position of points, a and b are semi major and semi minor axis, respectively, and c is the shape parameter which describes the shape of the ellipse. For c = 2, the bar is elliptical; c < 2 correspond to a disky shape and c > 2, a boxy shape (Figure 1.2).

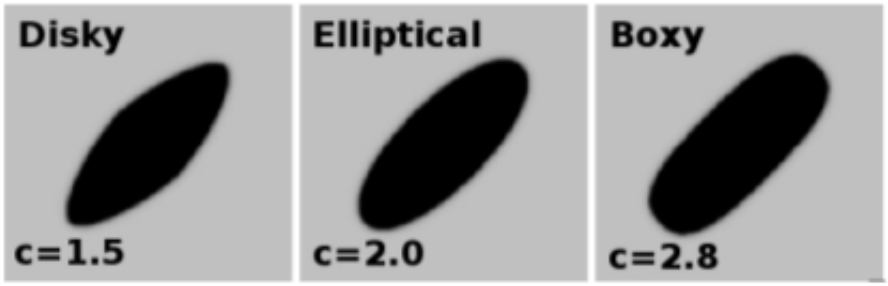

Figure 1.2: *Morphology of bars that are simulated with BUDDA. All the three bars have the same ellipticity (1-b/a) of 0.65 in this figure but have different shapes (Kim et al. 2015).*

Simulations done by Combes & Elmegreen (1993) showed that the bar gradient density is flatter for galaxies with massive bulges in comparison to less massive bulges. This suggest a relationship between the bulge to disk ratio and the bar properties.

1.2 Morphologies of barred galaxies

One of the earliest bar observations was done by W. Parsons in 1858. He identified a bar and an inner ring in NGC4725 with the 1.8 m Speculum reflector at Birr Castle in Ireland. Spirals with bars have

been call ϕ-type spirals by Curtis (1918) in reference to their visual appearance and later, rebaptised θ-type (Hubble 1926) since the bar never exceeded the spirals arms.

Finally the more appropriate name given was "barred spiral" contracted as "SB" (Hubble 1926). The non-barred spirals were called "normal" spirals. Realising the possibility of having intermediate bar structure between the non-barred and the true barred spiral, Sandage (1961) and de Vaucouleurs (1959) proposed the change of the term "normal" to "ordinary". So the ordinary spirals become "SA" and the intermediate and true barred spiral were respectively called "SAB" and "SB". de Vaucouleurs (1963) studied 1500 bright galaxies using large photographic plates. For a total of 994 spirals, he found 31 % SA, 28 % SAB and 37 % SB. This gives a total of 65 % of spirals having a bar structure in the blue light. Eskridge et al. (2000) determined bar fraction in the H band using a sample of 186 spirals from Ohio State University Bright Spirals Galaxy Survey. They found 56 % strongly barred and 16 % weakly barred galaxies. Their sample reveals no particular trend in the bar fraction as a function of morphology in both optical and H bands. Another study done by Menendez-Delmestre et al. (2007) gives a total fraction of 67 %. From a sample of 151 near infrared J, H and K_s images of spiral galaxies from 2 MASS, they identified bars by analyzing two-dimensional light distribution in combination with ellipticity and position angle. They found only 31 % of galaxies (from the total sample) with bar having the semimajor axis larger than 4 Kpc. Infrared bars where found to typically extend to one-third of the galactic disk. Galaxies morphologies can be studied by breaking it into different components. The basic elements (primary elements) are bars, spheroids and disks. The other components are represented by lenses that are elliptical-shape features between spheroid and disk, also inner and outer rings. Kormendy et al. (1979) studied a sample of 20 galaxies containing bars and lenses. He discovered that in 17 cases the bar fills the lens in one dimension. From these observations, Kormendy suggests that the lenses may derive from secular dissolution of the bar. Bulges of barred S0 seem to be different from those found in SA.

Dust lanes are believed to be tightly link to the bar strength (Athanassoula 1992b). They identified three main kind of dust lane: the type "a" are linear; type "b" are straight along the bar but curve in the vicinity and the type "c" are curved. The bar strength seems to increase as we move from type "a" to type "c".

Rings are often seen in barred spirals. They have active star formation and their average diameter is about 1.5 kpc (Figure 1.3). Some galaxies present an outer ring and pseudo-ring, respectively represented by (R) and (R').

Many barred galaxies present a ring drawn by the spirals arms configuration. The spirals arms form closed loops starting from one end to the other end of the bar.

1.3 Bar mass profile and shape

In galaxy evolution, structures like rings, bars, bulge and spiral arms are formed at a later stage after the disk forms. The evolution of the disk (mass and angular momentum redistribution; Athanassoula 2013) is lead by mergers and also by more internally driven mechanism referred to as secular evolution. With time the initially hot and dense universe cools down and stretches, reducing significantly galaxies'

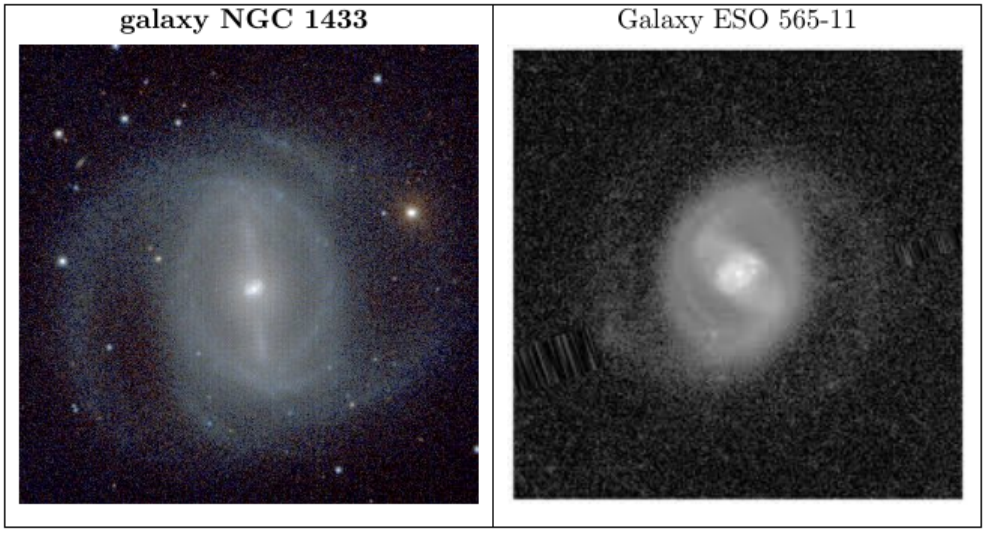

Figure 1.3: *NGC1433 (left), bar aligned with the inner ring and ESO565-11 (right), case of misalignment between the bar and the inner ring. Image from NED.*

interactions with each other. Thus, the late (more recent) evolution of galaxies are driven mostly by secular evolution (Kormendy & Kennicutt 2004). Bars are one of the most important structures in terms of mixing and driving the gas toward the center of the galaxy. The motion of the bar also creates an accumulation of stars in the central part of the galaxy (Sellwood and Wilkinson 1993). The high concentration of stars and the increase in the star formation rate due to the gas in the central part is observed as nuclear rings (Kim et al. 2012, Seo & Kim 2013). Bars, by their streaming motions redistribute stars inside the disk, provoking breaks in the disk luminosity profiles (Kim et al. 2014). Indeed in some galaxies, disk luminosity profiles, instead of having a sharp truncation (a single luminosity profile for the disk) there is a change in the slope, dividing the disk in two parts known as inner and outer disks. Profiles with a shallower inner disk and steeper outer disk and on the other hand with steeper inner disk and shallower outer disk are, respectively, type II and type III breaks (Pohlen et al. 2002 ; Pohlen and Trujillo 2006). Kim et al. (2014) found that if the disk break is not taken into account while doing the image fitting it leads to respectively up to 40 %, 10 % and 25 % change in disk scale length, bulge to total luminosity ratio (B/T) and bar to total luminosity ratio. Disk galaxies earlier than SBb have longer bars comparing to those later than SBb (Laurikainen & Salo 2002; Menendez-Delmestre et al. 2007). Studies done by Kim et al. (2014) have shown a correlation between the bulge to total luminosity ratio and the stellar mass of the galaxy. They found that bars in massive galaxies have a flatter profile compared to those in low mass systems, that show an exponential disk like profile (Figure 1.4). They suggested that bars in massive galaxies may have started with an exponential profile (disk-like) and became stronger with time (grabbing more stars) while in low mass galaxies the bar is still at the beginning of the growing process (and so has a disk-like profile).

1.4 Offset structures and lopsided disks

Bars in most of the Magellanic systems exhibit a bar which is offset from the galaxy disk center. The offset is frequently along the minor axis of the bar. The two best well known Magellanic systems are

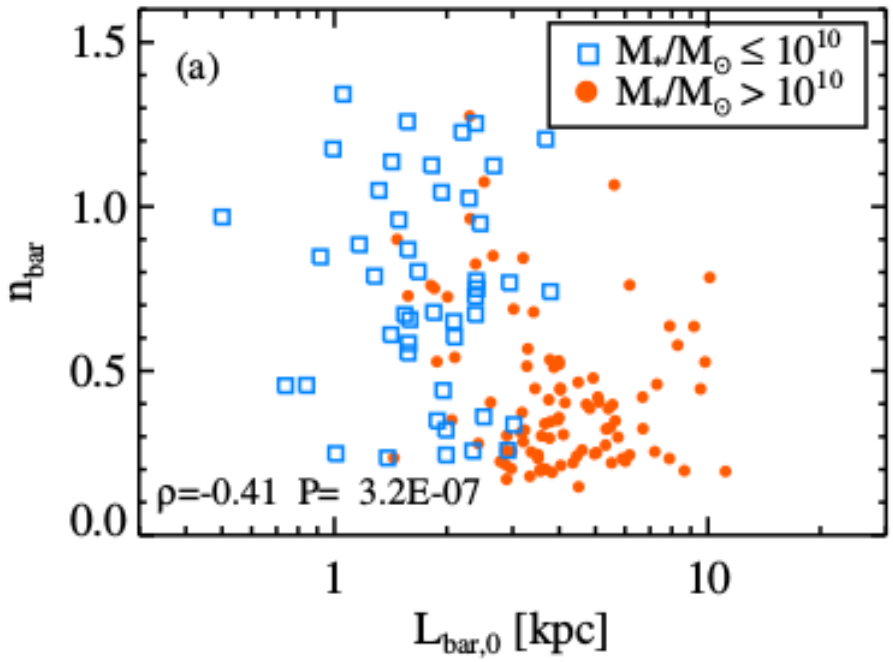

Figure 1.4: *Bar sérsic index against bar length. The masses galaxies are represented by filled circles and less massive by the squares (Kim et al. 2015).*

the Small Magellanic Cloud (SMC) and the Large Magellanic Cloud (LMC). Magellanic systems have been classified by de Vaucouleurs et al. (1972) as a specific group of disk galaxies. Systems like LMC have a specific morphology consisting of two spiral arms. One big and a second, smaller, starting from the end of the offset bar. In general they are low in mass, mean surface brightness and integrated absolute magnitude galaxies. The absence of bulge and lens in these galaxies in most of the cases, simplifies their photometric and kinematic studies. They are also very close to our own galaxy, the Milky Way. The LMC is even the closest galaxy making them perfect candidate for detailed studies. Magellanic systems are of great interest due to their position as transitional stage between the pure disk and irregular galaxy. So their studies will allow a better understanding of the Hubble sequence, but also the formation and evolution of bars and spiral arms.

The asymmetric mass distribution rise a couple of questions as follows: Does it have an effect on the global velocity field ? Or is the bar centered on the rotation center of the galaxy? Studies done by (Feitzinger 1980) on the LMC seems to show a difference between the bar center and the rotational center. On the other hand, the opposite was found by Pence et al. (1988) with the study of NGC4027. The studies of NGC4618, NGC2537 and LMC has shown a clear displacement of more than 1.5 kpc between the optical center and the rotational center. The computation of the rotation curves of those galaxies revealed large asymmetry on the rotation curve which seems to be a kinematic signature of Magellanic systems. The two dimensional luminosity decomposition done by Odewhan (1991) has shown that the bar will contribute 10% to 20% to the total luminosity while the smooth arm component contribute roughly 20% to 30% of the luminosity and the disk roughly 50%.

Lopsidedness is known as nonaxisymmetry on the mass distribution in the disk of spiral galaxies. Although noticed long time ago by astronomers (Sandage 1961), the lopsidedness phenomenon was first highlighted by Baldwin et al. (1980). They detected an asymmetry in the spatial extent of the atomic hydrogen gas in the outer region in the two halves of some galaxies and gave them the name

"lopsided"galaxies. Rix and Zaritsky (1995) defined A_1, the fractional amplitude of the first Fourier component (m=1) of surface brightness to be a quantitative measure of disk lopsidedness. Recently Bournaud et al. (2005) studied a much larger sample of 149 galaxies and found 1/3 of them to have 10% or more asymmetry in the amplitude of m = 1 Fourier component. The lopsided distribution of the HI can also be mapped kinematically (Schoenmakers et al. 1997; Swaters et al. 1999). Baldwin et al. (1980) mentions the asymmetric distribution of light and HI in spiral galaxies such as M101. They quantitatively defined a galaxy to be lopsided if the galaxy is more extended on one side than the other and where the density of HI on the two sides of the galaxy at least 2:1.

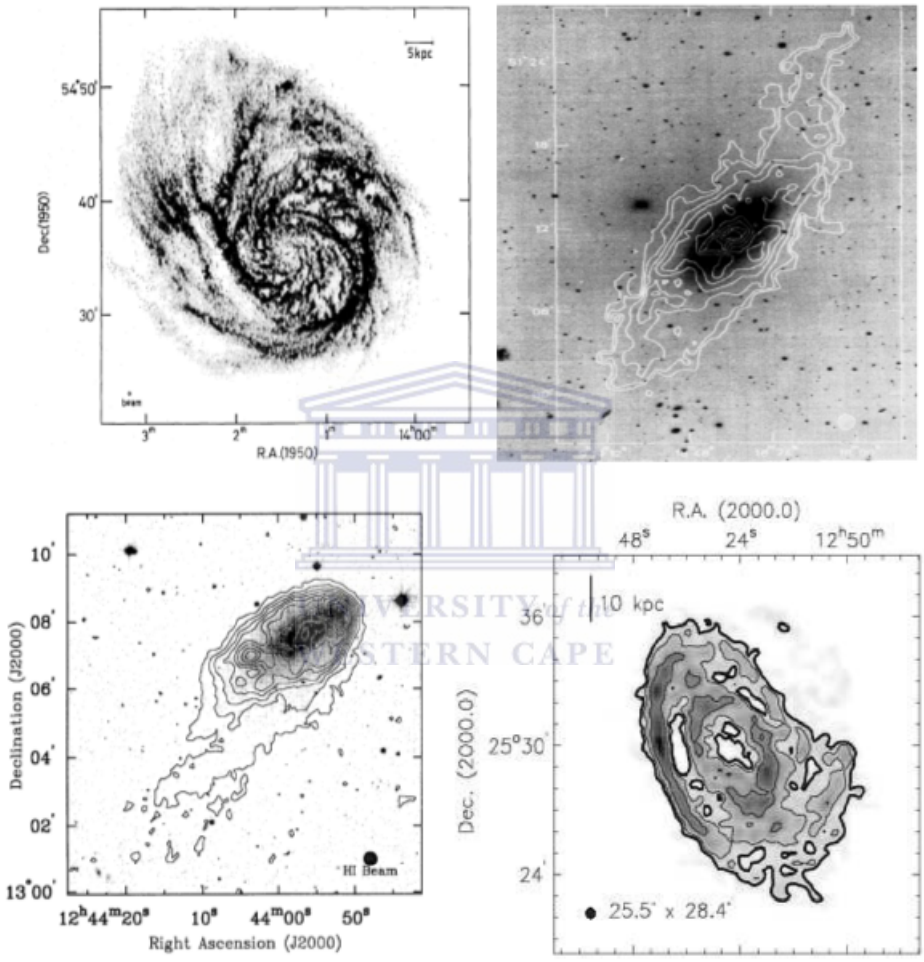

Figure 1.5: *Galaxies showing an asymmetry in the spatial extent of 2:1 or more in the HI distribution : M101 (top left, where the HI intensity is plotted here as gray scale) and NGC 2841 (top right: here the HI contours are superimposed on an optical image). Other typical examples are NGC 4654 (lower left: where HI contours are superimposed on an optical image) and UGC7989 (lower right, showing contours and grey scale of the HI intensity) Jog et al. (2009)*

1.5 Bar fraction evolution with redshift

Bar fraction is usually defined as fbar = number of barred disk/number of all disk galaxies.
In the local universe the bar fraction is 35 % for strongly barred galaxies (Sandage & Tammann 1987; de Vaucouleurs 1991). More recent work gives a total bar fraction of 0.65 for all barred galaxies (Whyte et al. 2002; Menendez-Delmestre et al. 2007) This result has been consistent with a lot of

works over decades and found to be the same for both optical and infrared. Looking further back in time (z > 0.5) this bar fraction decreases sharply leading to the conclusion that possibly disk galaxies were dark matter dominated or too hot to form a bar (Abraham et al. 1999; Vanderden Bergh et al. 1996).

Sheth et al. (2003) found four barred spiral a z > 0.7 for an initial sample of 95 galaxies. They haven't seen an obvious decrease of fbar and this might be due to the resolution of the instruments used (NICMOS with a resolution of 0.15"). Sheth et al. (2008b) used COSMOS data to study the evolution of bar fraction.

Unlike all previous studies, the sample is very large (2157 luminous face on galaxies vs a maximum of 187 using Advanced Camera for Survey (ACS)) spread over 0.2 <z <0.84. They found a decrease in the bar fraction (SB + SAB) from 65 % in the local universe to about 20 % at z = 0.84 while the strongly barred spirals (SB only) decrease from 30 % up to 10 %. Also the bar fraction seems to remain constant for massive spirals and decrease only with low masses spirals. Other remarkable founding was a significantly greater number of bulge dominated in comparison to non-bulge dominated barred spirals at high redshift.

The first step of this project is to analyse all disk galaxies in the *Spitzer* Survey of Stellar Structure in Galaxies (S4G) to identify offset bars and create a first and definitive catalogue of these structures in the nearby Universe. We will also fit each offset bar with the two dimensional fitting programme GALFIT to derive the basic properties of the bar and the host galaxy. Specifically we will derive the size, shape and profile of each bar, and calculate the light/mass ratio contained in the bars relative to their host galaxies. This will be compared to the properties of the more "regular" bars in more massive systems.

Chapter 2

The Spitzer Survey of Stellar Structure in Galaxies (S^4G) Sample

2.1 Description of the sample

Spitzer Survey of Stellar Structure in Galaxies (S^4G) is a magnitude and size limited survey of more than 2300 nearby galaxies at 3.6 and 4.5 μm. It is a deep survey compared to all the preceeding studies reaching 1 σ surface brightness limit of 3.6 μm(AB) = 27 mag arcsec^{-2} equivalent to a stellar surface density $<< 1 M_{\odot}$ (Figure 2.1).

Figure 2.1: *Image from NASA's Spitzer Space Telescope, taken in infrared light, shows where the action is taking place in galaxy NGC 1291. The outer ring, colored red in this view, is filled with new stars that are igniting and heating up dust that glows with infrared light.*

So S^4G can detect stars in the galaxies mostly dominated by gas (typical HI surface density of a few $M_{\odot}pc^{-2}$). The motivation for S^4G was to create a survey deep enough to understand the structure

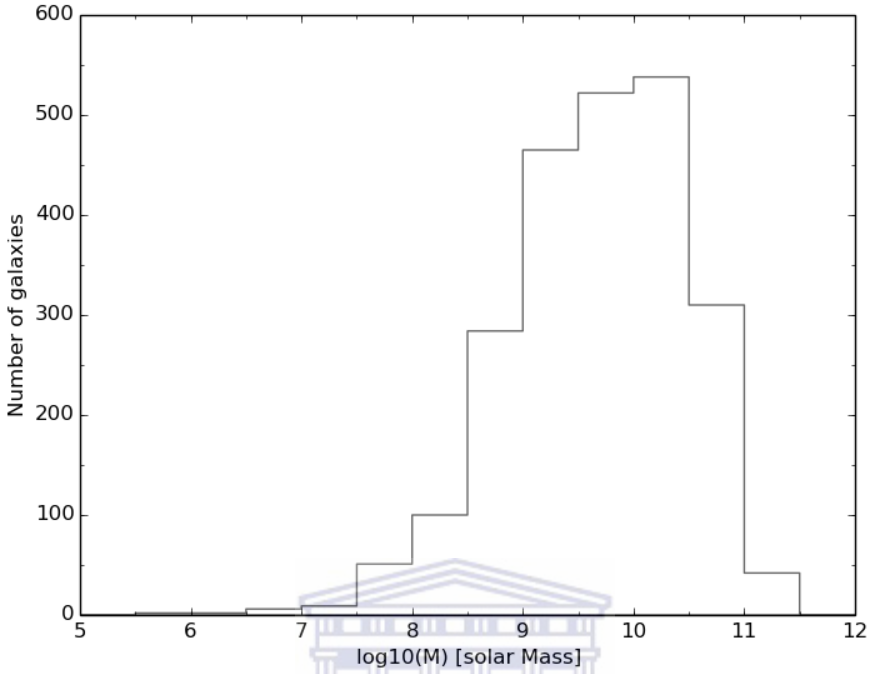

Figure 2.2: *Histogram of mass for S^4G sample.*

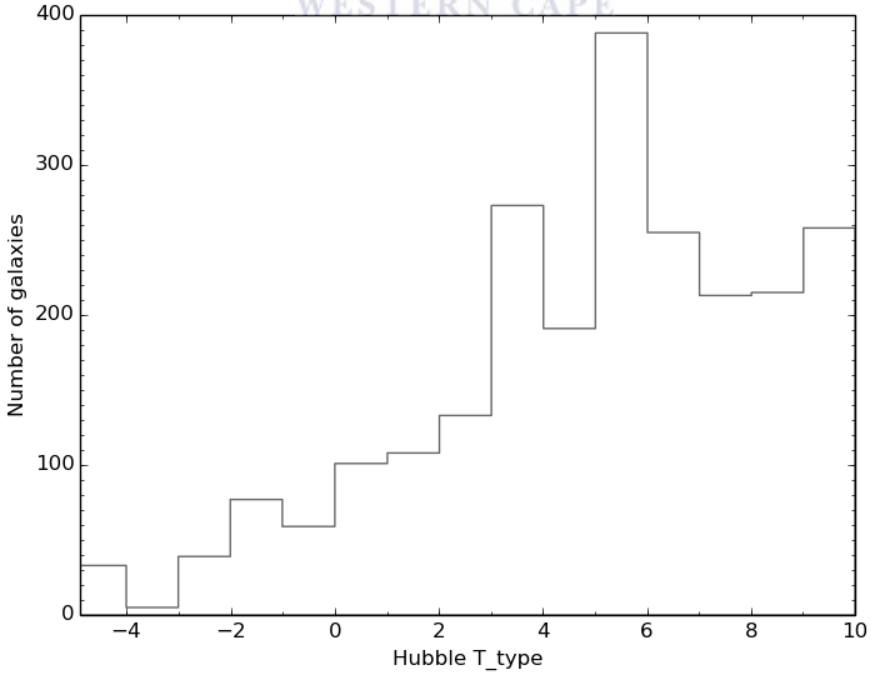

Figure 2.3: *Distribution of Hubble parameter T for S^4G sample. The data were determined from HyperLEDA data base.*

of all morphological types, and galaxies in a wide range of environments. S^4G select all galaxies with

radial velocities $v_{radio} < 3000$ km/s corresponding to a distance < 40 Mpc for Hubble constant (H_0) = 75km/s/Mpc and an isophotal angular diameter for the blue light $D_{25} > 1.0$'. This size cut (D_{25} >1.0') was to make sure that the galaxy is large enough to study it internal structures. For instance at the distance of 40 Mpc (corresponding to S^{4}G most far away galaxy), 1' will be almost equal to 11.6 Kpc (reasonable size to see all the features inside the galaxy). The total corrected blue magnitude has to be <15.5 with $|b| > 30^o$ using HyperLEDA (Paturel et al. 2003) to minimize the unresolved Galactic light contribution from the Milky Way disk. By using v_{radio} from HyperLEDA, the S^{4}G sample is limited by the data that are available in HyperLEDA. The comparison of our sample using v_{radio} to compare to a sample base instead of $v_{optical}$ velocity reveal that Some relatively small size and early type (gas-poor) are missing from S^{4}G sample. This decreases the population of early type in comparison to late type. Figure 2.2 and Figure 2.3 show respectively the mass and morphological type distribution of the S^{4}G sample.

Chapter 3

Analysis

3.1 Identification of regular and offset bars

The galaxies classified as irregulars (in HyperLEDA), mergers or strongly interacting and highly inclined (i > 65^o) have been firstly excluded. The identification was done using three methods namely visual inspection, ellipse fit technique and finally GALFIT. After excluding all the irregulars, mergers etc. we were left with 1522 galaxies from the initial sample of 2532 nearby galaxies. A meticulous visual inspection (each galaxy in S^4G) was done through imaging application SAOImage DS9. The ellipse fit for each galaxy was displayed on top of the original image in order to have a better view of all the substructures inside the galaxy. Moreover, using the tools available in DS9 to adjust the color the brightness and the contrast we were able to identify the presence of bars and bulges inside the galaxy disk and see whether the bar is offset or normally centered. The second method used both the position angle (PA) and ellipticity derived from the ellipse fit. The task ellipse in IRAF (Jedrzejewski 1987) to map galaxies contours followed by isophotes. According to this method, the ellipticity, ϵ = 1 - b/a (where b and a are respectively the semi-minor and major axises) decreases as we move from the round center area (bulge-dominated) to the disk (Figure 3.1). The classic signature of a bar fit with ellipses is the enhancement of the ellipticity in the bar region while the position angle stays relatively constant. The end of the bar is seen through an abrupt drop of the ellipticity followed by huge perturbation of the position angle. The presence of arms in the bar region can cause a constant change in the PA and ellipticity therefore hiding any signature from the bar. Indeed the presence of spiral arms in the bar region induces in some cases the drop of the position angle far from the bar end, so the semi major axis corresponding to the maximum ellipticity (ϵ max) is chosen to be the end of the bar. Due to the fact that the peak of ϵ is sometimes a flat region instead of a single point, a systematic error bar of $\delta\epsilon > 0.01$ is applied to ϵ max. A threshold of $\epsilon > 0.2$ is chosen to make a difference between a simple oval structure inside the disk and a bar (Karin Menendez-Delmestre et al. 2007). In some of the galaxies (Figure 3.2) only the ellipticity present the signature of a bar presence. The position angle increase regularly rather than being constant in the bar region. The cases are classified as "candidate" barred spirals and need a closer visual inspection.

After combining the visual method and the method defined by Karin Menendez-Delmestre et al.

(2007), we were able to find a considerably reduced sample of 102 offset structures made of 36 bar, 35 spiral, 31 candidate spirals barred and one edge on (available in Table 3.1). After many additional inspections and taking account of the two dimensional fitting, our final result is 49 offset barred galaxies in the nearby universe probe by S^4G.

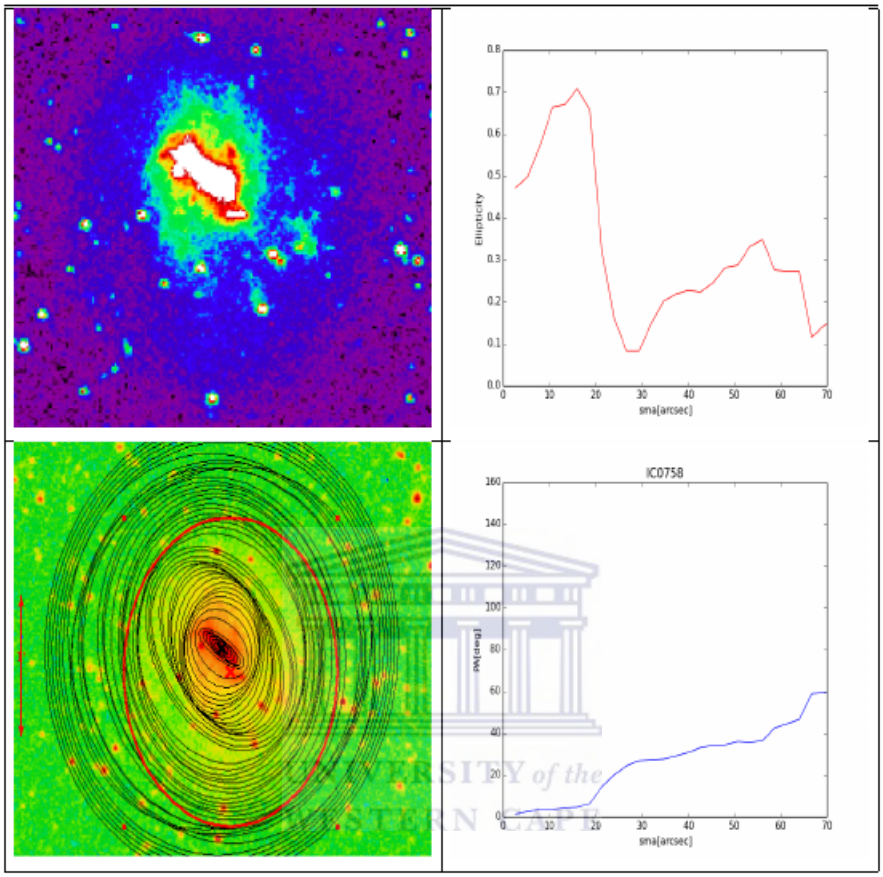

Figure 3.1: *Top left : IC0758 3,6 μm image. Bottom left: IC0758 image with ellipse fit over plotted. Top and bottom right are respectively ellipticity and PA as a function of semi major axis in arcsecond. One can see that ellipticity increase monotonically and drop abruptly while the position angle still constant.*

Table 3.1: All the offset structures in S^4G

Name	Classification	Longitude	Latitude	Redshift	Morphological Type
ESO054-021	SPIR	57.454551	-71.635581	0.004773	SAB(rs)dm
ESO079-007	CB	12.517568	-66.552204	0.005561	SA0
ESO187-051	SPIR	316.88834	-54.950367	0.004687	SB(s)m
ESO341-032	CB	315.889158	-39.446309	0.009213	SB(rs)m
ESO342-050	SPIR	322.062601	-37.861329	0.008876	SA(rs)c ?
ESO358-015	SPIR	53.27847	-34.80705	0.004631	SBm
ESO409-015	999	1.38364	-28.099908	0.002459	Double?
ESO443-080	SPIR	197.79023	-28.01012	0.007055	SB(s)m
ESO444-037	CB	201.7536	-30.07641	0.006331	SB(s)dm
ESO510-058	CB	211.155747	-24.833142	0.007795	SB(s)cd?
ESO539-007	SPIR	4.701543	-19.007968	0.010670	SAB(s)m
ESO544-030	SPIR	33.7386	-20.21175	0.005365	SB(s)dm
C0163	B	27.311743	20.711025	0.009170	SBdm
C0758	B	181.049601	62.505431	0.004253	SB(rs)cd
C1251	CB	257.553509	72.410525	0.004036	Scd
C2828	SPIR	171.795633	8.731073	0.003466	S0?WR
C4536	B	228.322299	-18.137098	0.007612	SB(s)dm
C5273	B	344.861151	-37.702888	0.004312	SB(rs)cd
NGC0150	CB	8.564448	-27.803522	0.005284	SB(rs)bc
NGC0244	SPIR	11.44343	-15.59657	0.003140	S0 ?
NGC0772	SPIR	29.831391	19.007664	0.008246	SA(s)b
NGC0899	SPIR	35.47107	-20.8238	0.005214	B(s)m
NGC1051	B	40.260387	-6.935825	0.004320	SB(rs)m
NGC1326A	CB	51.2868	-36.36308	0.006108	SB(s)m
NGC1338	B	52.227253	-12.153353	0.008259	(R')SAB(rs)b
NGC1359	B	53.449101	-19.492207	0.006581	SB(s)m?
NGC1385	CB	54.368701	-24.501198	0.005000	SB(s)cd
NGC1679	B	72.479197	-31.965522	0.003509	SB(s)m
NGC1688	B	72.098881	-59.800265	0.004095	SB(rs)dm
NGC1705	SPIR	73.555973	-53.360988	0.002112	SA0-
NGC1800	CB	76.606801	-31.954077	0.002692	B(s)m
NGC2101	SPIR	86.60085	-52.08862	0.004016	B(s)m
NGC2541	CB	123.667218	49.061618	0.001828	SA(s)cd
NGC2550	CB	126.142735	74.012323	0.007579	Sb
NGC2701	CB	134.773903	53.771599	0.007759	SAB(rs)c
NGC2793	CB	139.1943	34.43168	0.005627	SB(s)m
NGC3023	CB	147.468653	0.619035	0.006268	SAB(s)c
NGC3061	B	149.050248	75.866441	0.008196	(R')SB(rs)c
NGC3067	SPIR	149.587799	32.370092	0.004923	SAB(s)ab?
NGC3246	B	156.674245	3.861968	0.007185	SABdm
NGC3381	B	162.103649	34.711411	0.005434	SB WR

Table 1-continued

Name	Morphological	Longitude	Latitude	Redshift	Morphological Type
NGC3445	SPIR	163.648112	56.990824	0.006831	SAB(s)m
NGC3447	CB	163.349772	16.773345	0.003559	Mult
NGC3627	B	170.062528	12.991503	0.002425	SAB(s)b
NGC3659	B	170.939545	17.818502	0.004287	SB(s)m?
NGC3664	B	171.100947	3.324848	0.004607	SB(s)m
NGC3686	B	171.933239	17.224113	0.003856	SB(s)bc
NGC3846A	B	176.061724	55.034941	0.004790	SB(s)m
NGC3906	B	177.418986	48.42613	0.003200	SB(s)d
NGC3985	CB	179.175556	48.334026	0.003163	SB(s)m
NGC4027	B	179.87611	-19.2653	0.005574	SB(s)dm
NGC4189	B	183.446907	13.424757	0.007055	SAB(rs)cd?
NGC4234	CB	184.288151	3.683112	0.006761	(R')SB(s)m
NGC4273	CB	184.98355	5.343328	0.007932	SB(s)c
NGC4276	B	185.031128	7.691909	0.008733	S(s)c
NGC4351	CB	186.006393	12.204898	0.007667	SB(rs)ab
NGC4416	B	186.694731	7.918558	0.004637	SB(rs)cd
NGC4430	B	186.860045	6.262747	0.004840	SB(rs)b
NGC4618	CB	190.387044	41.150802	0.001815	SB(rs)m
NGC4625	B	190.469657	41.273867	0.002071	SAB(rs)m
NGC4630	SPIR	190.62968	3.9604	0.002458	B(s)m?
NGC4632	SPIR	190.6333	-0.082499	0.005747	SAc
NGC4668	B	191.383344	-0.535808	0.005457	SB(s)d
NGC4781	B	193.599219	-10.537113	0.004203	SB(rs)d
NGC4980	SPIR	197.291774	-28.641644	0.004767	SAB(rs)a ?
NGC5002	CB	197.658982	36.634275	0.003639	SBm
NGC5112	B	200.4852	38.73459	0.003252	SB(rs)cd
NGC5474	SPIR	211.255537	53.662209	0.000911	SA(s)cd
NGC5486	SPIR	211.854122	55.102954	0.004637	SA(s)m
NGC5691	B	219.472372	-0.398855	0.006238	SAB(s)a
NGC5713	CB	220.047696	-0.28888	0.006334	SAB(rs)bc
NGC5744	CB	221.658841	-18.512337	0.008856	Sa
NGC5915	SPIR	230.387934	-13.091746	0.007580	SB(s)ab
NGC5954	SPIR	233.645938	15.200128	0.006535	SAB(rs)cd
NGC6889	CB	304.721395	-53.956999	0.008456	SBbc?
NGC7154	B	328.837836	-34.814275	0.008726	SB(s)m
NGC7541	SPIR	348.682822	4.533923	0.008969	SB(rs)bc
NGC7694	SPIR	353.31534	-2.702694	0.007609	m
NGC7713	CB	354.062415	-37.938058	0.002322	SB(r)d
PGC012068	B	48.659276	-4.774324	0.007397	B(s)m
PGC012981	SPIR	52.38849	-15.23836	0.006294	SB(s)m

Table 1-continued

Name	Morphological	Longitude	Latitude	Redshift	Morphological Type
PGC014487	SPIR	61.804195	-17.20395	0.006191	SB(s)dm
PGC036274	CB	175.34505	-6.47948	0.005764	SAB(s)m
PGC041965	SPIR	188.90715	-7.87676	0.003269	SAB(s)dm
PGC045195	SPIR	196.12994	-3.57232	0.004536	SAB(s)dm
PGC066559	CB	319.928542	-7.55205	0.009093	SB(s)dm
PGC069339	SPIR	339.337551	-8.46084	0.009376	B(s)m
UGC03070	SPIR	67.748556	-2.003287	0.008389	SAB(s)b
UGC04549	SPIR	131.089447	58.841971	0.004300	Sdm?
UGC05612	B	156.02775	70.8822	0.003372	SB(s)dm
UGC05676	SPIR	157.268904	54.716456	0.004763	SBdm
UGC05832	B	160.701825	13.459817	0.004056	SB?
UGC06157	CB	166.604961	17.50796	0.009867	SA(s)dm
UGC06309	B	169.443402	51.476739	0.009573	SB?
UGC06320	SPIR	169.571898	18.847192	0.003753	S?
UGC07239	CB	183.536952	7.776652	0.004083	m
UGC08084	B	194.593312	2.792704	0.009263	SB(s)dm
UGC08303	SPIR	198.323333	36.2175	0.003149	AB(s)m
UGC08733	CB	207.162281	43.412834	0.007799	SBcd
UGC09215	B	215.863206	1.726241	0.004660	SB(s)d
UGC09380	SPIR	218.6634	4.26256	0.005647	m LSBG
UGC09661	B	225.51476	1.841294	0.004143	SB(rs)dm
UGC12682	CB	353.72235	18.22668	0.004647	m

Table 3.2: Offset bars galaxies and their fitting parameters

Name (1)	Stellar mass (2)	Morphological type (3)	Luminosity distance (4)	Redshift (z) (5)	Physical angular size (6)
ESO341-032	9.76	0.1	39.7378	0.009213	0.168
ESO510-058	9.952	6	33.5852	0.007795	0.171
IC0163	9.877	5.9	39.551	0.09170	0.162
IC0758	9.551	8	18.2745	0.004253	0.092
IC4536	9.98	3.2	32.7921	0.076000	0.162
IC5273	10.02	5.1	18.5288	0.004312	0.068
NGC1051	9.26	9.9	18.5633	0.004300	0.071
NGC1338	10.1	5.2	35.597	0.008259	0.153
NGC1359	9.917	5.9	28.3282	0.006581	0.122
NGC1679	9.537	6	15.069	0.003509	0.069
NGC1688	9.68	8.0	17.5934	0.004100	0.082
NGC1800	8.74	5	11.5532	0.002692	0.054
NGC3023	9.854	-2	26.9744	0.006268	0.146
NGC3061	10.3	5.5	35.3237	0.008200	0.164
NGC3246	9.88	9	30.9425	0.007185	0.165

Table 2-continued

Name (1)	Stellar mass (2)	Morphological type (3)	Luminosity distance (4)	Redshift (z) (5)	Physical angular size (6)
NGC3381	9.892	3.2	23.3703	0.005434	0.126
NGC3447	9.433	-2.4	15.2843	0.003559	0.093
NGC3627	10.8	1.5	10.4052	0.002400	0.071
NGC3659	9.942	7.7	18.4211	0.004287	0.107
NGC3664	9.531	5.9	19.801	0.004607	0.115
NGC3686	10.2	9.8	16.5636	0.003800	0.099
NGC3846A	9.521	7.9	20.5904	0.004790	0.106
NGC3906	9.365	9.8	13.7383	0.0032	0.077
NGC4027	10.59	6.2	23.975	0.005574	0.133
NGC4189	10.4	7.9	30.3796	0.007000	0.161
NGC4234	10.07	4.8	29.107	0.006761	0.156
NGC4276	10.08	1.5	37.6536	0.008733	0.194
NGC4416	9.747	-2	19.9304	0.004637	0.114
NGC4430	9.8	5.0	20.8061	0.004800	0.118
NGC4618	9.466	7.8	7.78412	0.001815	0.051
NGC4625	9.07	9.8	8.8838	0.002100	0.056
NGC4668	9.23	6.6	23.4696	0.005400	0.13
NGC4781	10.09	4	18.0589	0.004203	0.105
NGC5002	8.901	7.9	15.0288	0.003639	0.087
NGC5112	10.11	8.6	13.9173	0.003252	0.079
NGC5691	10.17	8	26.8447	0.006238	0.138
NGC7154	9.96	9.5	37.6232	0.008700	0.155
NGC7713	9.554	8.8	9.96243	0.002322	0.029
PGC012068	9.286	-6	31.8606	0.007397	0.134
PGC066559	9.524	8.1	39.2166	0.009093	0.159
UGC05612	9.506	8	14.4791	0.003372	0.072
UGC05832	9.173	-1.9	17.4254	0.004056	0.103
UGC06157	9.618	9.7	42.5799	0.009867	0.216
UGC06309	10.4	-4.8	41.3019	0.009500	0.201
UGC07239	9.434	6.8	17.4704	0.004083	0.104
UGC08084	9.576	8.8	39.955	0.009263	0.204
UGC08733	9.592	-1.9	33.6025	0.007799	0.165
UGC09215	9.807	4	20.0296	0.004660	0.108
UGC09661	9.18	9	17.8003	0.004143	0.095

Column (1)- the common name of a galaxy; column (2)-Stellar mass; column (3)- Hubble stage parameter T; column (3)-Luminosity distance

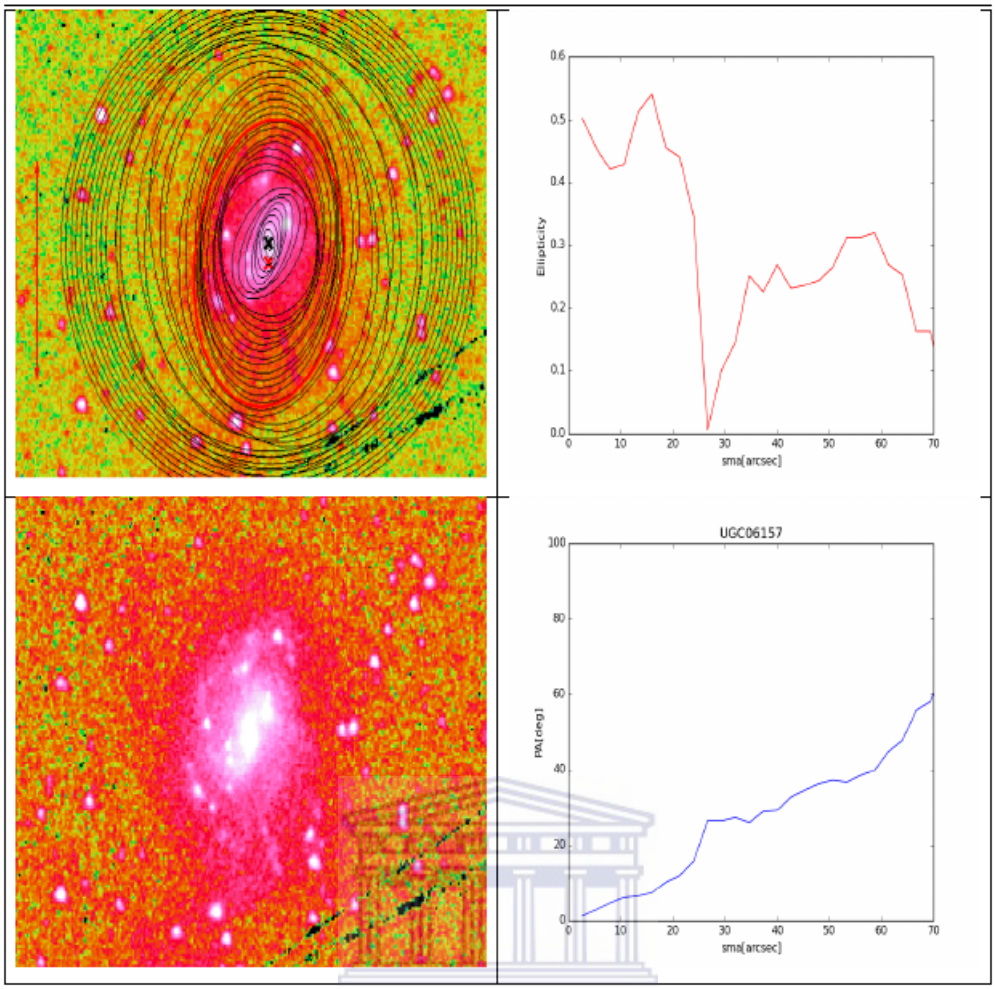

Figure 3.2: *Top left : UGC06157 3.6 µm image with ellipse fit overplotted. Bottom left: UGC06157 image. Top and bottom right are respectively ellipticity and PA as a function of SMA in arcsecond. One can notice that ellipticity increases monotonically and then drops abruptly , but PA increases continuously.*

3.2 Introduction to Ellipse(Iraf)

The fits have been done using a radial increment of 2 arcsecond along the semimajor axis. This profile (small step size: 2" increment) is better to measure structure like bars in details (Figure 3.4). The center is maintained fixed but the position angle PA and the ellipticity are set free. The required input parameters or files for ellipse fit are the galaxy image (fits file), the position of the photometric center, the initial position angle and ellipticity. The display of the image using DS9 is helpful to guess the initial parameters need for the fitting.

Fitting process

The image is measure using an iterative method (Jedrezejewsk 1987). Each isophot is fitted at a predefined fixed semi-major axis length (2" in this case). From the initial guess of the center (X,Y), the position angle and the ellipticity; the image is sampled following an ellipse and produce a one dimensional intensity distribution function of the ellipticity (E). The accuracy of the fitting is checked

using least-squares fitting to the following function:

$$\chi^2_\nu = \frac{1}{Ndof}\sum_{x=1}^{nx}\sum_{y=1}^{ny}\frac{(fdata(x,y) - fmodel(x,y))^2}{\sigma(x,y)^2} \tag{3.1}$$

Ndof is the number of degrees of freedom in the fit (Ndof $\approx$ $nx \times ny$). (See description of the parameters in equation(3.3)).

Table 3.3: Ellipse fit output parameter for IC0758. Only the parameter relevant to our study have been selected.

Semi-major axis (arcsec) (1)	Intensity mJy/sr (2)	Ellipticity (3)	Position angle deg (4)	Magnitude (AB mag/arsec^2) (5)
2.6667	0.6398	0.4725	52.3651	21.5815
5.3333	0.5260	0.4986	57.0224	21.7943
8.0000	0.4564	0.5748	56.9660	21.9484
10.6667	0.4379	0.6643	55.3238	21.9933
13.3333	0.3804	0.6707	55.4077	22.1460
16.0000	0.3578	0.7082	56.0585	22.2125
18.6667	0.2849	0.6585	59.0104	22.4599
21.3333	0.1912	0.3218	54.4213	22.8929
24.0000	0.1428	0.1592	44.6413	23.2101
26.6667	0.1136	0.0829	27.3321	23.4586
29.3333	0.0956	0.0829	-4.3996	23.6457
32.0000	0.0894	0.1482	-4.3996	23.7180
34.6666	0.0833	0.2022	-11.4061	23.7955
37.3333	0.0744	0.2186	-7.4264	23.9182
40.0000	0.0656	0.2274	1.1649	24.0544
42.6666	0.0581	0.2233	10.7760	24.1862
45.3333	0.0579	0.2458	23.9981	24.1901
48.0000	0.0556	0.2820	-156.001	8 24.2336
50.6667	0.0532	0.2879	-156.001	8 24.2828
53.3333	0.0561	0.3323	36.9300	24.2237
56.0000	0.0505	0.3482	38.3527	24.3382
58.6667	0.0434	0.2761	42.3937	24.5033
61.3333	0.0351	0.2731	38.9119	24.7343
64.0000	0.0307	0.2731	38.9119	24.8776
66.6667	0.0256	0.1161	28.5791	25.0751

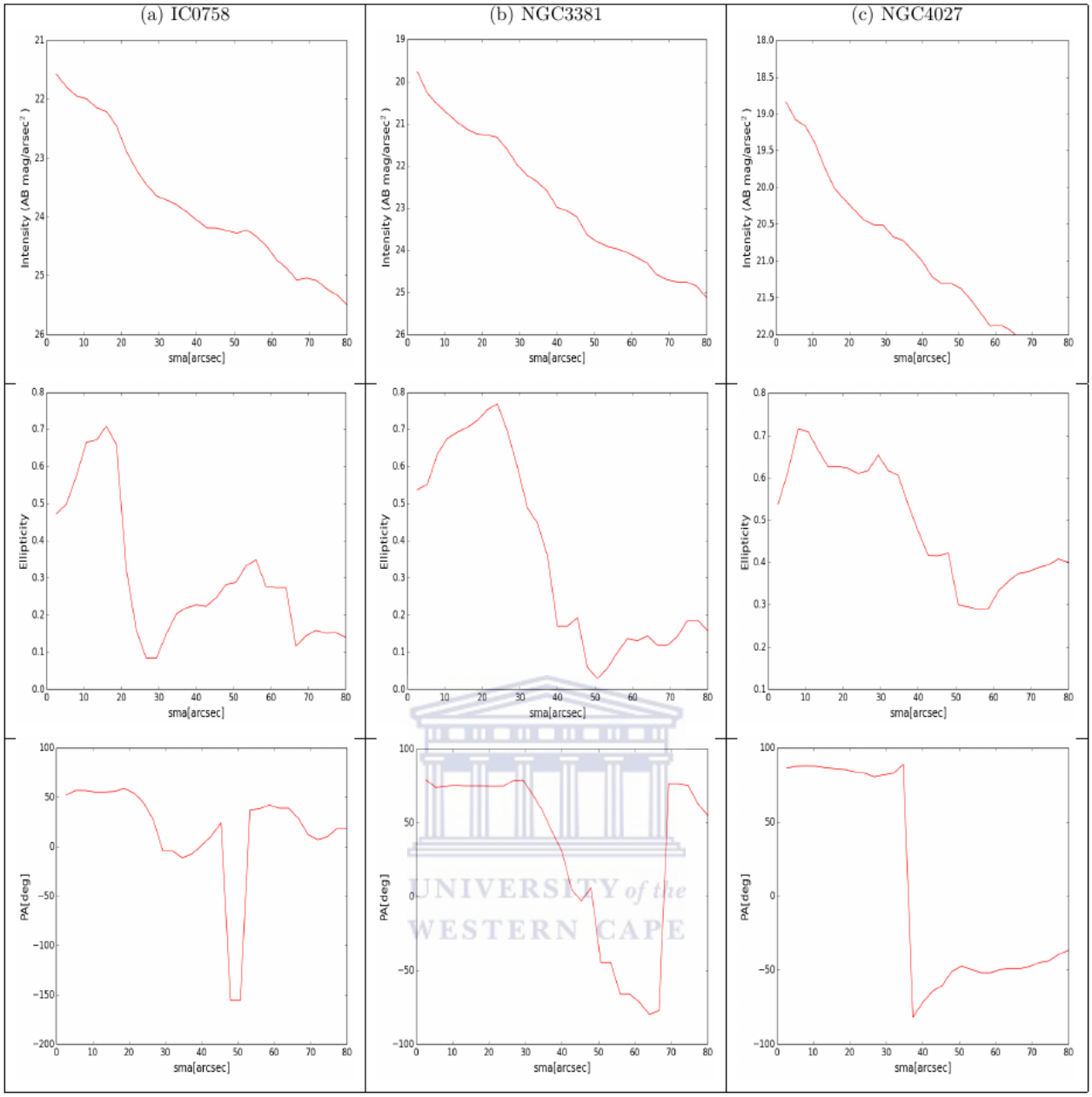

Figure 3.3: *Panel (a) , (b) and (c) represent respectively the radial profiles for IC0758, NGC3381 and NGC4027 from the surface photometry of 3.6 μm S^4G images. In each panel we have on top: The surface brightness profile. Middle: The variation of the ellipticity with the semi-major axis. Bottom: Position angle (PA) against the radius.*

3.2.1 Introduction to GALFIT

3.2.2 Definition

GALFIT is a two dimensional fitting algorithm designed to extract structural components from galaxy images. It has been successful at modeling the light distribution in spatially well-resolved, nearby galaxies. This algorithm is able to simultaneously fit a galaxy with an arbitrary number of components (Figure 3.5). GALFIT has a number of different models that can be used as initial inputs for the decomposition:

$$y = y_0 + A_1 * sin(E) + B_1 * cos(E) + A_2 * sin(2 * E) + B_2 * cos(2 * E) \tag{3.2}$$

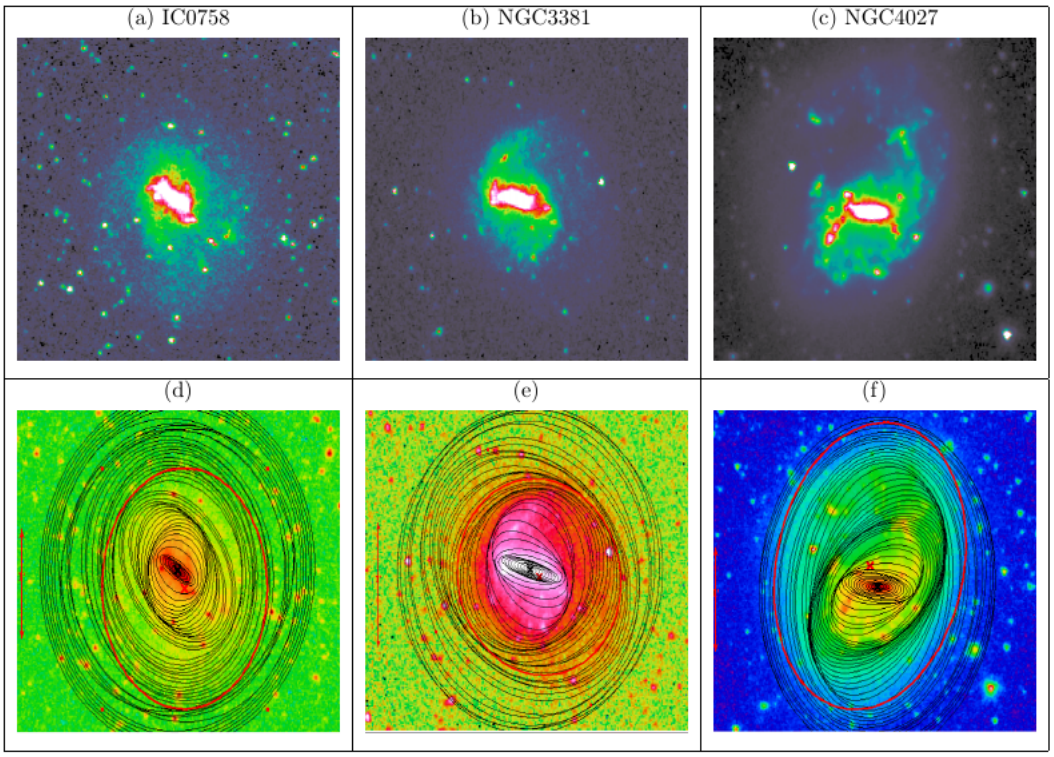

Figure 3.4: *From top left to top right we have 3.6 µm image of (a) IC0758; (b) NGC3381; (c) NGC4027. Bottom left to right represent respectively the 3.6 µm image of (d) IC0758, (e) NGC3381 and (f) NGC4027 with the ellipse fit overplotted.*

Where A_1, A_1, B_1 and B_1 are the harmonic amplitudes for a given ellipse geometry and show the deviation of the parameter with respect to the true one.

The output of ellipse is given in the form of a table containing more than 40 columns. Each column represents different values for a parameter at a given position along the semi-major axis.
The following table represent some of the parameters (more important for our study).

- **One component input files**

To fit one component (e.g a bulge or a disk) we use a Sérsic function and make an initial guess (by looking at the galaxy image) five free parameters: the total magnetude of the galaxy (m), its effective *radius*[1], the Sérsic index(n), isophotal minor-to-major axial ratio (q) and the position angle (PA). If the algorithm does not converge (i.e. when the Sérsic index is too big $n > 10, q < 0.05$ and Re is very large or very small - i.e. unphysical parameters) we change the initial guess to better fit the galaxy.

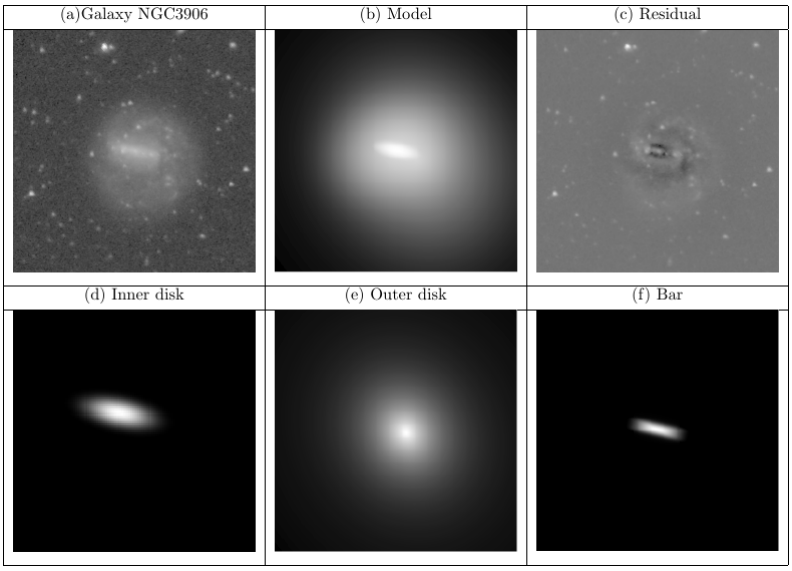

Figure 3.5: *From the top left to the bottom left we have: (a) 3.6 µm image of NGC3906; (b)the model; (c) the residual; (d) the inner disk; (e) the outer disk and (f) the bar*

- **Two components input files**

For the two components input (e.g bulge and disk) we use the same Sérsic function as the previous case, except that now for the first guess:

$$Re(bulge) = 0.5Re(image)$$

$$m(bulge) = m(image) + 1$$

To fit the disk we use "expodisk" when the galaxy estimated inclination b/a $\geq$ 0.2. Here the free parameters are scale length (hr) and the integrated magnitude of the disk (mdisk). For a first guess one can use the following relationships:

$$hr = 0.25 \times Rgal$$

$$mdisk = m(image) + 1$$

When b/a $\leq$ 0.2 we use "edgedisk" which has four free paramaters: the central brightness (μ_0), hr (like in expodisk model), the radial scale length (hz) and the position angle of the disk (PA). The first guesses are:

$$\mu_0(image) + 3$$

$$hz/hr = 0.1$$

• Multicomponent input files

To fit more than two components, one follows the same process as for two components, but then adding the functions we need. For example, if we want to fit the bar in addition to the bulge and the disk, we add a Ferrers bar model. The free parameters then are: the surface brightness at effective radius of the bar (μ_e), the outer truncation $radius^2$ (Rbar), the axial ratio (qbar) and the position angle (PA). The following relation can be use to make initial guesses:

$$\mu_e(bar) = \mu_e(image) + 3$$

$$Rbar = 0.25 \times Rgal$$

$$qbar = 0.5$$

$$PA(bar) = PAdisk + 90$$

```
#  Input menu file: GALFIT.03

#  Chi^2/nu = 10.729,  Chi^2 = 695822.188,  Ndof = 64852

================================================================================
# IMAGE and GALFIT CONTROL PARAMETERS
A) NGC3906.phot.1_nonan.fits     # Input data image (FITS file)
B) NGC3906imblockII.fits      # Output data image block
C) NGC3906_sigma2012.fits_ns     # Sigma image name(made from data
                                    if blank or "none")
D) PSF-1.composite.fits          # Input PSF image and (optional)
                                   diffusion kernel
E) 5                   # PSF fine sampling factor relative to data
F) NGC3906.1.finmask_nonan.fits      # Bad pixel mask (FITS image
                                       or ASCII coord list)
G) none                # File with parameter constraints(ASCII file)
H) 569  829  240  500  # Image region to fit (xmin xmax ymin ymax)
I) 50     50           # Size of the convolution box (x y)
J) 21.097              # Magnitude photometric zeropoint
K) 0.750  0.750        # Plate scale (dx dy)   [arcsec per pixel]
O) regular             # Display type (regular, curses, both)
P) 0                   # Choose: 0=optimize, 1=model, 2=imgblock,
                         3=subcomps

# INITIAL FITTING PARAMETERS
#
```

```
#   For component type, the allowed functions are:
#       sérsic, expdisk, edgedisk, devauc, king, nuker, psf,
#       gaussian, moffat, ferrer, and sky.
#
#   Hidden parameters will only appear when they're specified:
#     Bn (n=integer, Bending Modes).
#     C0 (diskyness/boxyness),
#     Fn (n=integer, Azimuthal Fourier Modes).
#     R0-R10 (coordinate rotation, for creating spiral structures).
#     To, Ti, T0-T10 (truncation function).
#
# ------------------------------------------------------------------
#   par)   par value(s)   fit toggle(s)    # parameter description
# ------------------------------------------------------------------

# Component number: 1
 0) sersic                 #  Component type
 1) 699.9920 370.7670 0 0 #  Position x, y
 3) 15.0828     1          #  Integrated magnitude
 4) 20.4378     1          #  R_e (effective radius)   [pix]
 5) 0.5096      1          #  Sersic index n (de Vaucouleurs n=4)
 6) 0.0000      0          #     -----
 7) 0.0000      0          #     -----
 8) 0.0000      0          #     -----
 9) 0.2150      1          #  Axis ratio (b/a)
10) 79.8930     1          #  Position angle (PA) [deg: Up=0, Left=90]
 Z) 0                      #  Skip this model in output image?  (yes=1,
                           no=0)

# Component number: 2
 0) expdisk                #  Component type
 1) 699.9920 370.7670 0 0 #  Position x, y
 3) 13.0901     1          #  Integrated magnitude
 4) 22.5976     1          #  R_s (disk scale-length)  [pix]
 5) 0.0000      0          #     -----
 6) 0.0000      0          #     -----
 7) 0.0000      0          #     -----
 8) 0.0000      0          #     -----
 9) 0.8691      0          #  Axis ratio (b/a)
10) 28.1464     0          #  Position angle (PA) [deg: Up=0, Left=90]
 Z) 0                      #  Skip this model in output image?  (yes=1,
```

```
no=0)

================================================================
```

3.2.3 GALFIT Input Images

A) The Sigma Image

The sigma image is a map containing the uncertainties in the flux for every pixel. The map is used in the calculation of the χ^2_ν, which is the square of the difference between the real data and the model fit divided by the standard deviation sigma (σ). The equation is the following :

$$\chi^2_\nu = \frac{1}{Ndof} \sum_{x=1}^{nx} \sum_{y=1}^{ny} \frac{(fdata(x,y) - fmodel(x,y))^2}{\sigma(x,y)^2} \tag{3.3}$$

Ndof is the number of degrees of freedom in the fit (Ndof $\approx$ $nx \times ny$).
fdata(x,y) is the observed data at pixel position (x,y); fmodel is the best fit produce by GALFIT at pixel (x,y) and σ is the deviation of the flux at the position (x,y). The first thing to do when we generate the sigma image is to make sure that the image is in units of counts (instead of other units such as counts/second). Then the creation of the sigma image follows these steps:

1. The header of real data contain informations about the ADU, the GAIN, the Ncombine etc.. GALFIT uses these parameters to convert the pixel ADUs into electrons ($Nelectrons = ADU \times GAIN \times Ncombine$).

2. Nelectrons is added to the RMS of the sky in quadrature (RMS is multiplied by $\sqrt{Ncombine}$).

3. GALFIT then divides the square root of the result in step two by the Gain in order to convert the electrons into ADU and creates the final sigma image.

$$electron(inADU) = \sqrt{step(2)image}/Gain$$

B) Point spread function (PSF)

The PSF is the image of a single point source with nothing around and no sky background. It is the three dimensional diffraction pattern of light emitted from the infinitely small point source in the specimen and transmitted to the image plane by reflecting and refracting on the optics (telescope aperture), atmosphere ect. In astronomy only far-field PSFs are used so the image obtained is normally flat. The point spread function is obtained with a theoretical model or from an image.
An ideal PSF must be isolated from everything else, have a very high signal to noise (S/N) and zero background. It should also match the shape of the image, be centered in the image and enough large

to enclose all the light.
To extract the PSF from an image, we select a star within that respect the conditions above. Then we just cut a small region around it. This is done in IRAF as the following:
$> imeopydata.fits[xmin : xmax, ymin : ymax]psf.fits$
$> imarithpsf.fits - skyvaluepsf.fits$

C) Object masking

The masking can be done by using a SExtractor segmentation image or manually.
GALFIT can take the SExtractor segmentation image directly as a bad pixel mask: all non zero pixels in the segmentation image are ignored by GALFIT in the fit. Manually we select the region to be masked with DS9. So with the programs DS9poly.c and nillpoly we created the mask image.

3.2.4 GALFIT functions

⋆ Sérsic profile

Sérsic profile or Sérsic model is a mathematical function that describes how the intensity I of the galaxy varies with distance R from it center up to the edge. It is the generalisation of de Vaucouleurs law ($r^{1/4}$).

The simple Sérsic profile can fit bulge dominated systems to disk systems (e.g. n = 1, fits the dwarf ellipticals well whereas $r^{1/4}$ bulges and ellipticals are fit by higher values of n (Graham 2002).
The Sérsic profile has the form:

$$\sum(r) = \sum_e \exp\left[-\kappa\left(\left(\frac{r}{r_e}\right)^{1/n} - 1\right)\right] \tag{3.4}$$

$\sum_e$ is the surface brightness of the pixel at the effective radius r_e.The effective radius r_e is the distance from the center at which half of the total flux is inside the circle of radius r_e. κ is a variable use to perform the profile. The parameter n, called the "Sérsic index" controls the degree of curvature of the profile. When n is small (big) the profile is less (more) centrally concentrated.

The flux integrated out to r = ∞ for a Sérsic profile is:

$$F_{tot} = 2\pi r_s^2 \sum_e e^{\kappa} n \kappa^{-2n} q / R(C_0, m) \tag{3.5}$$

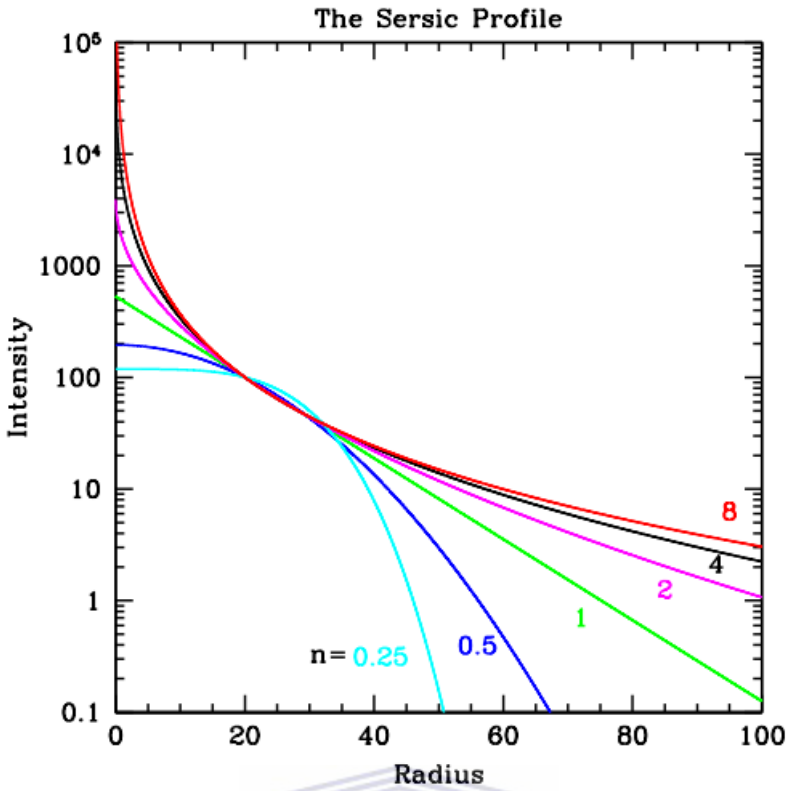

Figure 3.6: *Sérsic profile for different values of the concentration variable n (Chien Y. Peng et al. 2010). When n is large the central core is steep and outer wings are extended. A low n has a flat core and sharply truncated wings.*

⋆ The Exponential Disk Profile

The Exponential function is used to describe the galactic disks, it looks like the following:

$$\sum(r) = \sum_0 \exp\left(-\frac{r}{rs}\right) \tag{3.6}$$

$$F_{tot} = 2\pi r_s^2 \sum_0 q/R(C_0, m) \tag{3.7}$$

r is the galactocentric radius. rs is the length scale of the disk and $\sum_0$ is the surface brightness of the pixel at the center of the galaxy. It is a special case of Sérsic for n = 1.
The relation between r_s and r_e in this case is $r_e = 1.678 r_s$.

⋆ The Modified Ferrers Profile

The Ferrer profile has a flat core and an outer truncation. α is the parameter that represent the truncation sharpness, β controls the central slope. According to it characteristics (flat core and sharp truncation), Ferrer 2 is a good fit for galaxy with bars and/or bar lenses.

$$\sum(r) = \sum_0 \left[1 - \left(\frac{r}{r_{out}}\right)^{2-\beta}\right]^{\alpha} \tag{3.8}$$

$\sum_0$ surface brightness at the origin

This profile is only defined for r $\leq r_o ut$ and take the value 0 for r $= r_o ut$.

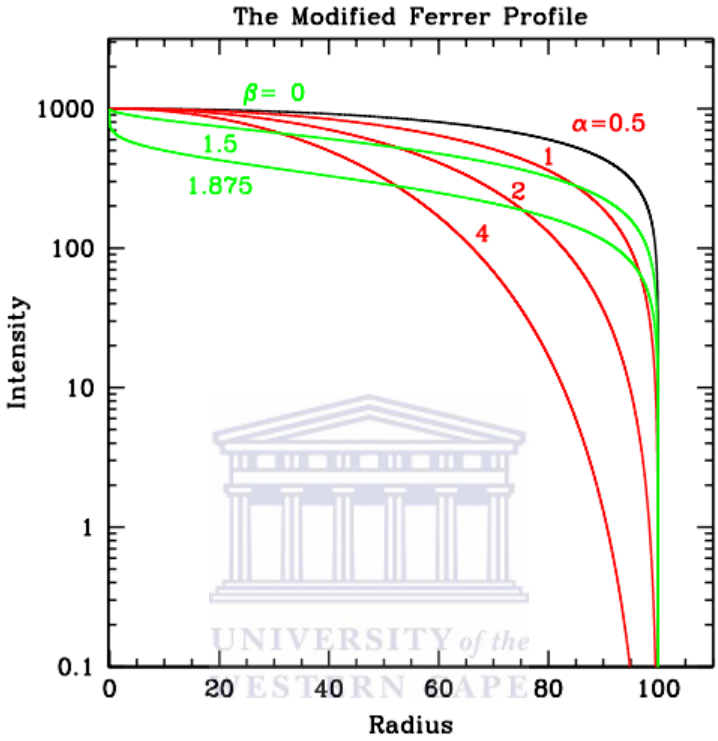

Figure 3.7: *The modified Ferrer Profile (Chien Y. Peng et al. 2010). The black reference curve parameters are r_{out} = 100, α = 0.5, β = 2 and $\sum_0$ = 1000. The red and green curves have the same parameters as the reference curve except respectively for the parameters α and β.*

Chapter 4

Results

We investigated all the galaxies in S^4G and we found 49 offset barred disk galaxies within the entire population. From our offset barred disk galaxies, we selected a sub-sample of low mass offset barred galaxies with $8.6 < \log_{10}M_*/M_\odot < 9.8$. We chose this mass range to encompass the mass range for low

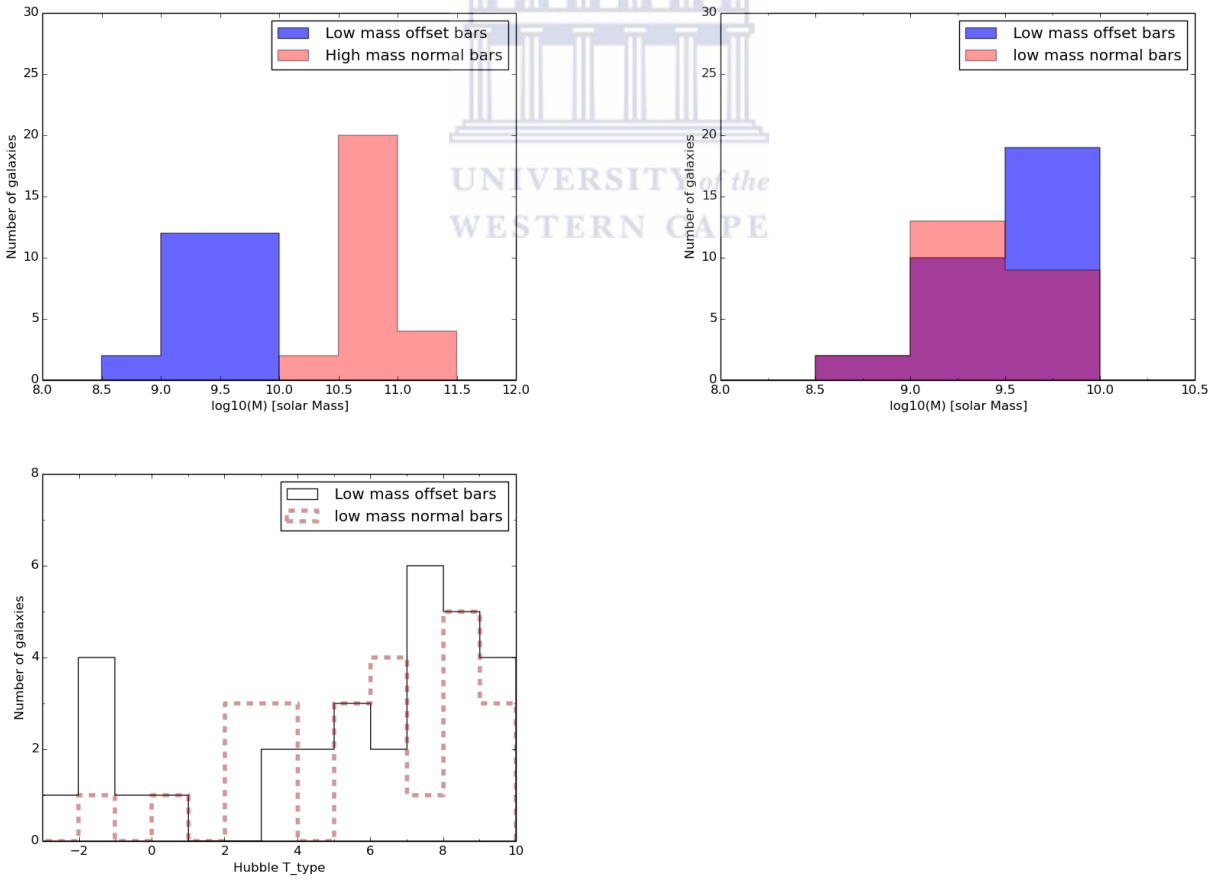

Figure 4.1: *-(top left): Histograms showing respectively the low mass offset in blue and high mass normal galaxies in orange. We can see the distinct separation between the two samples -(top right): Low mass offset in blue and low mass normal galaxies in orange. Here the two samples almost overlapped allowing us to make a strong comparison. -(Bottom left): Displays the low mass offset (filled black line) and low mass normal (dashed orange line) barred galaxies. We have the presence of all the morphological types in comparable proportion for both samples.*

mass dwarfs and Magellanic systems where the majority of galaxy evolution is likely occuring today (Sheth et al. 2008a; de Swardt et al. 2015). Apart from the samples of offset barred, we also created two other samples, namely low mass normal and high mass normal barred galaxies from S^4G (see Figure 4.1). They have been selected among disk barred galaxies with inclination $< 65^o$ and presenting a clearly centered bar and hosting no known AGN. For more precautions, we took galaxies already classified as disk barred galaxies in S^4G and double check them using the selection method used for the offset sample. The low mass normal sample is restricted to the same mass range as than our low mass offsets bars in order to compare only differences due to the displaced position of the bar. The high mass normal sample was chosen to have the most massive disk barred galaxies from S^4G. The low mass normal and high mass normal contain respectively 24 and 26 galaxies. We determined basic parameters such as bar shape, ellipticity, disk scale-length etc. and studied their variations. Low mass offset barred galaxies were compared to both low mass normal and high mass normal barred galaxies.

A number of studies suggest interaction as the cause of the lopsided structure of Magellanic type galaxies (Odewahn 1994, Robotham et al. 2012). However several other investigations have shown that actually only few of the lopsided galaxies or offset bars are in an interaction with a nearby galaxy (Wilcots and Prescott 2004). Simulations done by Springel (2005) show an offset due to interaction with a dark matter sub halo. They consider a Magellanic type galaxy with a thick stellar disk too hot to create bar, then allow an encounter with a dark matter sub halo. Some studies have shown that the lopsidedness can be stable and the disk, displaced from the dynamical center is allowed to rotate around the center (Levine et al. 1998, Noordermeer et al. 2001). In these cases the offset can be long-lived if they appear in dark matter potentials with inner cusps (i.e the central part of galaxy is halo dominated). Minors mergers with low mass companions and asymmetric accretion from the cosmic web also lead to perturbation in the velocity field of the host galaxy. With the large proportion of barred galaxies in the local universe, one would expect a higher number of offset barred galaxies, however, a low proportion is found. With 1500 barred disk galaxies, from S^4G only 49 were classified as offsets. This could be due to the constraints put on our selection process (ex: inclination $< 65^o$). Also our definition of offset (what is the minimum separation for a bar to be considered as offset). Since we used visual inspection and also GALFIT to quantify the offset, the accuracy of the program may affect our results. Offset barred galaxies were believed to be abundant in low mass galaxies; The magnitude and size limit of S^4G could have bias our study. On the other hand, due to the expansion of the universe, galaxies at low redshift are more isolated reducing galaxy-galaxy interactions which is one of the cause for offset bars.

4.1 Shape of Offset Bars

The parameter C_0 in GALFIT is used to evaluate the shape of the bar. It is the equivalent of the parameter C in equation (1.3), but unlike C, $C_0 < 0$ represent a disky and $C_0 > 0$ for boxy shape. $C_0 = 0$ represent an ellipse. The Figure 4.2a, shows a wide range of boxiness indices without any

correlation to the galaxy masses. Nevertheless, a notable fraction of highly offset bars seems to have

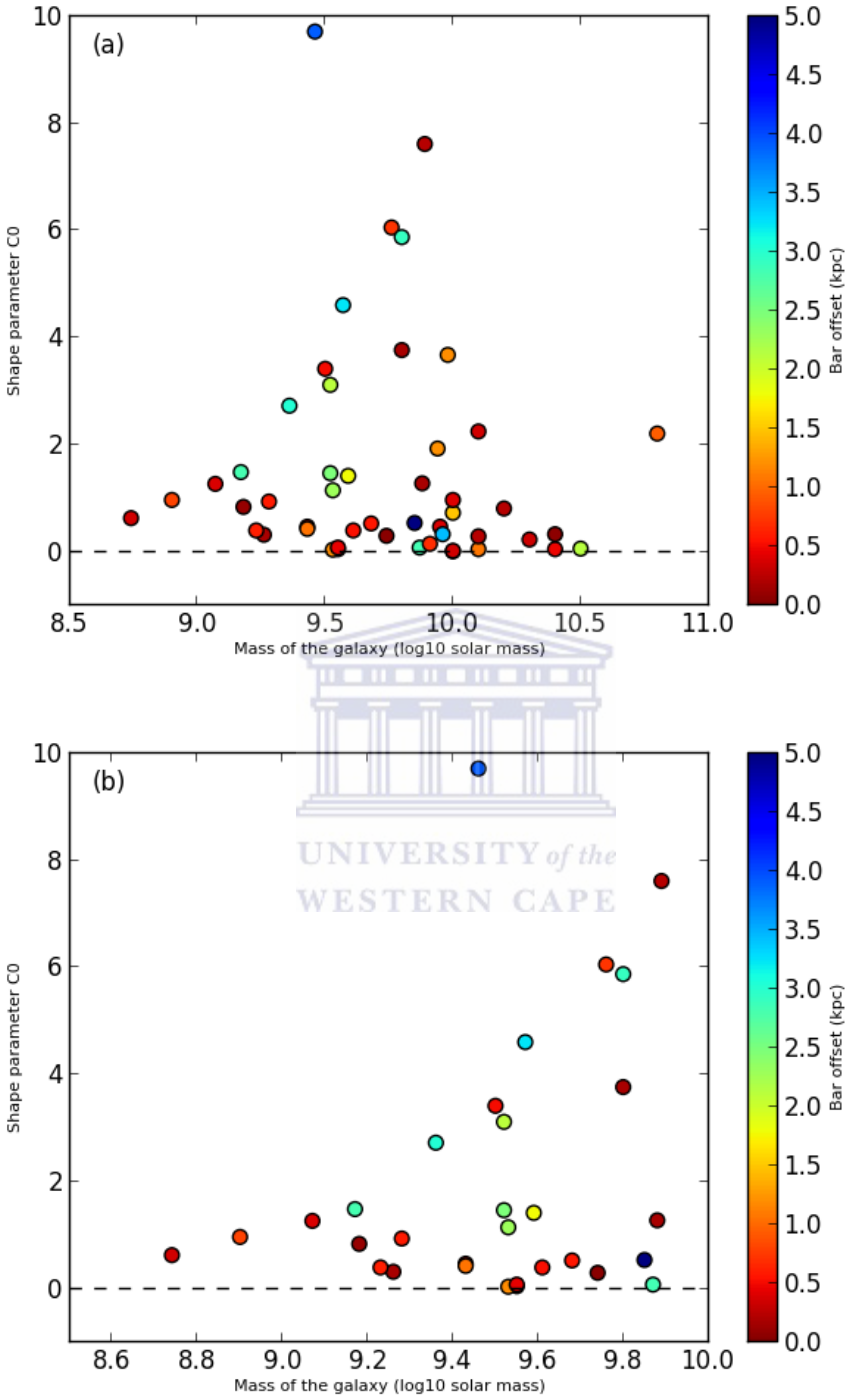

Figure 4.2: *Offset bars shapes versus theirs masses. The third dimension represent the offset between the bar and the disk of the galaxy. -(Top): Total sample of offset bars, -(Bottom): Sample of low mass offset bars. The distribution of the bars shape parameter (C_0) relative to the galaxies masses shows a range of boxiness. In Magellanic systems mass range (picture b), the most boxy bars are found within higher mass galaxies and the boxiness seems not to be related to the offset of the bar, nevertheless, a notable fraction of highly offset have* $0 < C_0 < 2$.

$0 < C_0 < 2$ and just few galaxies have a parameter $C_0 > 2$. From the original sample of 49 galaxies, 12 or (24%) have $C_0 > 2$ and 37 or (76%) have $0 < C_0 < 2$. The majority of the bars parameter

lies between $0 < C_0 < 2$. While the much high mass ($\log_{10}M_*/M_\odot > 10$) galaxies seem to have C_0 confined between 0 and 4, our low mass offset barred galaxies have a wider span of C_0 from 0 up to 8. This observation once more confirm that a lot of processes affecting galaxies evolution occur in this specific mass range.

In Figure 4.3 the offset barred sample has been divided according to the morphological type. Early types (dark red dashed) and late types (orange). We considered (only for Figure 4.3) early-types to SBa the rest (SBb and later) as late types. The frequencies have been calculated by normalising the number of galaxy by the total number in the sample. The morphological type distribution reveals a dominance of early type at high C_0 while late types are nearly confined between 0 and 2 ($\approx 90\%$). All the $C_0 > 6$ are early types offset barred disk galaxies.

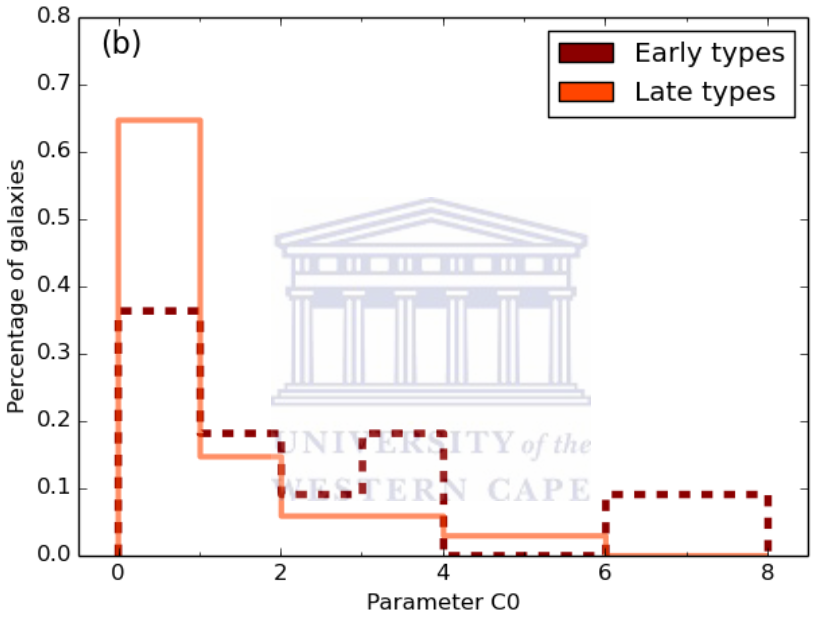

Figure 4.3: *Shape parameter C_0 distribution with the frequency of galaxies. Early types (dark red dashed) and late types (orange). We considered early-types to SBa the rest (SBb and later) as late type. The morphological type distribution reveals a dominance of early type at high C_0 while late types are nearly confined between 1 and 2 ($\approx 90\%$). All the $C_0 > 6$ are early types offset barred disk galaxies.*

Athanassoula (1990) on their analysis of 12 barred (SBO) spirals found no correlation between high shape parameter (see parameter C in equation (1.3)) value with the presence of substructures like rings or lenses, however, found bars in early type galaxies to be boxy. No conclusions were drawn about late type galaxies since their sample was only made of early type galaxies. In a large study of 144 normal barred spirals from S^{4}G, Kim et al. (2015) found that *all* bars were boxy in shape. We also find the same result here for the "offsets" bars, suggesting that all bars form in the same way! Our complete sample of offset bars (49 galaxies) shows no presence of disky bars (all the offset bars are boxy). Some values of the shape parameter (C_0) were close to 0, but still boxy. In few cases the bar looks visually more boxy than the result given by GALFIT. A visual inspection reveals strong spirals arms in the bar region leading to an underestimation of the bar boxiness (case found in 4 galaxies). The highest values of the shape parameter were found in late type offset barred galaxies with a wider C_0 distribution from 0.05 up to 8. After having investigated all the offsets bars from S^{4}G used as

representative of the local universe, all the offsets bars are also boxy. Our results in addition to Kim et al. (2015) suggest strongly that all kind of bars normals or offsets are boxy from the beginning of their formation and only get more boxy with time.

4.2 Luminosity Ratio and Bar Length

The sample of 49 galaxies identified (using mid infrared data 3.6μm) from S^{4}G as offset barred galaxies have been decomposed into their different components, namely the disk, the bulge and the bar. The program used (GALFIT) allows us to determine the bar length and the light distribution parameters for all the components (Figure 4.4). From this information we were able to reconstruct

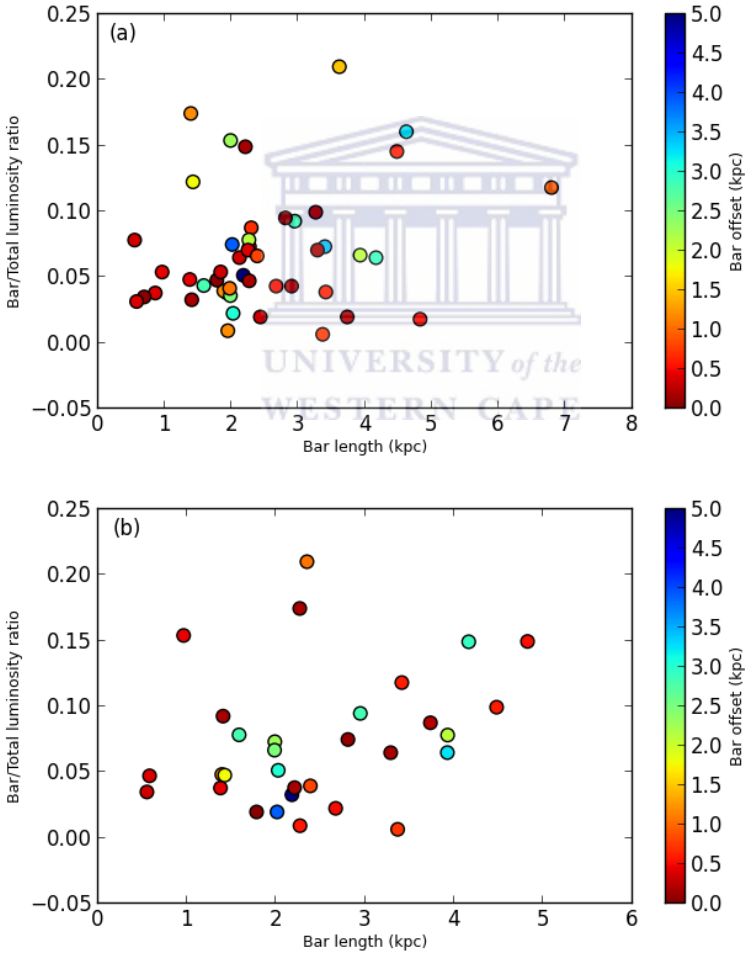

Figure 4.4: *The ratio bar luminosity/total luminosity against the bar length. -(Top): Total offset barred galaxies sample. The bar to total luminosity ratio is in the range 0.006 to 0.21 for bar-length (l_{bar}) between 0.55 and 6.8 kpc. More than 80% of the galaxies have Bar/T less than 0.1 and the overall average is $\approx$ 0.072 with the average offset bar length of 2.5 kpc. -(Bottom): offset barred galaxies reduced to Magellanic system mass range (8.5 and 10.1 $log_{10}M_*/M_\odot$ solar mass). The average Bar/T has slightly increased (Bar/T = 0.074), showing that most of the high mass offset barred galaxies present a bar with less contribution to the total light of the galaxy than low mass offset barred disk galaxies.*

the contribution to the total light of the bulge, the disk and the bar using respectively equations (3.4) (3.6) and (3.8). Our objective was to analyse the light contribution of the bar with respect to the total light diffused by the galaxy (Bar/T). Bar/T is a marker of the bar prominence in the galaxy. From this section up to the end of the document the morphological types are divided into early, intermediate and late types (Table 4.1).

Table 4.1: morphological type classification for all the samples

Samples \ T types	-3 < T ⩽ 2	2 < T ⩽ 6	6 < T ⩽ 10	Total galaxies
High mass normal	6	8	12	26
Low mass normal	2	9	13	24
High mass offset	3	8	7	18
Low mass offset	7	7	17	31

Throughout the document we considered $T < 5$ early type and $T \geqslant 5$ late type, this table shows more details by the subdivision into three groups. The T types between 2 and 6 are considered as intermediate between early and late morphological types.

In Table 4.1 we have classified galaxies in each sample into 3 distinct morphological type groups namely early, intermediate and late type respectively for $T \leqslant 2$, $2 < T \leqslant 6$ and $T > 6$. Despite the small size of our different samples, the late types seem to dominate the low mass samples as compared to high mass samples exhibiting a predominance of early and intermediate types. S^4G is a nearby (low redshift) survey of galaxies, so we expected to find many late type galaxies even in our high mass samples as we can see in Table 4.1. We also noticed a significant number of early types in the low mass offsets sample compared to the low mass normals one. The high mass offsets barred galaxies are dominated by intermediate morphological types.

4.2.1 Offset barred galaxies sample

In Figure 4.4a the bar to total luminosity ratio is in the range 0.006 to 0.21 for bar-length (l_{bar}) between 0.55 and 6.8 kpc with only one galaxy having $l_{bar} > 5$ kpc in the offset barred galaxies sample. We have almost the entirety of bars lying between bar length 0.55 and 4 kpc. More than 80% of the galaxies have Bar/T less than 10 % and the overall average is ≈ 0.072. So the mean contribution of the offset bars to the total luminosity ratio is $\approx 7.2\%$ with the average offset bar length of 2.5 kpc.

4.2.2 Comparison between offsets and normals Luminosity Ratio - Bar Length

Trying to have a comparative idea of offset barred galaxies, we showed the bar/total luminosity ratio against the bar length in Figure 4.5. Low mass offset barred galaxies are color coded as a function of the bar offset distance from the photometric center and in filled gray square the low mass normal barred galaxies. The galaxies were all chosen from S^4G, except the fact that in the latter sample, the bars of the galaxies are aligned with the photometric centers. The alignment of the bar and the

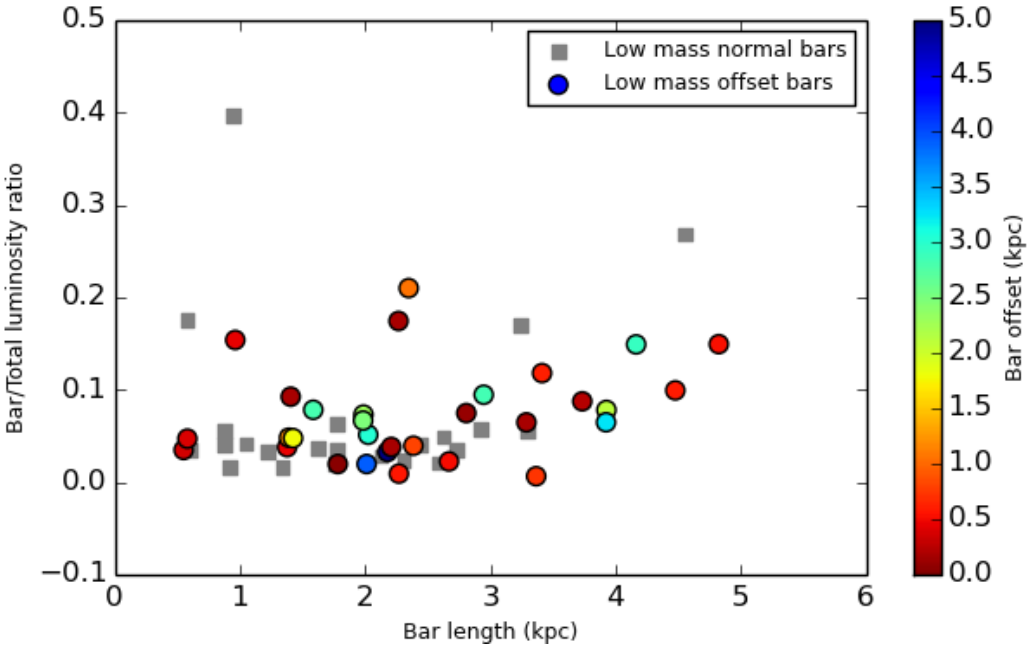

Figure 4.5: *The ratio bar luminosity/total luminosity against the bar length for the sample of offset bars. Comparison between low mass offset and low mass normal barred galaxies. The low mass offset are represented by color coded circles and the low mass normal in gray squares..*

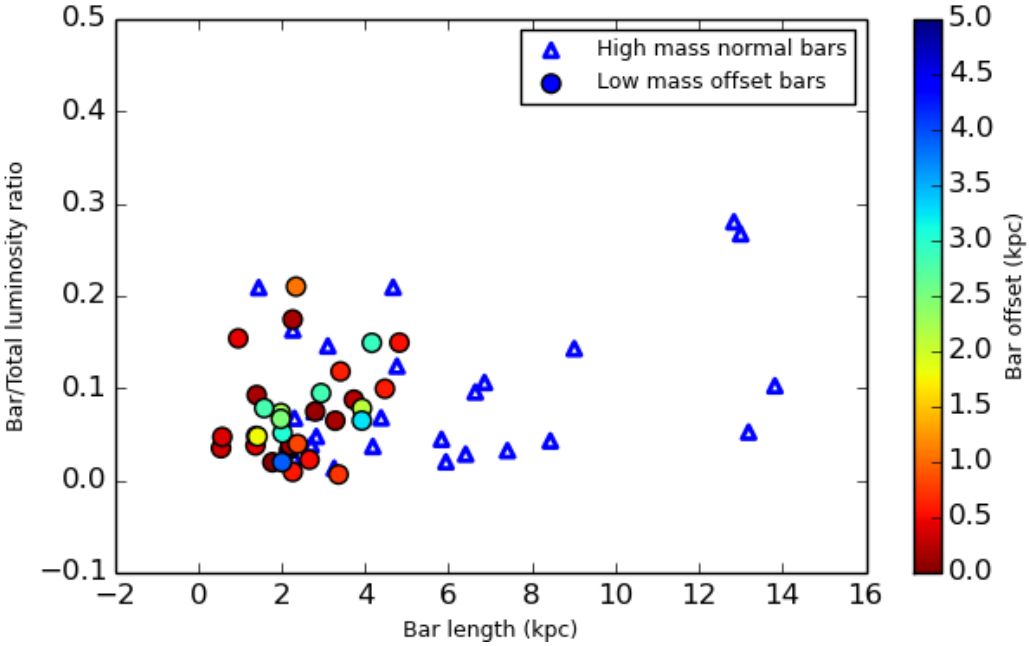

Figure 4.6: *Comparison between low mass offset bars and high mass normal barred galaxies. The low mass offset are represented by color coded circles and the high mass normal in blue triangles. The offset sample present a double slope which decreases for low bars length and increases as the bars become longer. The low mass normals are completely scattered*

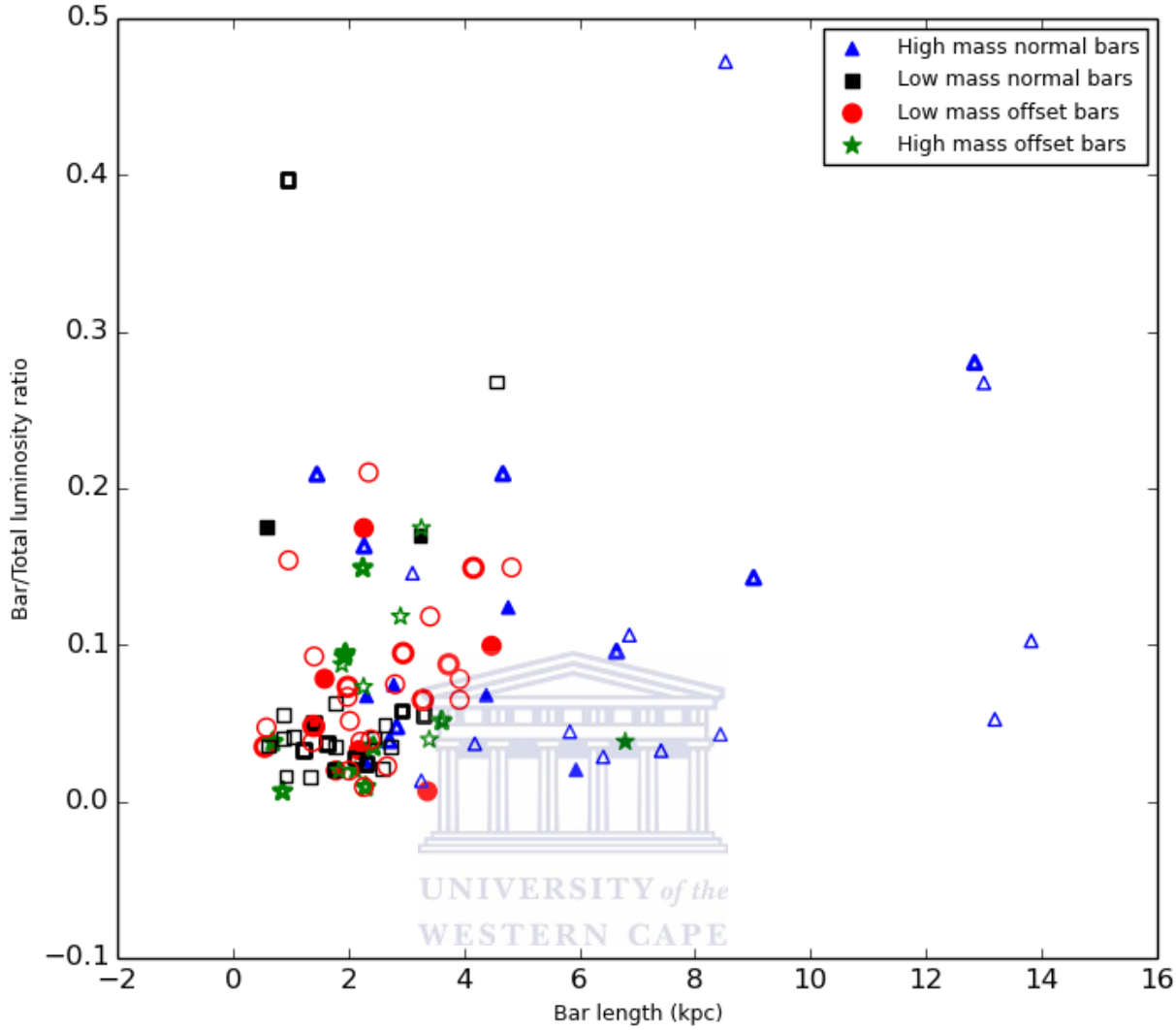

Figure 4.7: *Comparison of all the samples. Low mass offset, low mass normal, high mass offset and high mass normal barred galaxies are respectively represented by red circles, black squares, green stars and blue triangles. Inside each sample, the filled data points represent the early types, the thick and thin respectively for intermediate and late types. The high mass offset bars seem to be scattered, thus do not follow the same trend than the low mass offset. The average Bar/T of low mass normals, offsets and high mass normals are respectively 7 %, 7.4 % and 11 %.*

photometric center was confirmed by GALFIT fitting in addition to the visual inspection. Indeed GALFIT has the ability to locate the center of the different substructures of the galaxies.

Using GALFIT we measure the Bar to Total luminosity for the offset and normal bar populations. The Bar/T varies from 0.65 % to 21 % for the low mass (logM 8.5-9.8) offset barred galaxies. The average Bar/T value for the low mass offset bars is 7.4 %. In comparison, the Bar/T varies from 1.6 % to 40% for the low mass normal barred galaxies. But the majority of the low mass barred spirals have a Bar/T $<$ 10 %. The average Bar/T for low mass normal bars is 7% similar to the value of 7.4 % for the low mass offset bar population.The average bar length of the low mass normals is lower with the value 1.9 kpc against 2.5 kpc for the low mass offsets. High mass normal barred galaxies

have been selected from S^4G using the same criteria than low mass normals. We have also compared our high mass (blue triangles) with the low mass offset (coloured circles) in the same way than the previous comparison. Indeed by comparing our high mass normal (majority early types) and the low mass (mostly late types) offset barred galaxies, we expect to find clues that will make us have a better understanding of those odd offset feature mostly found in Magellanic systems. Are they the early stage of bars formation or something completely different?
Both low mass offset and high mass normal samples are represented in Figure 4.6. While the offset sample spreads almost uniformly from $\log_{10}M_*/M_\odot >= 8.5$ to 10, the high mass normals are concentrated between 10.5 and 11. The high mass normals galaxies are distributed from bar length = 0.55 to 14 kpc with an average value of 6.11 kpc. More than half of the normal bars have a length greater 5.3 kpc. Overall, the average bar contribution to the total light in the galaxy is about 7.4 % for the offset bars, 7 % for the low mass normal and an higher value of 11 % in the high mass normal sample.

Although the two distributions are different, low mass offset and normal bars have almost the same average contribution to the total light of their host galaxy. The average bar length for low mass offsets is almost half kpc higher than the low mass normal. This might indicate an increase of the star formation rate caused by the process responsible of the offset in the bar region but also in the disk so that the excess of luminosity in the bar is balance out by the disk.

4.3 Luminosity Ratio and Disk Scale-length

The disk scale-length (d_{scl}) is defined as the length at which the light of the galaxy decrease by a factor of e^1. d_{scl} is one of the best parameter used to quantify the light distribution within the disk. It's quantifies the evolution state of the disk. Early type galaxies have in general flatter disk (large d_{scl}) comparing to late types. We study the Bar/T vs the disk scale length to see if there is any connection between the bar and the disk strength over time.

4.3.1 Offset barred galaxies sample

The study of the offset bars in the bar/total luminosity ratio - disk scale-length plane shows a scatter of d_{scl} around 2.6 kpc (Figure 4.8a). The disk scale-length spread in a wide range from 0.87 up to 4.81 kpc. Overall, the Bar/T present a tentative increase relative to the disk scale-length. The large spread does not allow any conclusive statement. The study of only low mass offset reveals once again a double slop as seen in the previous section. The Bar/T decreases for lower disk scale-length up to d_{scl} = 2.6 kpc and increases (Figure 4.8b)

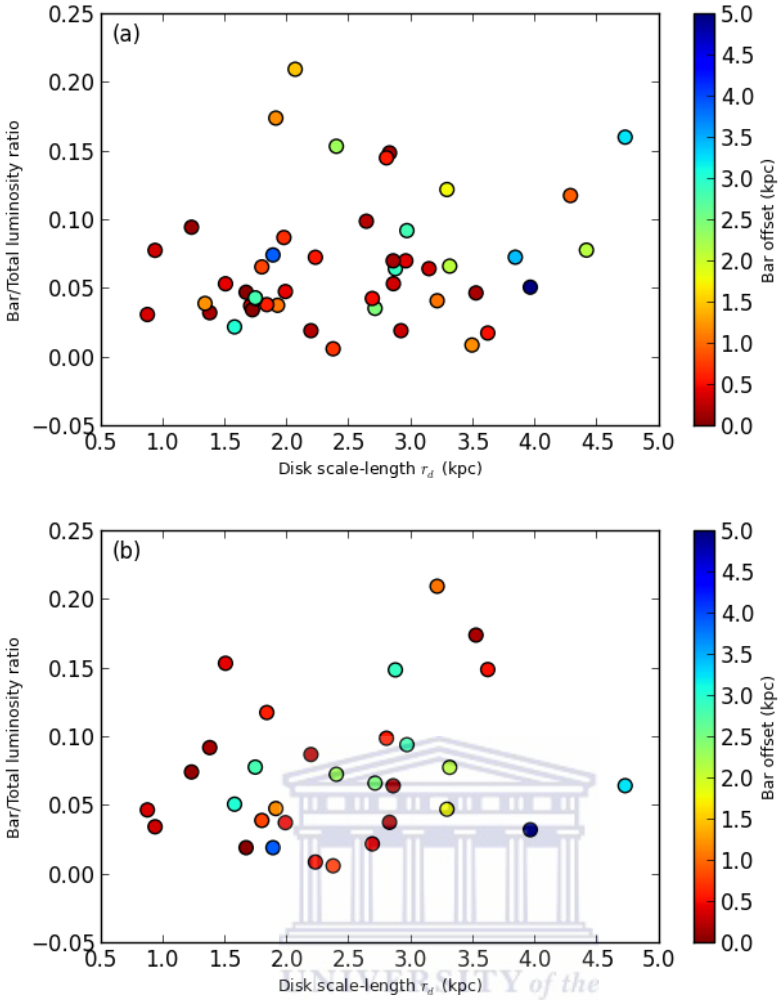

Figure 4.8: *The bar length against the disk scale-length. The data points are color coded as a function of the bar offset distance from the galaxy photometric center. -(Top): Total offset barred galaxies sample. Just a tentative increase. the data points are mostly scattered. -(Bottom): offset barred galaxies reduced to Magellanic system mass range. in the reduced sample one can see a double slop showing a decrease of Bar/T for low d_{scl} followed by an increase as the disk becomes stronger.*

4.3.2 Comparison between offsets and normals Luminosity Ratio - Disk Scale-length

Next we plotted the Bar/T luminosity ratio versus disk scale-length. We found that low mass offsets barred galaxies have higher disk scale-length compared to low mass normals barred galaxies with respective averages values 2.47 kpc and 2.02 kpc (Figure 4.9). While the offset sample seems to have an anti-correlation for low d_{scl} and a correlation for high d_{scl}, the normal sample displays no obvious relationship between Bar/T and d_{scl}, but gives a weak anti-correlation (correlation coeff = -0.39). This can be due to the fact that in the normal bar the disk becomes stronger faster than the bar, while in the case of offset bars, somehow the bar increases it amount of light much faster than the disk.
The disk scale-length and Bar/T are presented in Figure 4.10. The high mass normals barred galaxies show a slightly higher disk scale-length (mean disk scale-length ≈ 2.87) than the offsets barred galaxies (mean disc scale-length ≈ 2.47 kpc). The main feature is that the Bar/T for high normal barred galaxies decreases with the disc scale-length (correlation coefficient ≈ -0.56) while it as a double slope

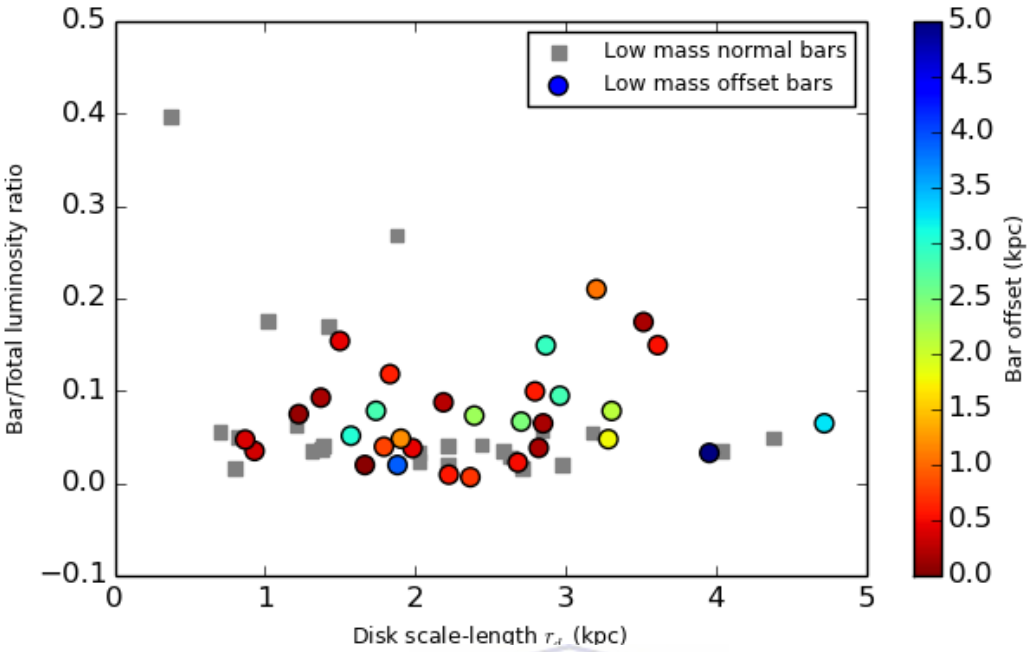

Figure 4.9: *The ratio bar luminosity/total luminosity against the disk scale-length. Comparison between low mass offset and low mass normal barred galaxies. The low mass offset are represented by color coded circles and the low mass normal in gray squares*

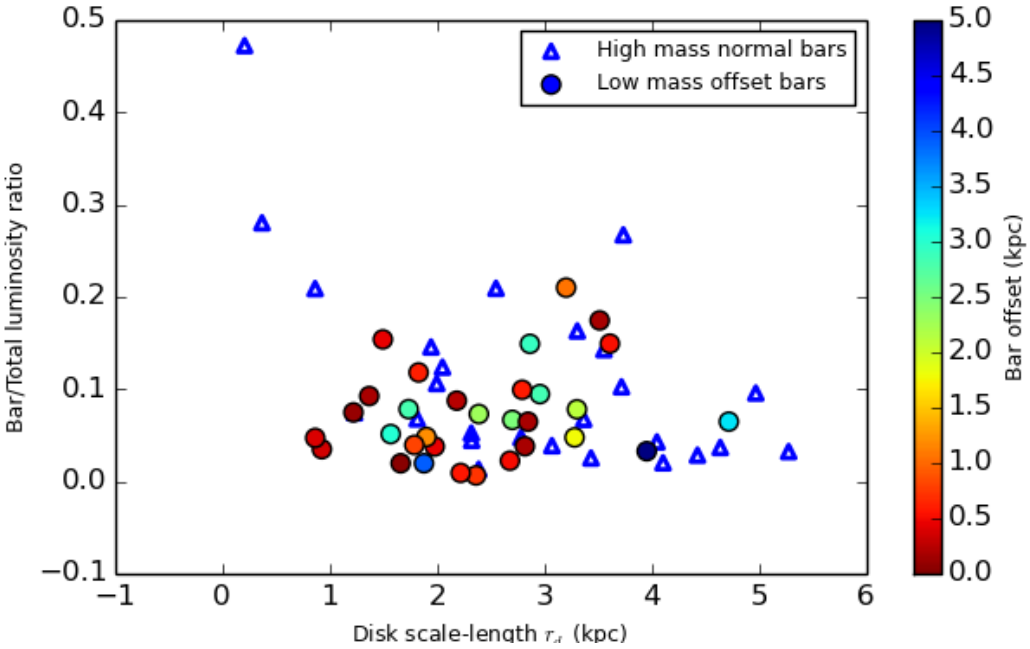

Figure 4.10: *Comparison between low mass offset and high mass normal barred galaxies. The low mass offset are represented by color coded circles and the high mass normal in blue triangles.*

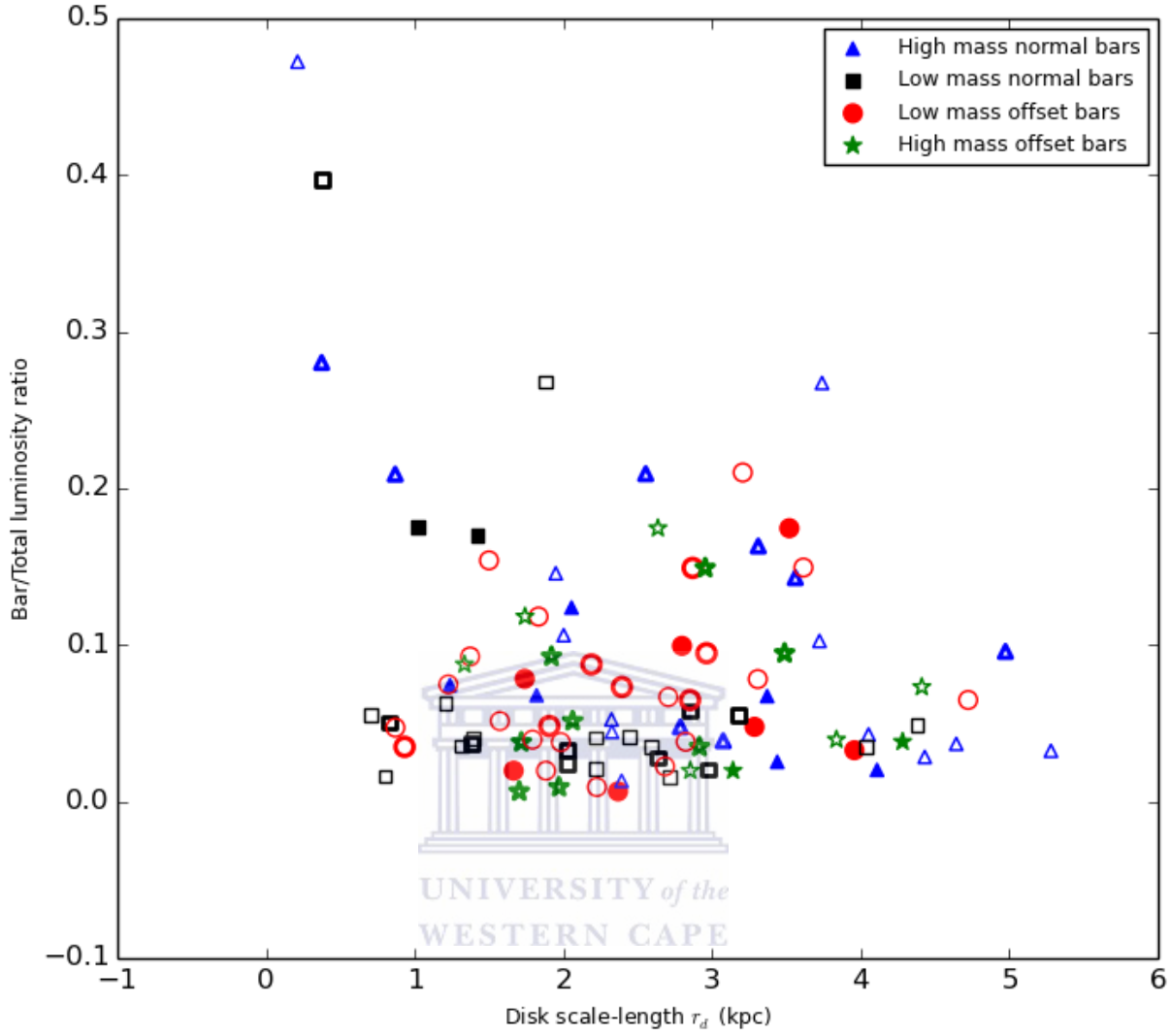

Figure 4.11: *Comparison all the samples. Low mass offset, low mass normal, high mass offset and high mass normal barred galaxies are respectively represented by red circles, black squares, green stars and blue triangles. Inside each sample, the filled data points represent the early types, the thick and thin respectively for intermediate and late types.*

in the low mass offset sample.

4.4 Relationship between l_{bar} - Disk scale-length

The disk scale-length has previously defined as been compared to the bar length in this section

4.4.1 Offset barred galaxies sample

The evolution of the bar length seems to have a moderate correlation with the disk scale-length (Figure 4.12a) resulting in a linear Pearson correlation coefficient of R = 0.56 (p-value = 0.00004). The dark line is the best fit between d_{scl} and l_{bar}. It can be represent by the following equation :

$$l_{\rm bar} = 0.74 \times d_{\rm scl} + 0.63 \tag{4.1}$$

In Figure 4.12b we have a sensibly stronger correlation between the bar length and the disk scale-length. The slope of a simple linear fit to the data is steeper for the low mass offset barred galaxies than the total offset sample but it likely not very significant. We find that as disk grow, bars grow and the behavior seems similar in both samples (Figure 4.12).

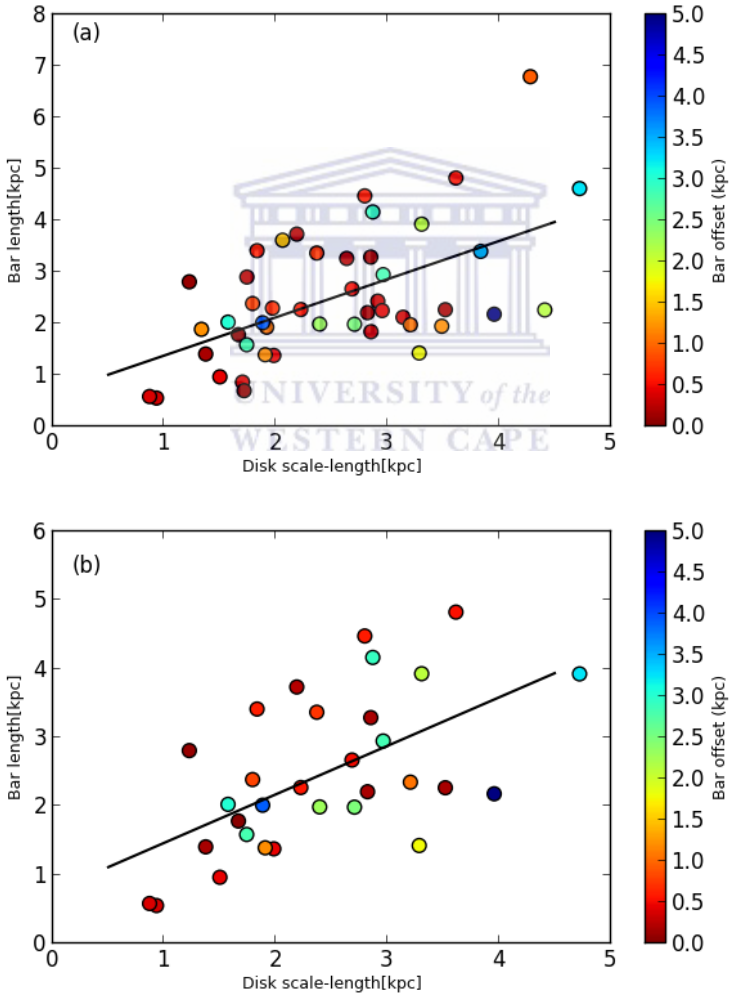

Figure 4.12: *The bar length against the disk scale-length. The data points are color coded as a function of the bar offset distance from the galaxy photometric center.The dark line is the best fit between d_{scl} and l_{bar}. -(Top): Total offset barred galaxies sample. One can see a correlation between the bar length and the disk scale-length such that the bar becomes longer with the increase of the d˙scl.-(Bottom): Offset barred galaxies reduced to Magellanic system mass range.* The correlation is tighter for the low mass offset.

4.4.2 Comparison between offset and normals l_{bar} - Disk scale-length

Next, we investigate the evolution of the bars as the disk scale-length increases. Figure 4.13 shows the

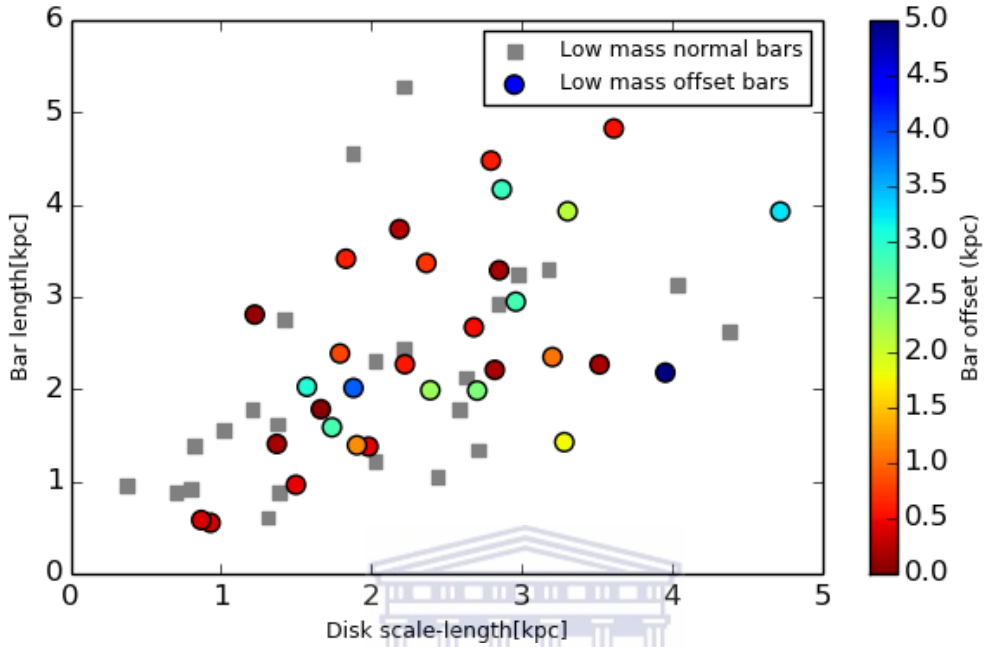

Figure 4.13: *The bar length against the disk scale-length. Comparison between low mass offset and low mass normal barred galaxies. The low mass offset are represented by color coded circles and the low mass normal in gray squares.*

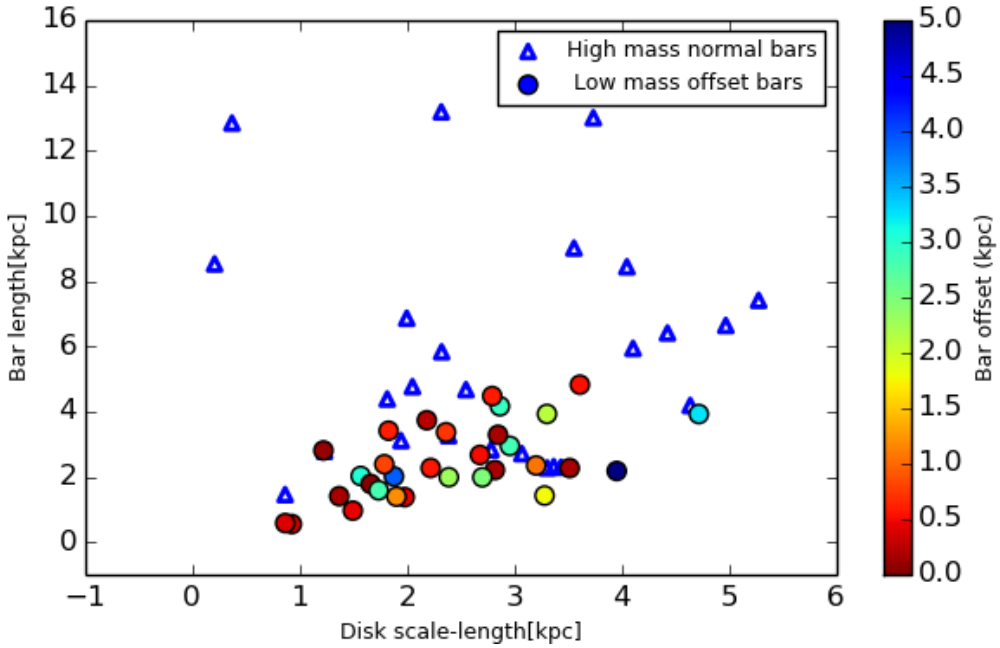

Figure 4.14: *Comparison between low mass offset and high mass normal barred galaxies. The low mass offset are represented by color coded circles and the high mass normal in blue triangles. Low mass offset and normal show a correlation between d_{scl} and l_{bar} while the high mass normal present no relationship between the two parameters.*

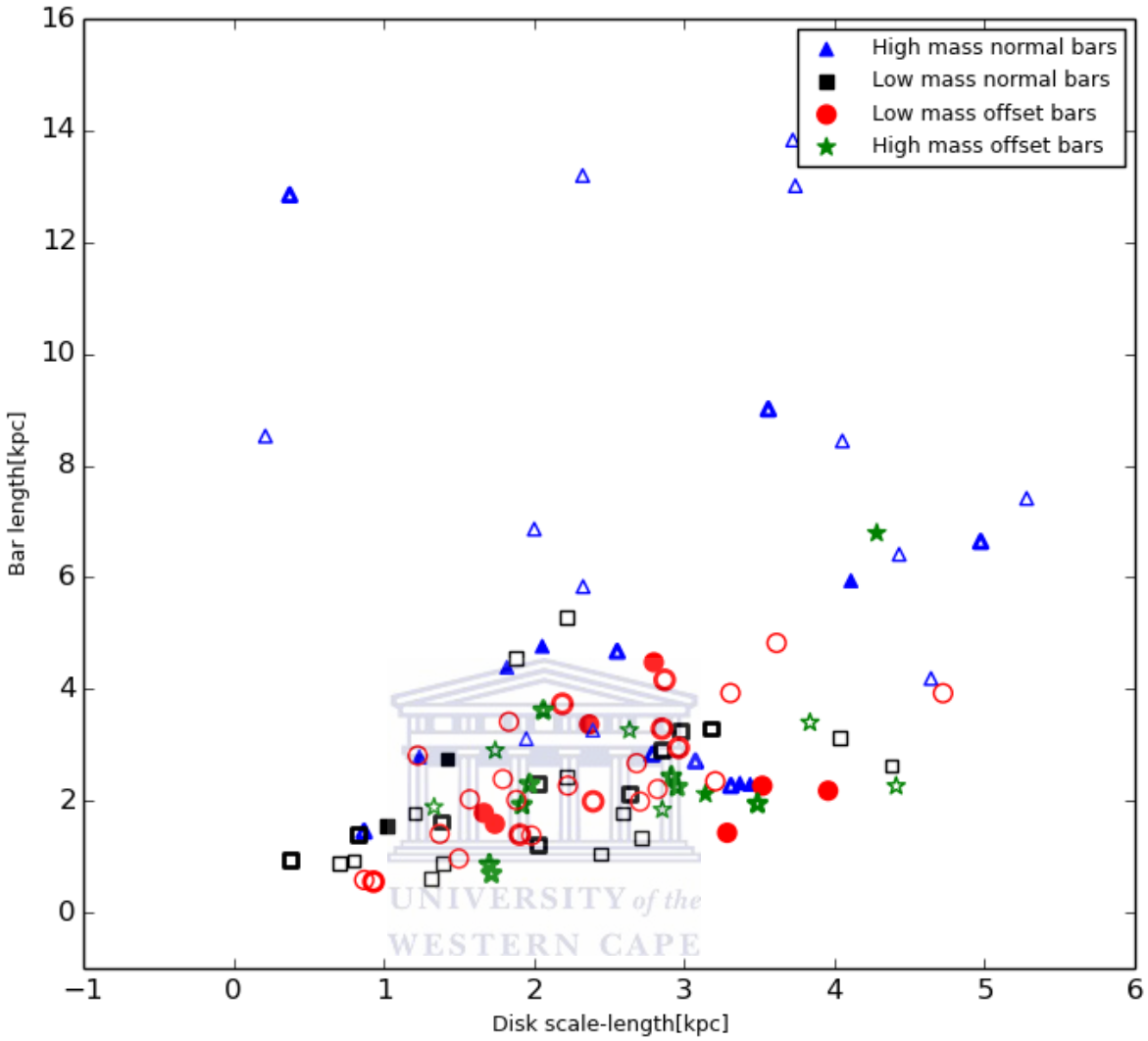

Figure 4.15: *Comparison all the samples. Low mass offset, low mass normal, high mass offset and high mass normal barred galaxies are respectively represented by red circles, black squares, green stars and blue triangles. Inside each sample, the filled data points represent the early types, the thick and thin respectively for intermediate and late types.*

bar length versus the disk scale-length for the two samples of low mass offset and low mass normal barred galaxies. As in the previous cases, the low mass offset barred are represented by colored circles and the low mass normal, by gray squares. The bar length increases as the disk light distribution becomes flatter but the correlation between the disk scale-length and the bar length is stronger for the low mass offsets than the low mass normals (the respective correlation coefficient are 0.68 and 0.5). In Figure 4.14 we have no visible relationship between the bar length and the disc scale-length for high mass normal barred galaxies but the low mass offsets l_{bar} increase with the disc scale-length (See Figure 4.12b).

In our investigations we found an increase of the d_{scl} as the bar becomes longer. But on the contrary some high mass galaxies have a very high bar length while the disk scale-length is still low. This might be caused by the bar being so strong that doesn't allow one to correctly measure the disk scale-length.

This trend was also seen by Seidel et al. (2016). They found in their analysis of 16 large barred galaxies that, in the early type sample, some of the very old bars were sitting in a young disk. This suggest that among the high mass galaxies, we might find galaxies with bars fully formed (long bar) but surrounded by disk materials which is still at the beginning of the formation process (low d_{scl}).

4.5 The variation of l_{bar}/D_{25} vs l_{bar}

The parameter D_{25} represents the length of the major axis of the galaxy at the 25 mag/arcsec^2 isophotal level, representing the diameter of the galaxy for a disk galaxy. We scale the bar length by the diameter of the host galaxy (l_{bar}/D_{25}) and investigate the variation with the bar length (l_{bar}) (see Figure 4.16).

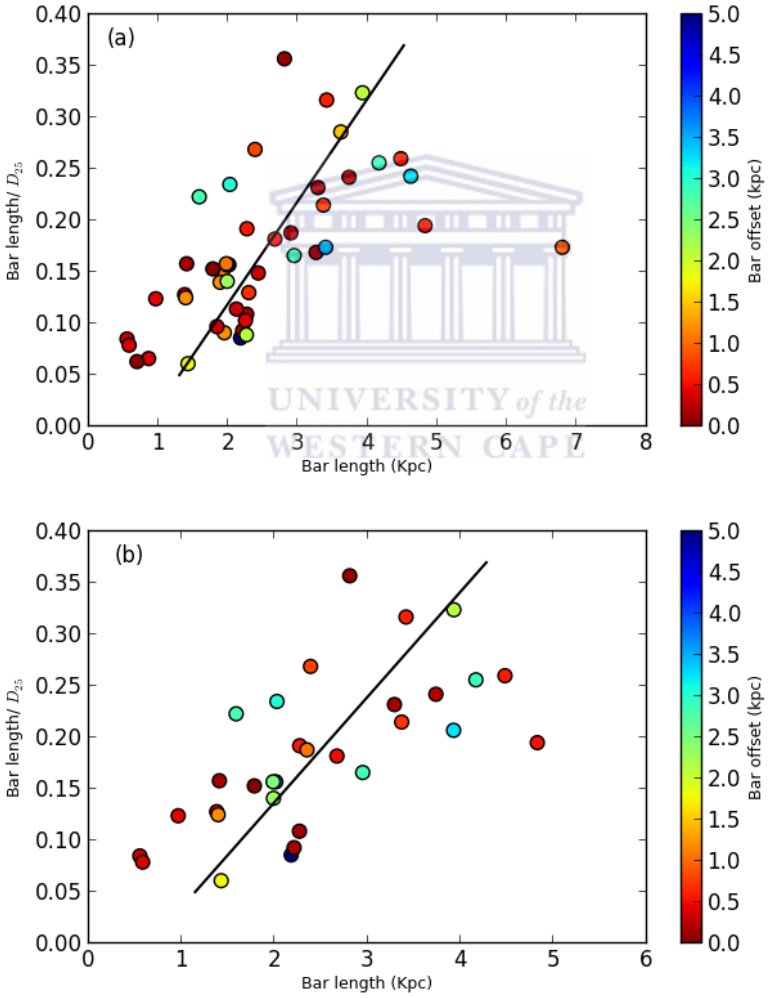

Figure 4.16: *The ratio bar length/D_{25} against the bar length. The data points are color coded as a function of the bar offset distance from the galaxy photometric center. -(Top): Total offset barred galaxies sample. -(Bottom): offset barred galaxies reduced to Magellanic system mass range. The black straight line in both sample represent the best fit. One can see a strong correlation between the ratio bar length/D_{25} and the bar length.*

4.5.1 Offset barred galaxies sample

The bar length gradient correlates with l_{bar}/D_{25} such that longer bars have higher l_{bar}/D_{25} (Figure 4.16a). Only one galaxy is really out of the general trend. This galaxy happens to be NGC3627 which is the galaxy presenting the longest bar in our total offset sample. It has also very strong spirals arms and a prominent bar (see picture in Appendix A). The linear Pearson correlation is R = 0.61 and p-value = 8.10^{-6}. We have a larger scatter as l_{bar}/D_{25} increases. The black straight line representing the best fit is defined as :

$$l_{bar} = 10.05 \times l_{bar}/D_{25} + 0.8 \tag{4.2}$$

The low mass offsets show a slightly higher correlation between l_{bar}/D_{25} and l_{bar} (due to the position of NGC3627 out of the general trend in the full sample of offset bars). The correlation coeff = 0.66 and P = 5.10^{-5} (Figure 4.16b).

4.5.2 Comparison between offsets and normals l_{bar}/D_{25}- l_{bar}

The average value for the bar length/D_{25} in both low mass offset and normal seems to be equal to 0.18 (Figure 4.17). We have the same behavior in the two samples showing a faster growth of the bar

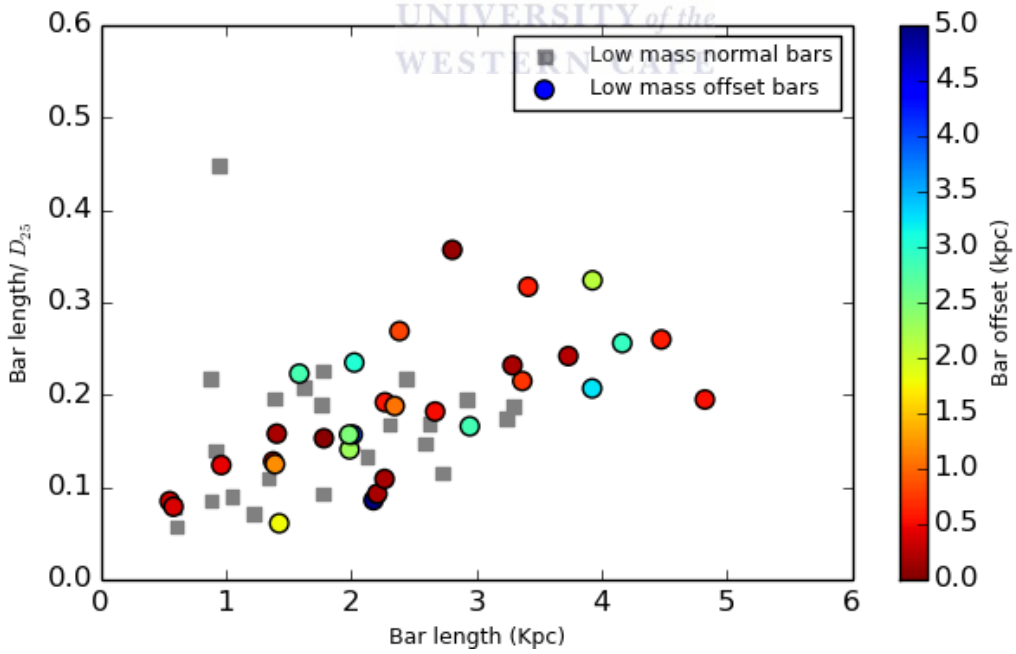

Figure 4.17: *The ratio bar length/D_{25} against the bar length.-(Top left): Comparison between low mass offset and low mass normal barred galaxies. The low mass offset are represented by color coded circles and the low mass normal in gray squares.*

length than the galaxy diameter for bars. This is shown respectively by the strong positive correlation (correlation coeff = 0.66) for the offset sample and a moderate correlation (correlation coeff = 0.49) for the normal sample. In Figure 4.18, the average bar length/D_{25} found for the low mass offsets and high

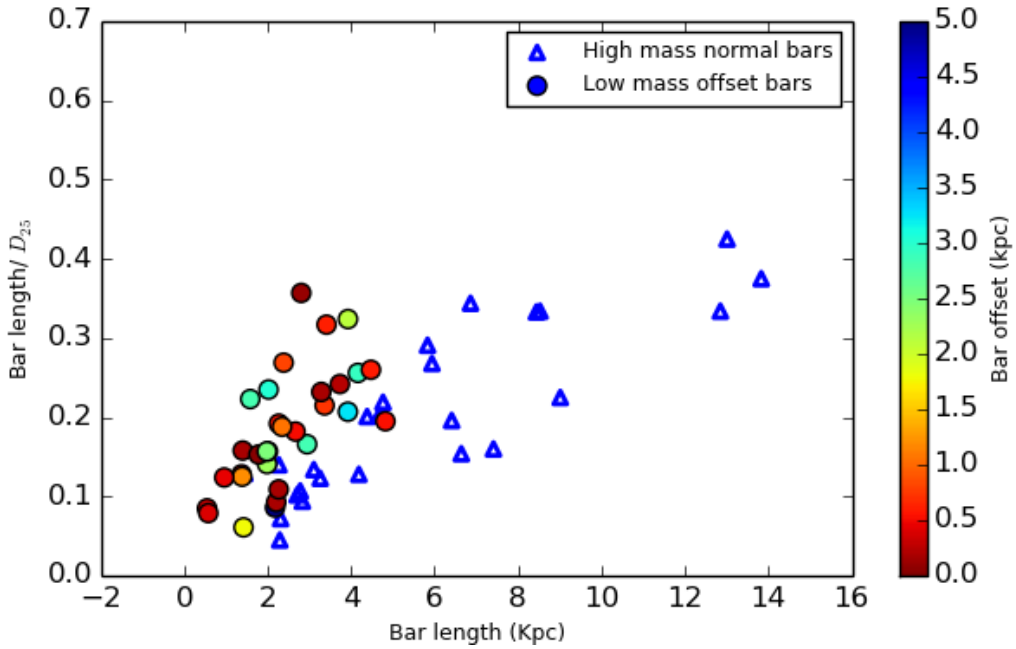

Figure 4.18: *-(Top right): Comparison between low mass offset and high mass normal barred galaxies. The low mass offset are represented by color coded circles and the high mass normal in blue triangles*

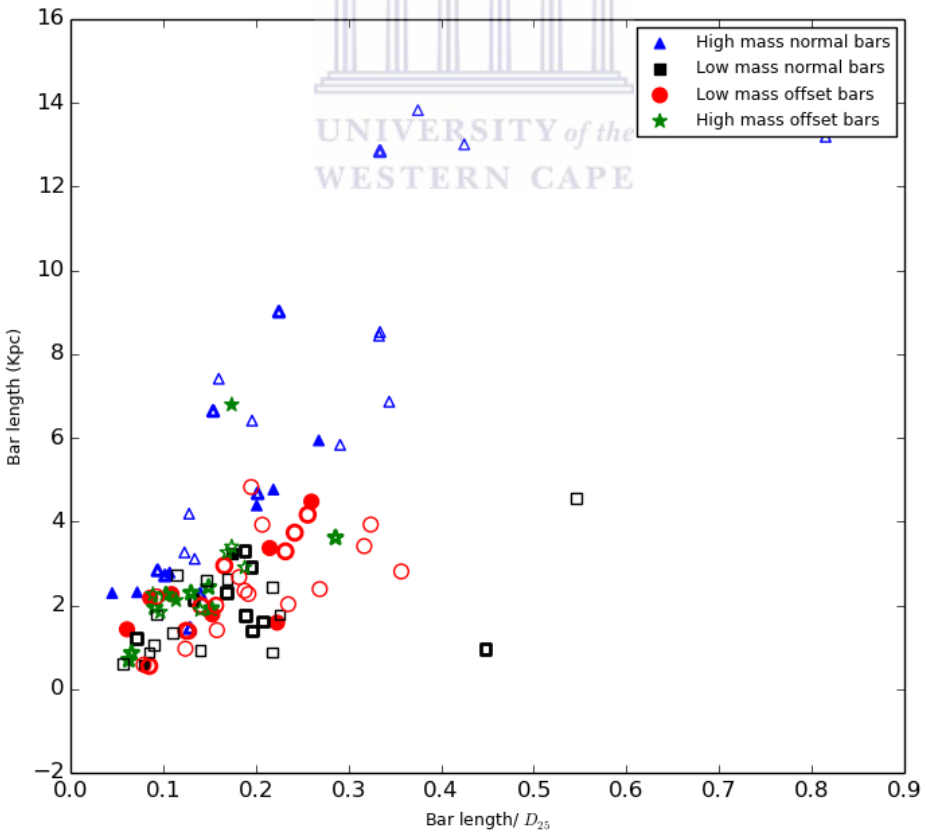

Figure 4.19: *Comparison all the samples. Low mass offset, low mass normal, high mass offset and high mass normal barred galaxies are respectively represented by red circles, black squares, green stars and blue triangles. Inside each sample, the filled data points represent the early types, the thick and thin respectively for intermediate and late types. In all the samples the bar grow as the apparent bar length expand at lower rate for high mass samples in comparison to low mass samples.*

mass normals barred galaxies are respectively 0.185 and 0.23. The high mass normals bar length/D_{25} increases as a function of the bar length at a lower rate in comparison to the low mass offsets barred galaxies. In conclusion, as the bar length increases, the apparent bar length increases in all the sample but at different rate. The highest increase is found in low mass offsets sample followed by low mass normal, high mass offset and high mass normal barred galaxies (see Figure 4.19). This is expected for normal bars, since some very big barred galaxies have their bar extending across their full diameter. It is also known that as the galaxy grows and becomes older, the bar growth slow down when the reserve of gas within the galaxy is exhausted (Athanassoula 2013). But given the off-centered position of offset bars, having such a big bar will perturb the rotation since the mass won't be symmetrically distributed around the dynamical center of the galaxy. The fact that we did not have very high mass off-centered barred galaxy might be a clue to that effect.

4.6 Relationship between Bar length and Ellipticity

The ellipticity (ell) has been defined as 1 - r_a/r_b, r_a and r_b are respectively the minor and the major

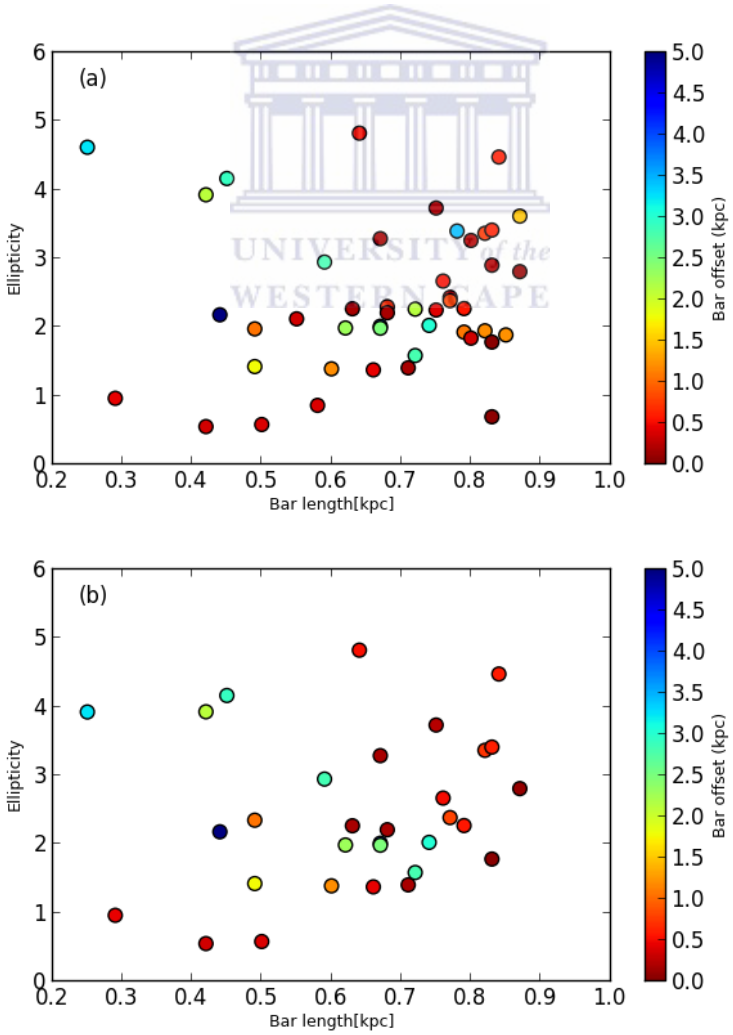

Figure 4.20: *The bar length against the ellipticity. The data points are color coded as a function of the bar offset distance from the galaxy photometric center. -(Top): Total offset barred galaxies sample. -(Bottom): offset barred galaxies reduced to Magellanic system mass range*

axises of the bar.

4.6.1 Offset barred galaxies sample

The mean value of the ellipticity in the total offset sample = 0.67. We observe slightly higher ellipticities with increasing bars length. The highly offset bars (offset > 2 kpc) have a wide range of ellipticity from 0.25 up to 0.75 but ellipticities greater than 0.75 are exclusively dominated by the presence of low offset (offset < 2 kpc) (Figure 4.20a). 5 galaxies from the top highest bar length are separated from the rest of the sample but still show the same increasing trend. More than half of the galaxies have bars with ellipticities greater than 0.7.
Like the total offset bar sample, the sub-sample shows the majority of galaxies having ellipticity > 0.6, with the average ellipticity value ≈ 0.63 (see Figure 4.20b).

4.6.2 Comparison between offsets and normals Bar length - Ellipticity

In average the low mass normals bars seems to be more elliptical than the offset bars (Figure 4.21). The mean ellipticity ≈ 0.7 for normals and 0.6 for offsets bars. Both low mass normals and offsets ellipticities increase with the bars length. We have the same correlation coefficient of R = 0.5 with p-value ≈ 0.01

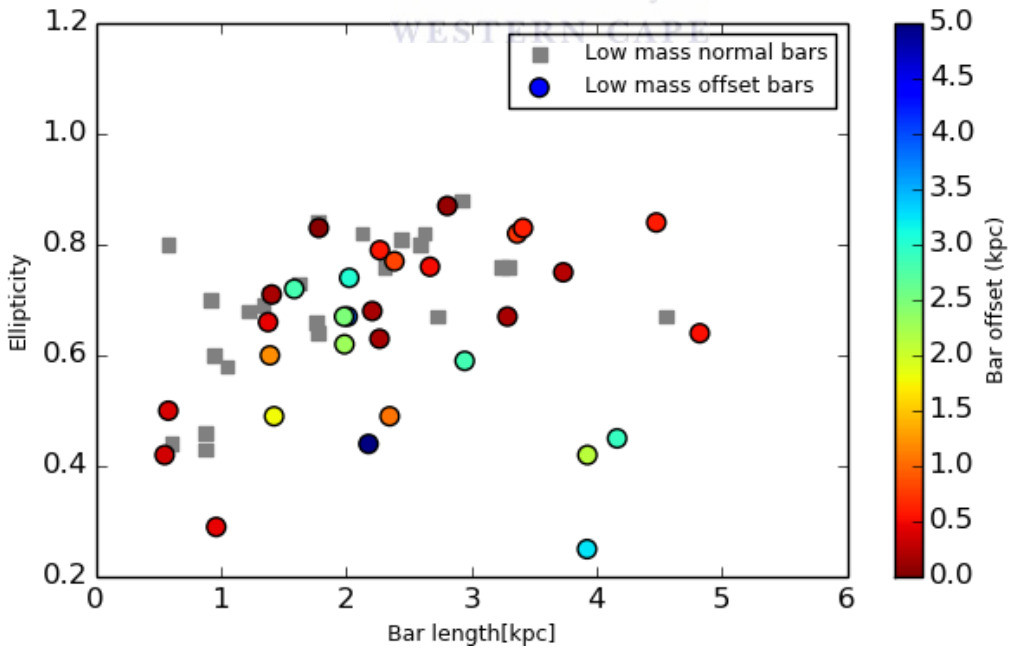

Figure 4.21: *The bar length against the ellipticity. Comparison between low mass offset and low mass normal barred galaxies. The low mass offset are represented by color coded circles and the low mass normal in gray squares.*

In Figure 4.22 the ellipticity of the bar his plotted versus the bar length for the two samples. The normals bars have an average ellipticity a bit higher (mean ellipticity ≈ 0.7) than the offset bars

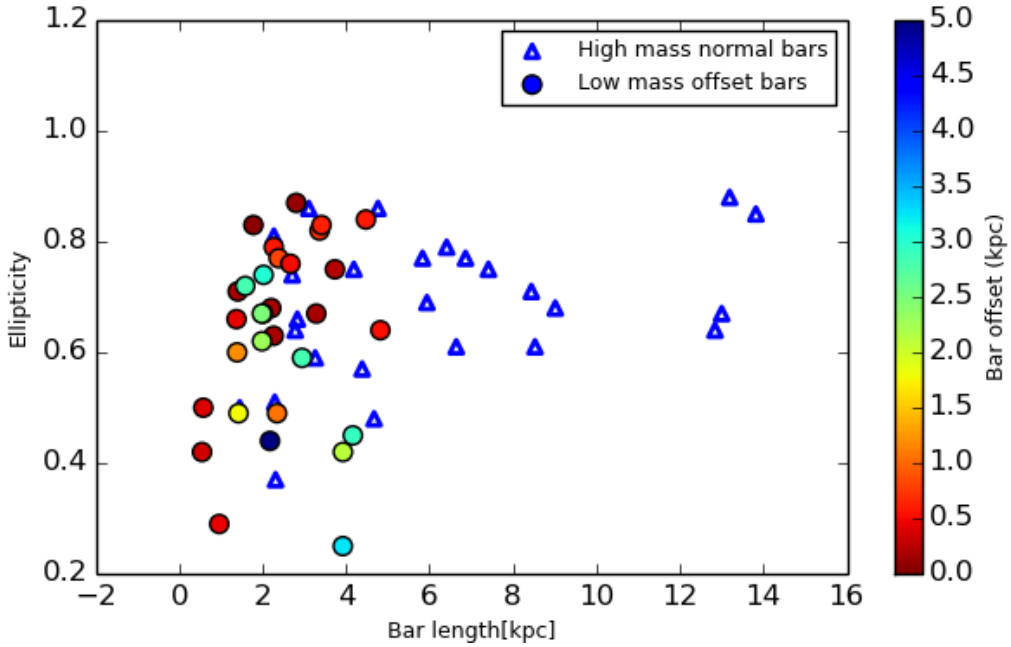

Figure 4.22: *Comparison between low mass offset and high mass normal barred galaxies. The low mass offset are represented by color coded circles and the high mass normal in blue triangles.*

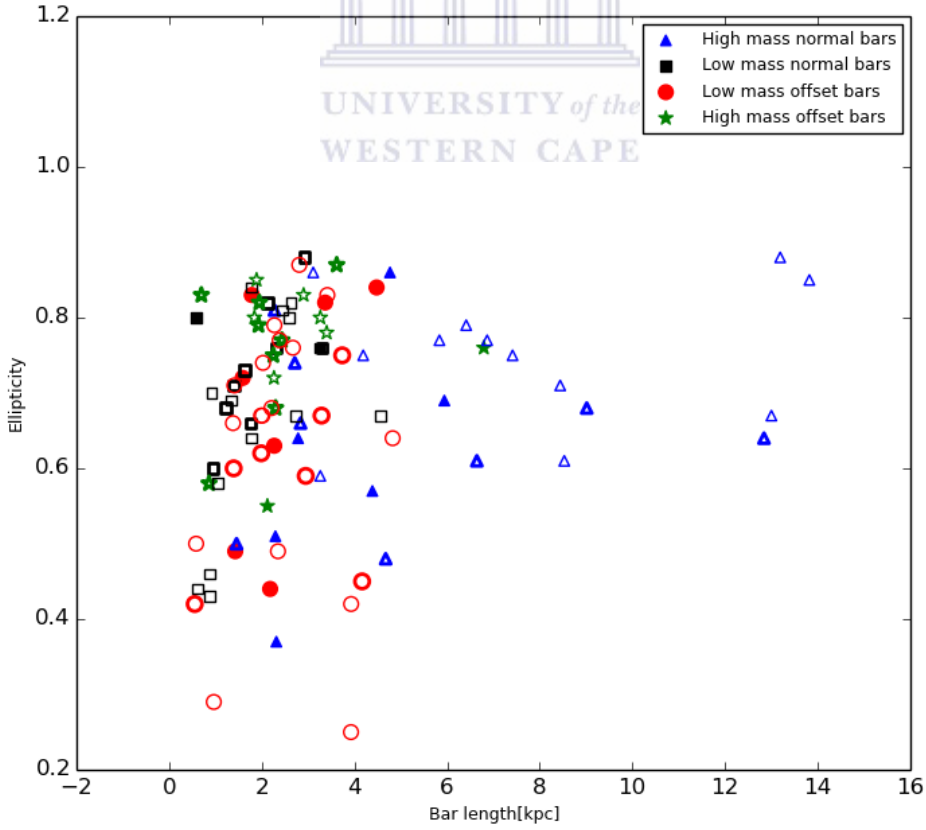

Figure 4.23: *Comparison all the samples. Low mass offset, low mass normal, high mass offset and high mass normal barred galaxies are respectively represented by red circles, black squares, green stars and blue triangles. Inside each sample, the filled data points represent the early types, the thick and thin respectively for intermediate and late types.*

(mean ellipticity ≈0.6). It seems to have a slight increase of the ellipticity for both samples as the bar becomes higher for bar length between 0 and 5 kpc. From the figure this upper limit represent the maximum bar length for the offset sample. From 5 kpc to 10 kpc the bar ellipticity decreases for normals bars and rise again beyond 12 kpc. It looks like the ellipticity of bars increases as they become longer up to a certain limit ($l_{bar} = 5$ kp) and begin to decrease followed by an increase at very high bar length. Since the bar length keep increasing while the ellipticity drops down, we can suggest a process that generate a greater expansion of the bar along it minor axis than it major axis.

4.7 Pixel statistic applied to our offsets and normals barred galaxy samples

Our initial sample of mid infrared galaxies from S^4G consists of 2352 nearby galaxies. In order to establish our catalog of nearby offsets barred galaxies, we inspected visually all the galaxies. We also used ellipse fit to identify the barred galaxies as we explained in chapter 3 section 1. But the presence of spirals arms in the bar region lead to imprecisions that require visual inspection before the final classification. GALFIT fitting, more than the decomposition of the galaxy image into it different substructures help to identify offsets barred galaxies. Indeed GALFIT is a 2 dimensional algorithm that can model the bulge, the bar, the disk, the spirals arms etc. but also find the position of their centers in the image in such a way we are able to identify offset structures after the fitting process. The problem is that running GALFIT is time consuming (sometimes more than ten runs with each run taking in average between 5 and 20 min to get the best fit !). With next generation more powerful telescopes, allowing to have larger samples of mid infrared data extending in a wider range of redshift, the need of automatic identification will be more than important.
In the following section, we applied the Gini Coefficient and the second order moment (M_{20}) method to those peculiar galaxies.

- Gini Coefficient

The Gini coefficient is a statistical method used to measure the inequity among values of a frequency distribution. For perfect inequality the Gini coefficient is equal to 0 and 1 for 100 % inequality for example (ex: a case where in a group, only one person has the whole wealth and the other have nothing) The Gini coefficient is also used in the study of galaxies to investigate whether the light is smoothly distributed or concentrated in few pixels (see Abraham et al. 2003). It is the ratio between the Lorenz curve (Lorenz 1905) and the curve of uniform equality (G/ $\frac{1}{2}$ square box in Figure 4.24). The Gini coefficient is based on Lorenz curve presented as follows:

$$L(p) = \frac{1}{\overline{X}} \int_0^p F^{-1}(u)du \tag{4.3}$$

In the case of galaxy studies, p is the percentage of the faintest pixels, F(x) is the cumulative distribution function and $\overline{X}$ is the mean of all pixels values.

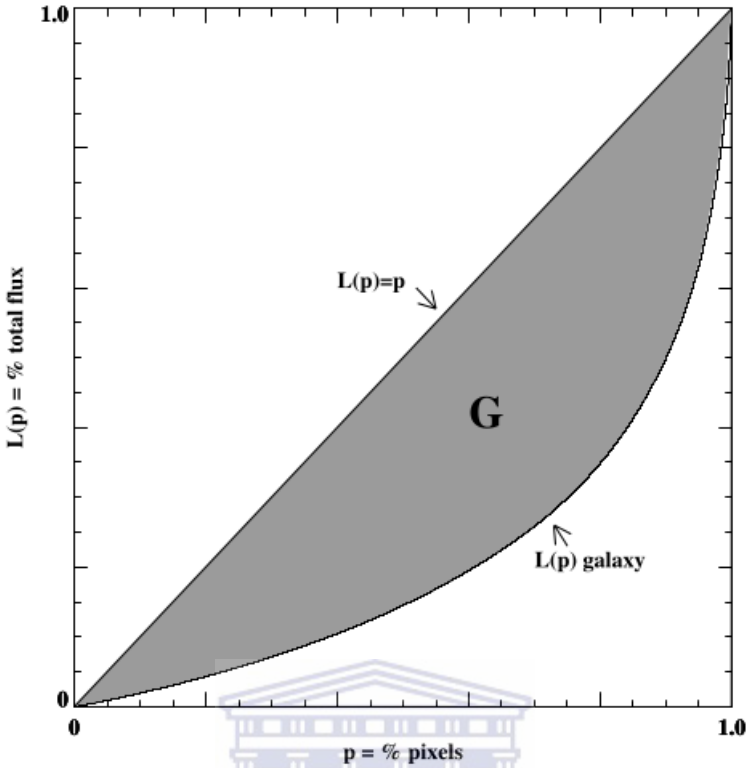

Figure 4.24: *Lorenz curve: the Gini coefficient is the area between the Lorenz curve of the galaxy's pixels and that of equitable distribution (shaded region). The given curve is for S0 NGC 4526,G = 059. (Lotz et al. 2004)*

$$G = \frac{1}{2\overline{X}n(n-1)} \sum_{i=1}^{n} \sum_{j=1}^{n} |X_i - X_j| \tag{4.4}$$

Where n is the total number of pixels and X denotes the mean brightness

- Second moment of brightness distribution

The second-order moment (M) is the sum over the brightness weighted by the distance to the center (d_i) square. It traces the spacial distribution of bright nuclei, bars, spiral arms and star clusters etc. (Lotz et al. 2004).

$$M_{tot} = \sum_{i=1}^{n} M_i = \sum_{i=1}^{n} X_i d_i^2 = \sum_{i=1}^{n} X_i[(x_i - x_0)^2 + (y_i - y_0)^2] \tag{4.5}$$

Where (d_i) is the distance the photometric center, (x_0) and (y_0) are the coordinate of the photometric center.

M_{20} is the normalized second order moment that takes into account the brightest pixels which contribute together to 20% of the galaxies flux. The normalization is done in order to avoid the dependence on the total galaxy flux and size.

$$M_{20} = log_{10}\left(\frac{\sum_{20\%} M_i}{M_{tot}}\right) \tag{4.6}$$

The high star formation rate in the spiral arm and clusters of stars in the galaxy disk can highly affect M_{20} such that in some rare cases, even a strong normal bar can have higher M_{20} than a low mass offset counterpart and vice versa. Indeed the further outermost layers in both samples (enclosed by red circles in Figure 4.25) are respectively IC0800 and NGC1055 in the normal and NGC4189 in the offset sample. The mid infrared image from S^4G reveals through DS9, either high star formation in the spiral arms or star clusters in the the disk of all the aforementioned galaxies.
In Figure 4.25 the filled thick empty and thin empty circles are, respectively, early, intermediate and late type galaxies in the offsets sample and likewise, filled, thick empty and thin empty triangles represent, respectively, early, intermediate in and late type normals galaxies. The furthermost outer layers are marked with red circles. Although the early and late type are mixed in both samples, almost all the outer layers in the normal sample are late types. The overall shape shows a tight correlation between M_{20} and G for all the galaxies. The offset barred galaxies are preferably located at low G and high M_{20} while normal galaxies have higher G and lower M_{20}. The graph shows the ability to separate the two sample with quite a good efficiency using G and M_{20}.

The most challenging part is the ability to disentangle the low mass offset and low mass normal galaxies. Indeed besides the offset of the bars, the two samples have the same properties. They share the same morphological distribution with a predominance of late type galaxies (see Figure 4.26) and the same mass range ($8.5 < \log_{10}M_*/M_\odot < 9.8$). We can nevertheless see an accumulation of offset barred galaxies between M_{20} ranging from -1.1 to -1.4 when the low mass normal barred galaxies span a wider range from -0.8 to -1.8. The low mass normal sample seems to be separated into two sub samples. One for M_{20} between -0.8 and -1.1 and the second for M_{20} starting from -1.4 to -1.8. Interestingly, the concentration zone of offset barred is almost deprived of low mass normal barred galaxies. The two samples are globally confined between G values of 0.1 and 0.4. only two galaxies are above the upper limit. Attempting to separate the two samples without ambiguity, using G and M_{20} will require an adaptation of M_{20} in such a way it takes more into account the offset of the bar than star forming regions and star clusters will make it a powerful tool to identify offset structures. One attempt will be to do a selective weight during the determination of M_{20}. In the determination of second order moment, the pixel value is multiply by the distance square to the photometric center, looking for compact groups of stars (bar-like) and giving them more weight can enhance significantly M_{20} value for offsets Structures (due to their greater distance to the center) in comparison to normals and allow a clearer separation of the two samples.

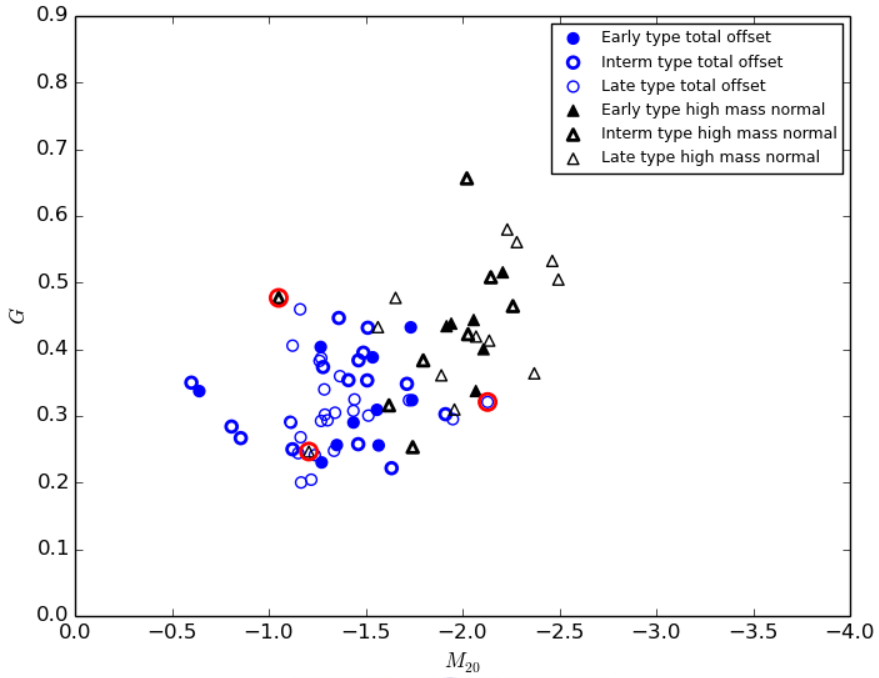

Figure 4.25: *Graph showing low mass offsets and high mass normals barred galaxies in G-M20 plane. The filled, thick empty and thin empty circles are respectively early, intermediate and late type barred galaxies in the offset sample. Likewise the filled, thick empty and thin empty triangles represent respectively early, intermediate and late type normals barred galaxies. The furthermost out layers are marked with red circles*

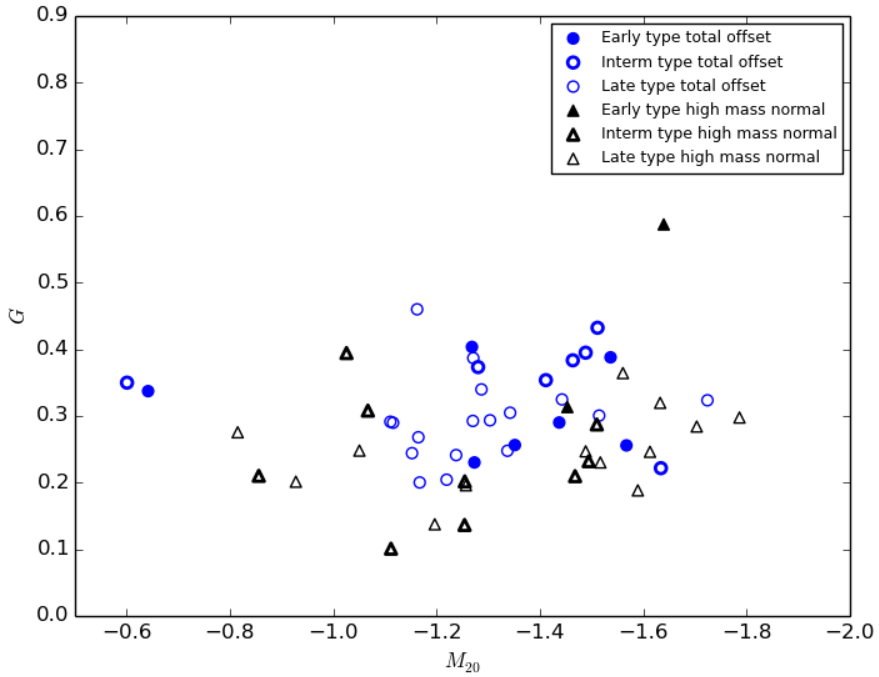

Figure 4.26: *Plot of the low mass offsets barred galaxies and low mass normals barred galaxies in G-M20 plane. The markers have the same representation than the previous figure.*

Chapter 5

Conclusion and outlook

In the Early Universe, galaxies evolution was likely dominated by mergers, but with its expansion, the rate of mergers decreases and the evolution of galaxies changes from being merger-driven to a more internally driven mechanism. The latest process was introduced by Kormendy (1979) as secular evolution. Bars are found to be one of the most important structures leading this secular evolution process within their host galaxy. Bars are present in more than 2/3 of the visible galaxies (de Vaucouleurs 1963). Simulations have shown them as a rigid and straight structures located at the center of some galaxies and their centered position is thought to stabilise the host galaxy in terms of their kinematics.

Some bars are, however, offset and seems to predominantly exhibit in low mass galaxies. Interaction between galaxies shouldn't be the only cause, since some of those offset structures like NGC3906 are completely isolated and show no visible sign of past or ongoing interaction (De Swardt et al. 2015). This was one of the motivations of the present project. The global aim is to investigate those offset structures and establish whether their offset is caused by bars in earlier stage formation process or induced by interaction, but by an unseen companion, namely a dark matter sub-halo. We expect a deeper understanding of their role in a broader picture of galaxies evolution.

We identified all the offset structures in the local universe using mid infrared data from the Spizer Survey of Stellar Structure in galaxy (S^4G). We note that (S^4G) is the largest and deepest mid infrared catalogue of nearby galaxies available up to now (Sheth et al. 2010). It is a survey of nearby galaxies to a magnitude limit of 3.6 μm(AB) = 27 mag arcsec^{-2}. The mid infrared data (free from extinction) used for our work were selected to have inclination less than 65^o. The combination of PA and ellipticity profiles, provided by ellipse fit was used for bar identification and in addition double check through visual inspection. We were able to identify all the offset galaxies within (S^4G) database. We also subdivided two other samples, one made of low mass normal barred galaxies and the second, a composition of high mass normal barred galaxies (the term "normal"is used for bars located at the photometric center of their host galaxies).

The two dimensional fitting programme GALFIT was used to fit our selected galaxies which are all offset barred disk galaxies, the selected low mass normal barred and the high mass normal barred galaxies. GALFIT separates the galaxy into it different components, namely the bar, the disk the bulge etc.

In our work we adopted three fitting options: The first is the disk and bar fitting for galaxies made of only a disk and bar. The second case is a three component fit (disk1, disk2 and bar) for galaxies with a bar and a disk presenting a break (see Taehyun Kim et al. 2014). The third option is a three components fit (bulge, disk, bar) for galaxies with a bulge.
The properties of offset and normal barred galaxies have been compared to similarities and/or divergences between the two groups. Our mains finding are presented as follows:

1) We have checked all the galaxies available in (S^4G) through visual inspection and ellipse fit. A confirmation of the offset was also given by GALFIT fit. From our initial sample of 2352 galaxies, 103 where offset and only 49 were classify as offset barred disk galaxies.

2) The bar shapes were modeled using GALFIT and all the bars are boxy. Early type offset barred galaxies have a broad range of boxiness (boxiness parameter C_0 from 0.1 up to 8) while the late type are more confined (boxiness roughly between 0.1 and 2).

3) The comparison of low mass offset, low mass normal and high mass normal reveals:

- The light contribution of offset bars (7.4 %) is slightly greater than low mass normal and less than high mass normal, respectively, 7.2 % and 11 % of the total luminosity of the galaxy. It has two slops in the offset sample. It decreases with bars and disk scale-length roughly less than 2.5 kpc and increases for higher values for low mass offset while it only decreases with high mass normals.

- The bar average length in low mass offset are longer than bars in low mass normals but more than two times shorter than the high mass normal bars.

- All the bar lengths increase as the galaxies grow but low mass offset bars grow more faster than normal bars.

- The bars ellipticity increases with bar length up to a limit of 5 kpc, corresponding to an offset bar length limit and decreases for high normal barred galaxies.

- The disk scale-length is on average slightly greater than low mass normal bars and less than high mass normal bars.

4) In an an attempt to make an automatic identification of offset bars, we applied a method to quantify the relative distribution of the galaxy pixel flux values (the Gini coefficient or G) and the second order moment of the brightest 20% of the galaxy's flux (M_{20}) to our samples in a comparative way and were able to differentiate high mass normal (low values of M_{20} and high values of G) from the offset sample (high values of M_{20} and low values of G).
Nevertheless we still have outliers due to high star formation rate in the spiral arms of some galaxies which can either increase or lower M_{20}. For low mass normal and offset separation, a modification

of M_{20} is needed to take into account the position of the off-centered bar to the photometric center; this will strengthen the ability to make a clear distinction between the two samples. However the low mass offset barred appear to be found preferably between M_{20} values of -1.4 and -1.1 and low mass normal out of this range. Both samples are below G values equal to 0.4.

An extension of this work will be to study the star formation rate (SFR) in low mass offset barred galaxies and compare to the SFR in low mass normal barred galaxies. The combination of simulation and isolated offset barred galaxy's data can be used as probes for dark matter sub halos if ever they are proved to be cause of offset bars ?

Appendix A

The Catalogue

The mid infrared image, the model derived with GALFIT and the residual of all the offset disk barred galaxies in S^4G are displayed (see chapter 3 section 1 for more details). The shape parameter C_0 of all the offset bars are added to the caption.

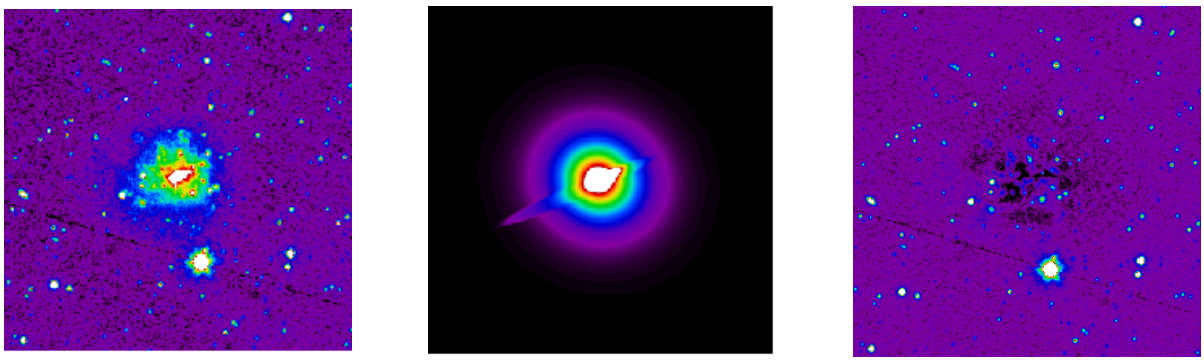

Figure A.1: ESO341-032. Left: Galaxy image, middle: The model and right: The residual. The shape parameter value is $C_0 = 6.06$.

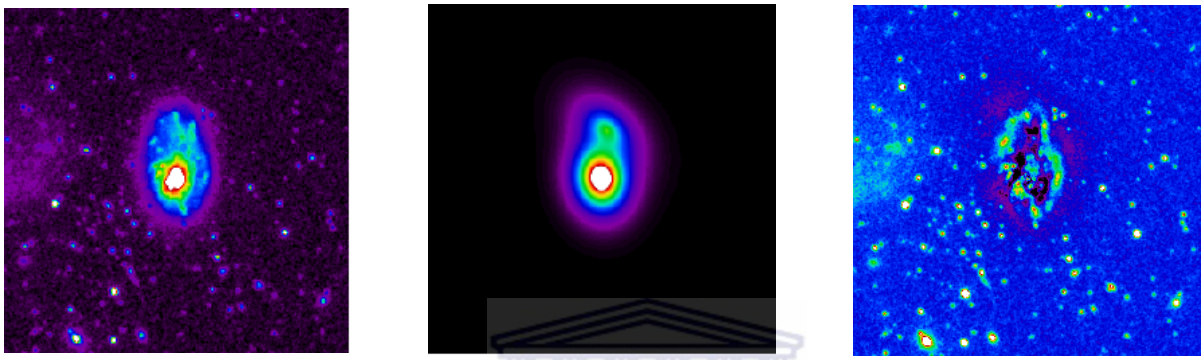

Figure A.2: ESO510-058. Left: Galaxy image, middle: The model and right: The residual. The shape parameter value is $C_0 = 0.47$.

Figure A.3: IC0163. Left: Galaxy image, middle: The model and right: The residual. The shape parameter value is $C_0 = 0.08$.

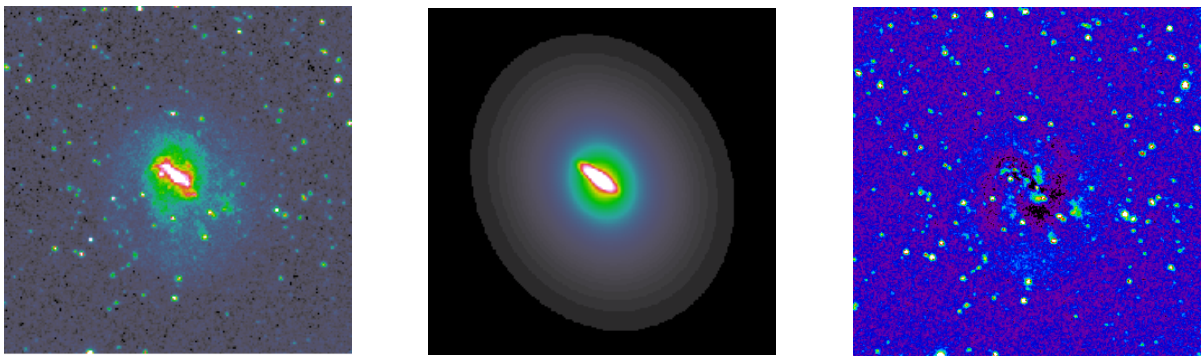

Figure A.4: IC0758. Left: Galaxy image, middle: The model and right: The residual. The shape parameter value is $C_0 = 0.05$.

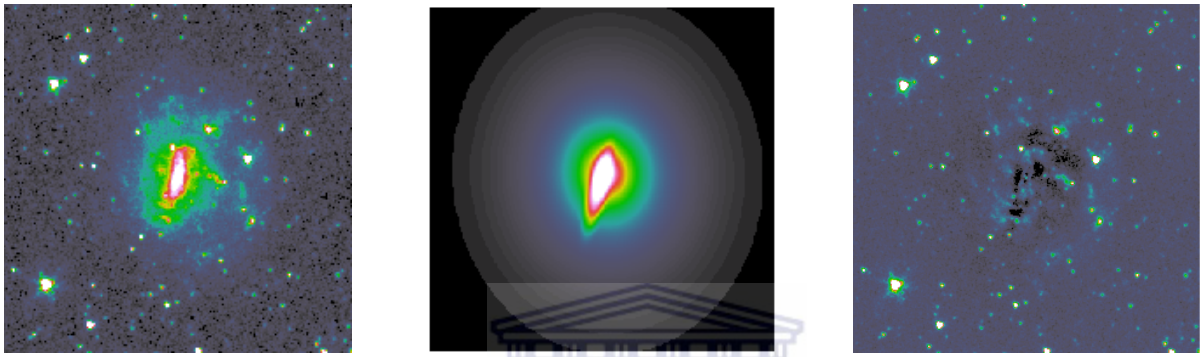

Figure A.5: IC4536. Left: Galaxy image, middle: The model and right: The residual. The shape parameter value is $C_0 = 3.68$.

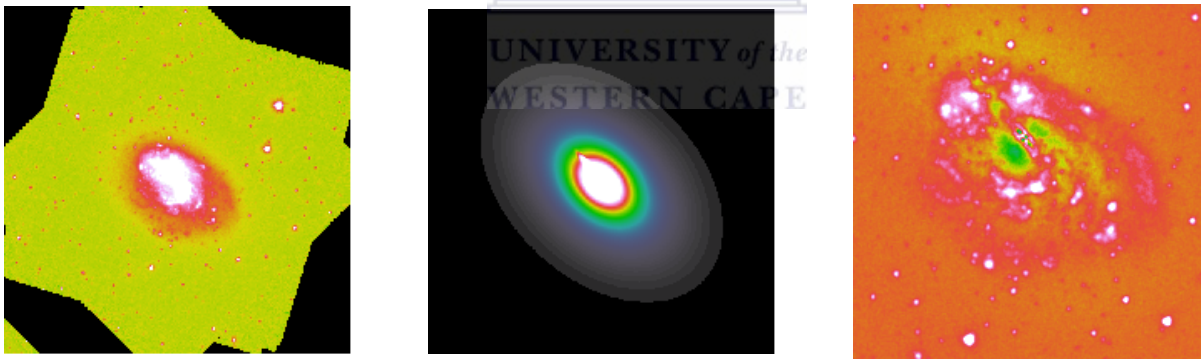

Figure A.6: IC5273. Left: Galaxy image, middle: The model and right: The residual. The shape parameter value is $C_0 = 0.01$.

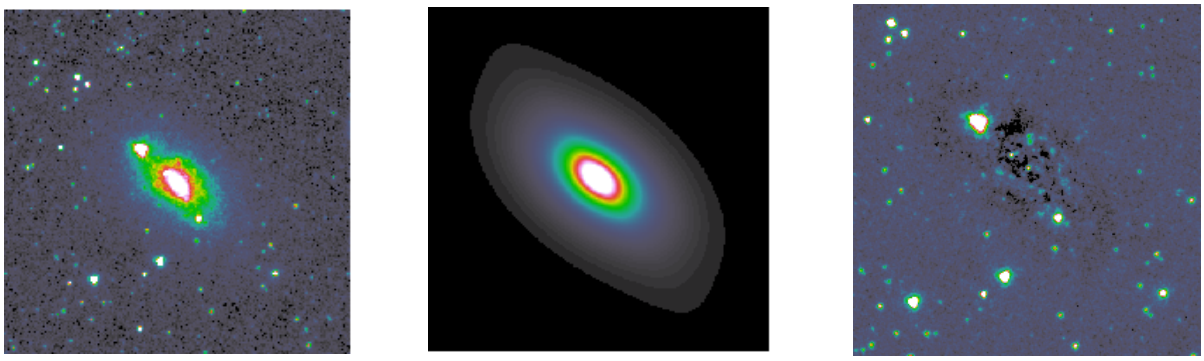

Figure A.7: NGC1051. Left: Galaxy image, middle: The model and right: The residual. The shape parameter value is $C_0 = 0.32$.

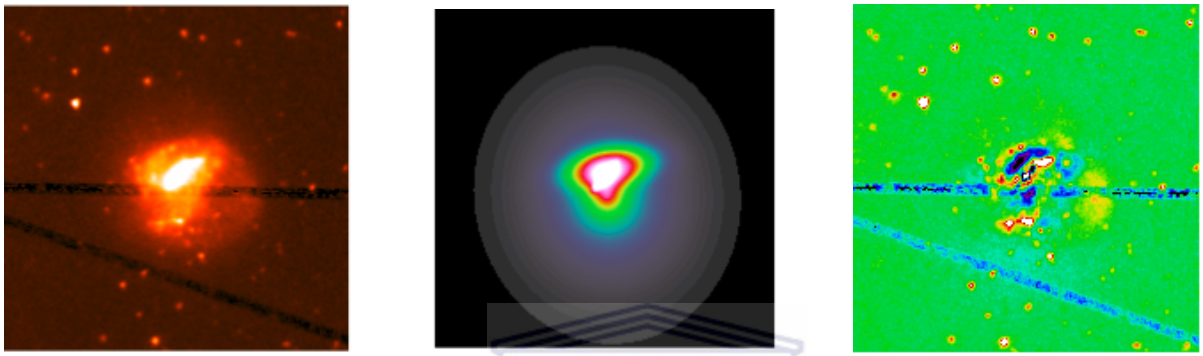

Figure A.8: NGC1338. Left: Galaxy image, middle: The model and right: The residual. The shape parameter value is $C_0 = 0.05$.

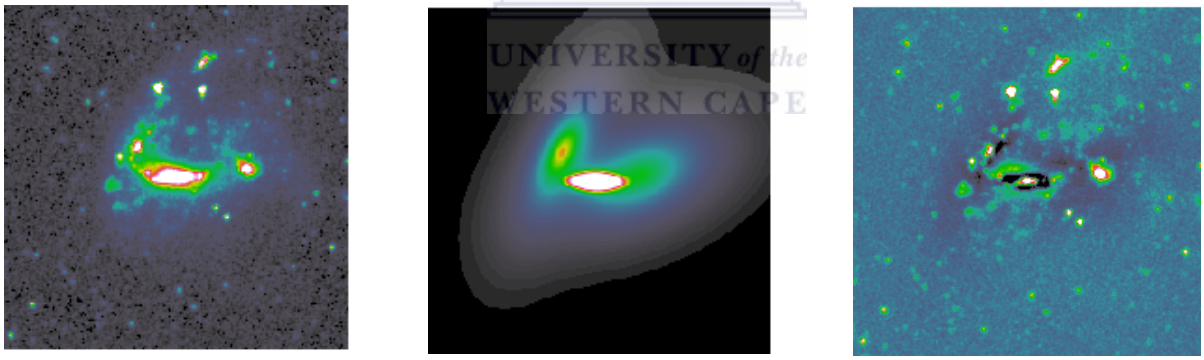

Figure A.9: NGC1359. Left: Galaxy image, middle: The model and right: The residual. The shape parameter value is $C_0 = 0.15$.

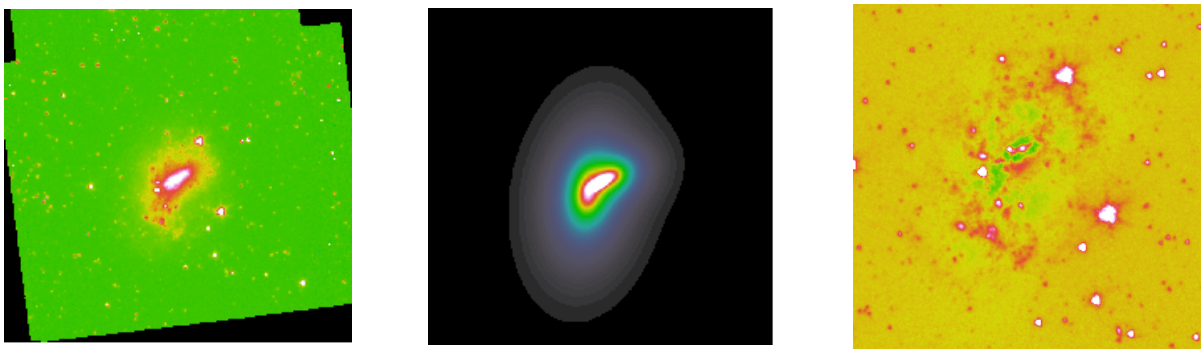

Figure A.10: NGC1679. Left: Galaxy image, middle: The model and right: The residual. The shape parameter value is $C_0 = 0.04$.

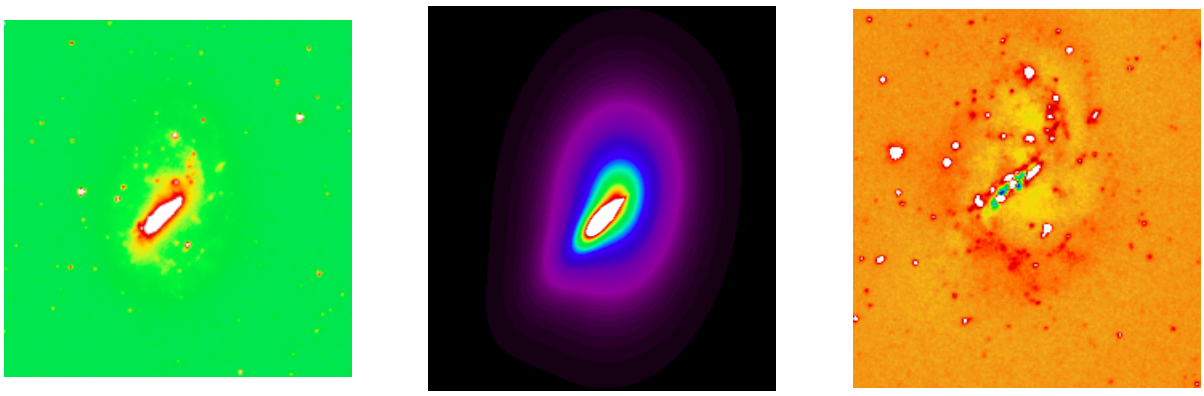

Figure A.11: NGC1688. Left: Galaxy image, middle: The model and right: The residual. The shape parameter value is $C_0 = 0.53$.

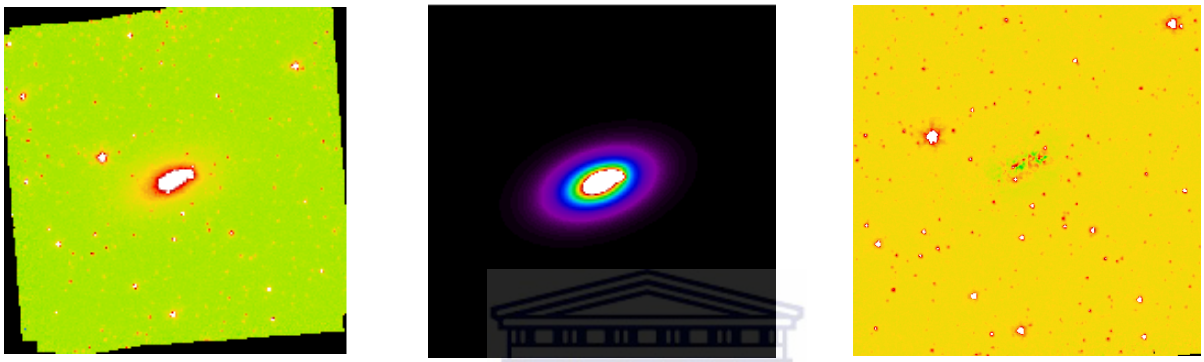

Figure A.12: NGC1800. Left: Galaxy image, middle: The model and right: The residual. The shape parameter value is $C_0 = 0.63$.

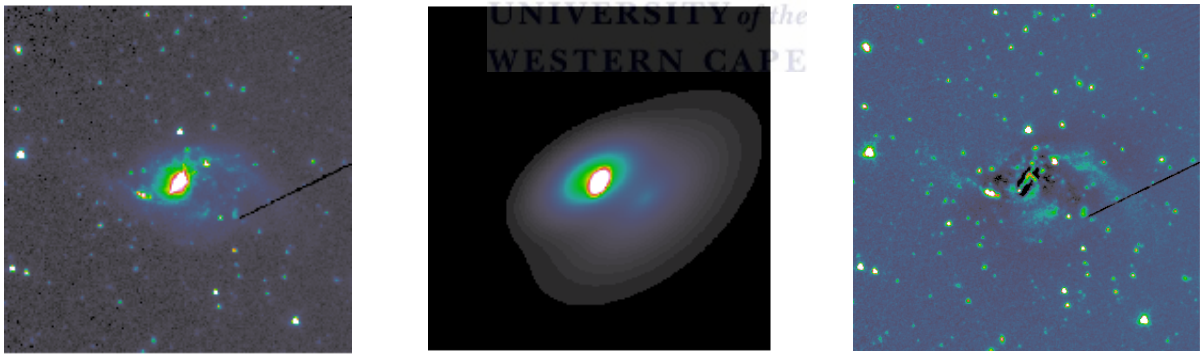

Figure A.13: NGC3023. Left: Galaxy image, middle: The model and right: The residual. The shape parameter value is $C_0 = 0.54$.

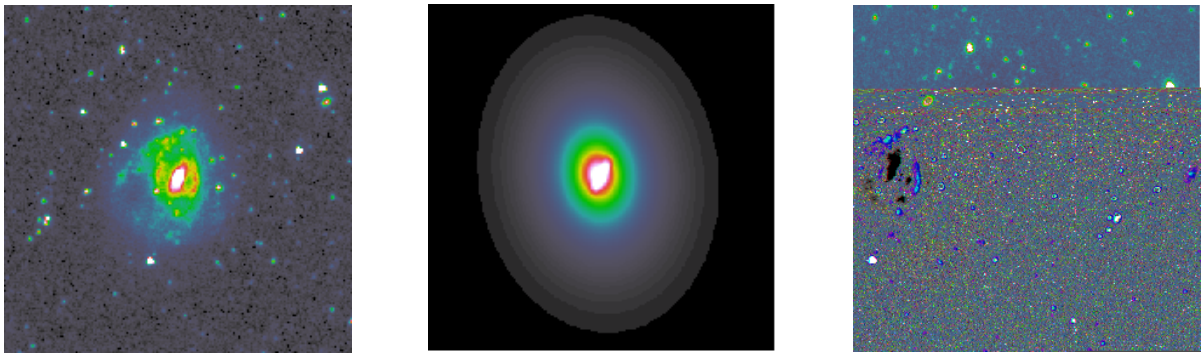

Figure A.14: NGC3061. Left: Galaxy image, middle: The model and right: The residual. The shape parameter value is $C_0 = 0.23$.

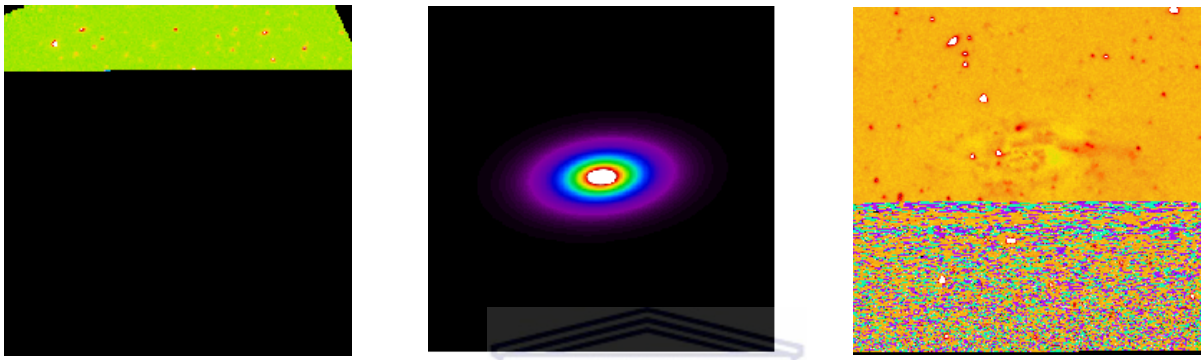

Figure A.15: NGC3246. Left: Galaxy image, middle: The model and right: The residual. The shape parameter value is $C_0 = 1.28$.

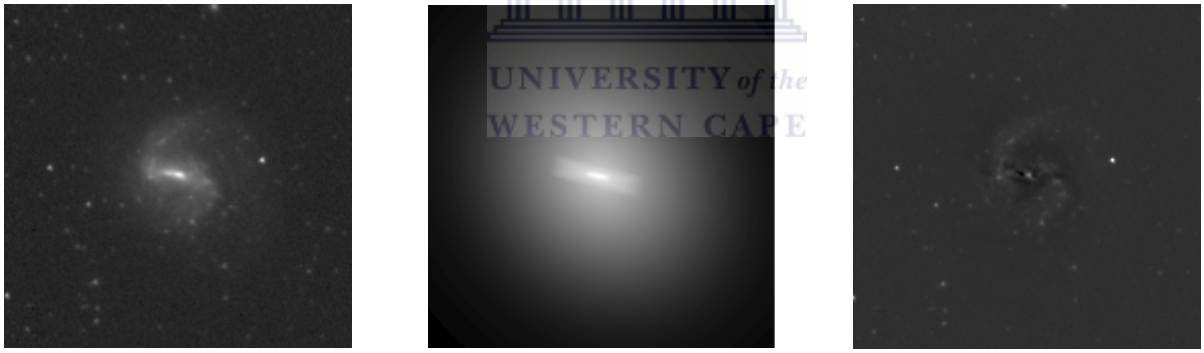

Figure A.16: NGC3381. Left: Galaxy image, middle: The model and right: The residual. The shape parameter value is $C_0 = 7.62$.

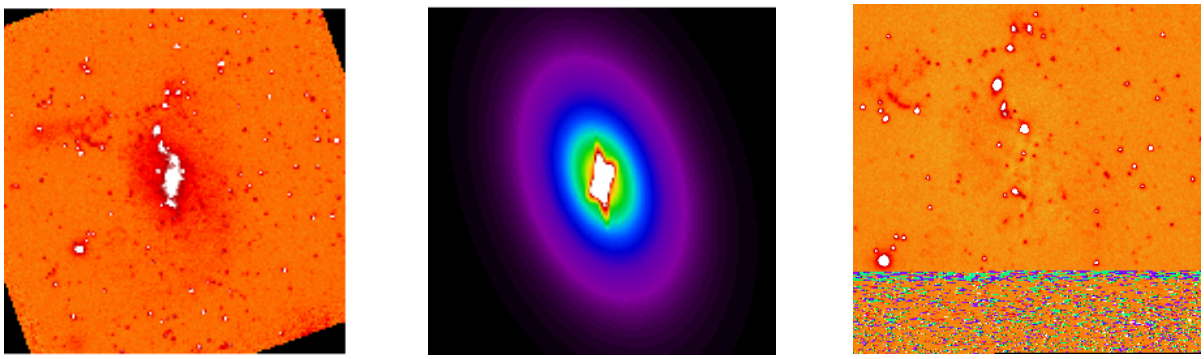

Figure A.17: NGC3447. Left: Galaxy image, middle: The model and right: The residual. The shape parameter value is $C_0 = 0.47$.

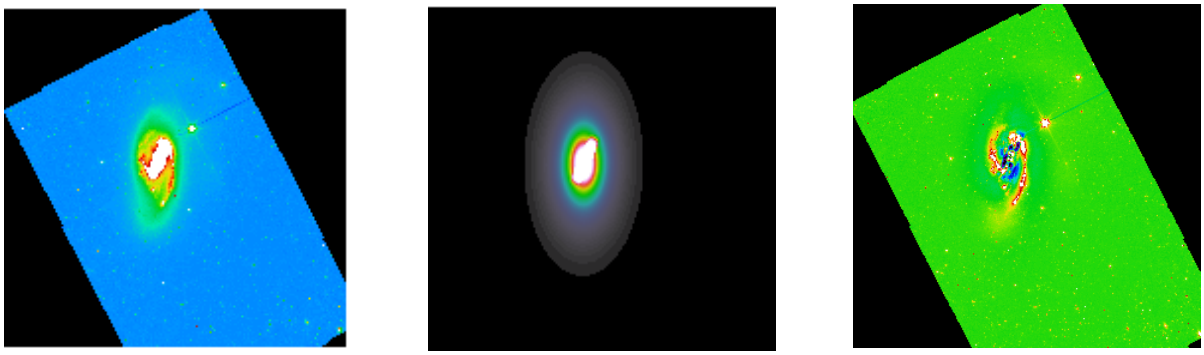

Figure A.18: NGC3627. Left: Galaxy image, middle: The model and right: The residual. The shape parameter value is $C_0 = 2.21$.

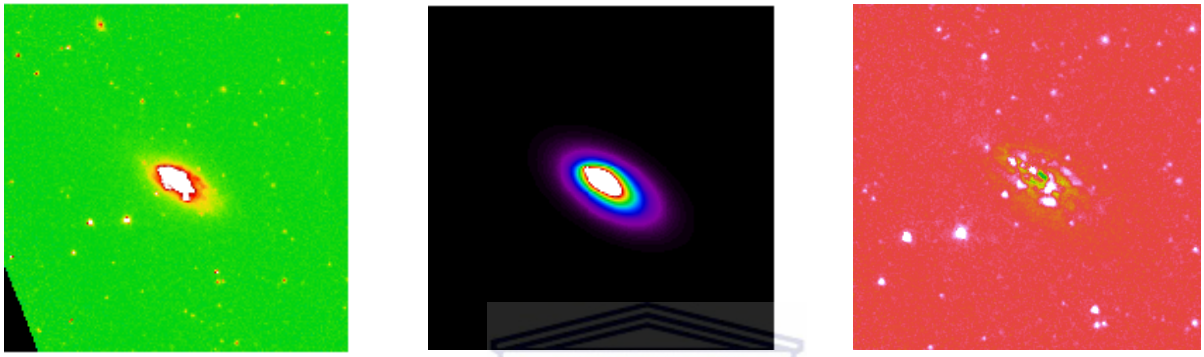

Figure A.19: NGC3659. Left: Galaxy image, middle: The model and right: The residual. The shape parameter value is $C_0 = 1.93$.

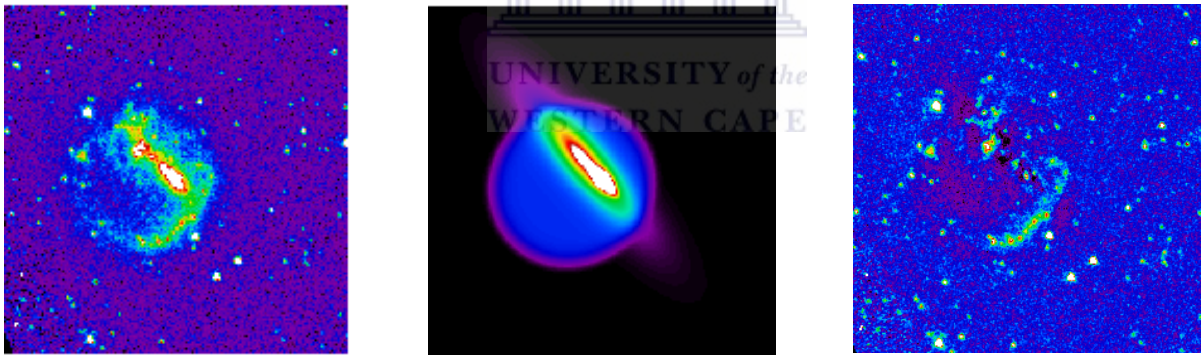

Figure A.20: NGC3664. Left: Galaxy image, middle: The model and right: The residual. The shape parameter value is $C_0 = 1.15$.

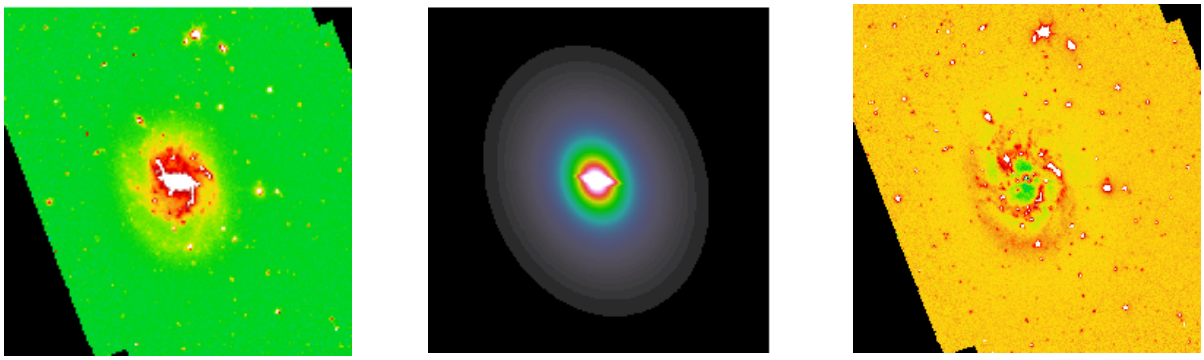

Figure A.21: NGC3686. Left: Galaxy image, middle: The model and right: The residual. The shape parameter value is $C_0 = 0.81$.

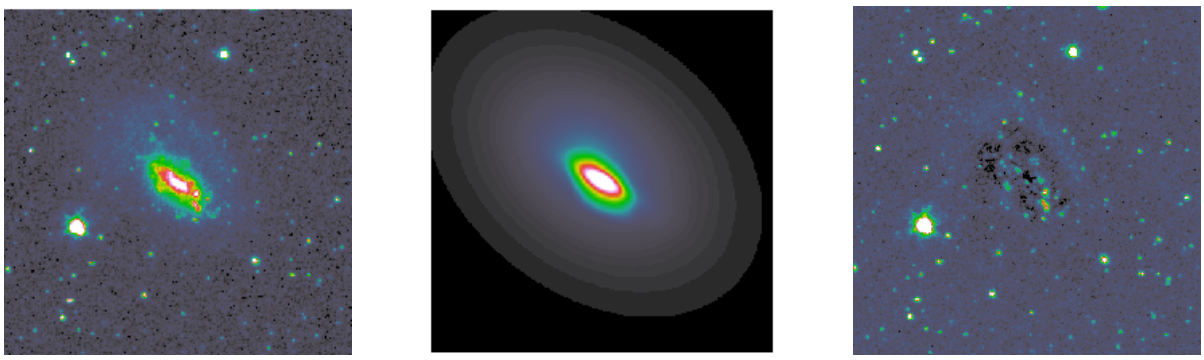

Figure A.22: NGC3846A. Left: Galaxy image, middle: The model and right: The residual. The shape parameter value is $C_0 = 3.12$.

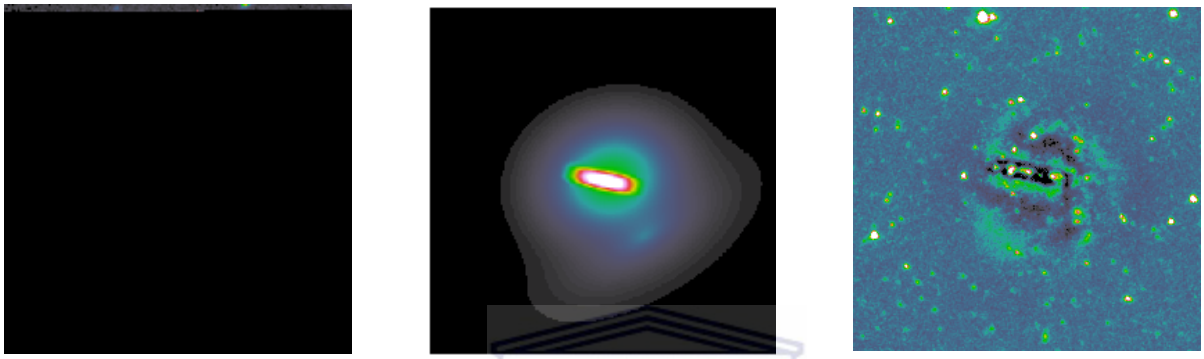

Figure A.23: NGC3906. Left: Galaxy image, middle: The model and right: The residual. The shape parameter value is $C_0 = 2.73$.

Figure A.24: NGC4027. Left: Galaxy image, middle: The model and right: The residual. The shape parameter value is $C_0 = 0.06$.

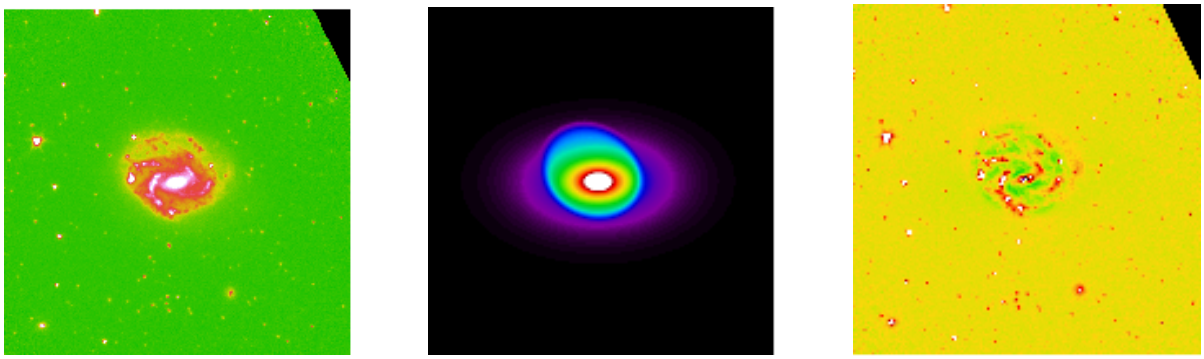

Figure A.25: NGC4189. Left: Galaxy image, middle: The model and right: The residual. The shape parameter value is $C_0 = 0.05$.

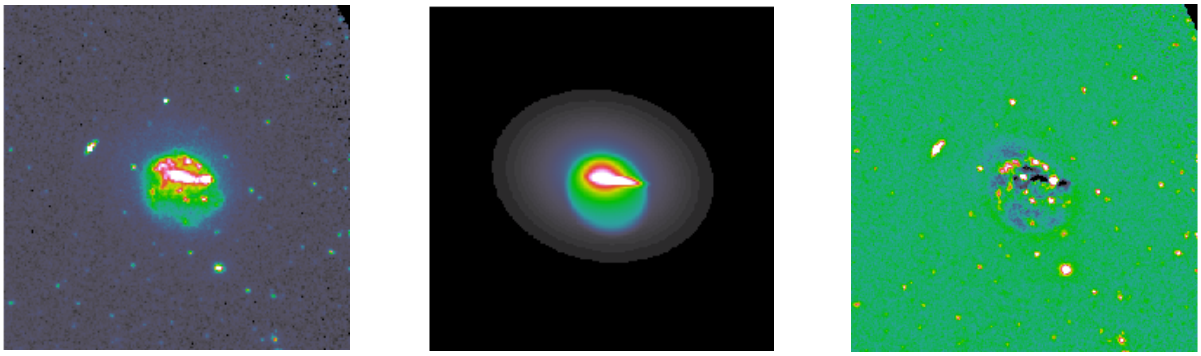

Figure A.26: NGC4234. Left: Galaxy image, middle: The model and right: The residual. The shape parameter value is $C_0 = 0.73$.

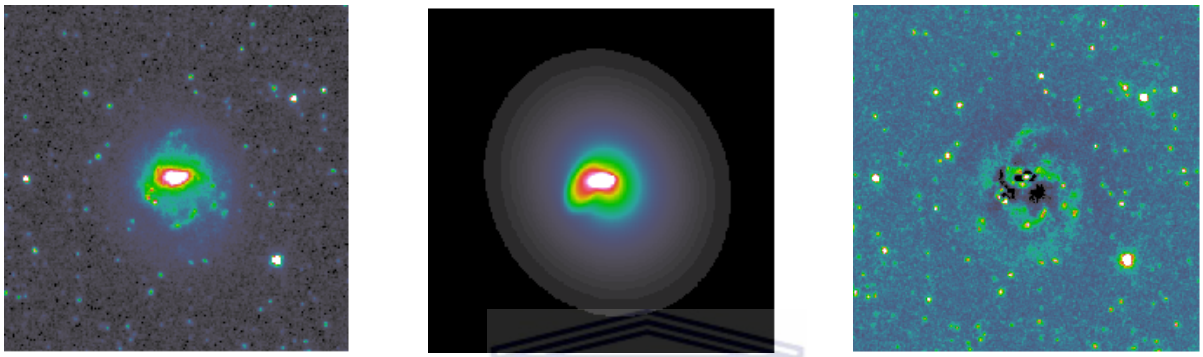

Figure A.27: NGC4276. Left: Galaxy image, middle: The model and right: The residual. The shape parameter value is $C_0 = 0.02$.

Figure A.28: NGC4416. Left: Galaxy image, middle: The model and right: The residual. The shape parameter value is $C_0 = 0.3$.

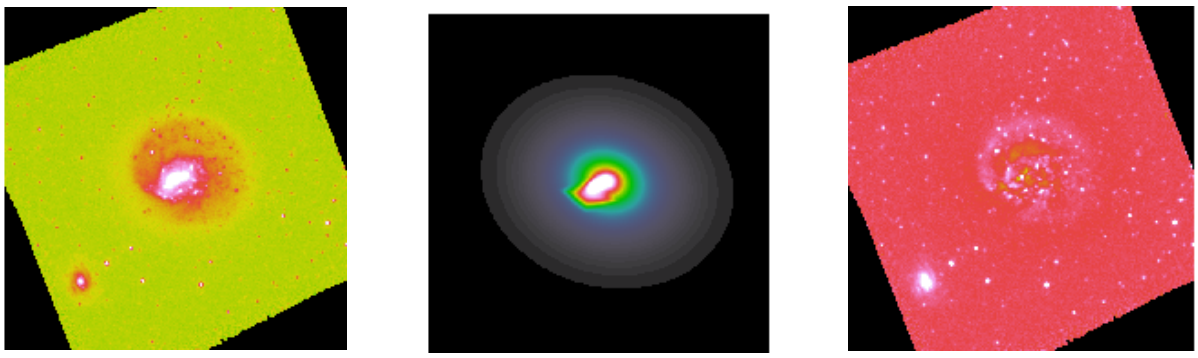

Figure A.29: NGC4430. Left: Galaxy image, middle: The model and right: The residual. The shape parameter value is $C_0 = 5.88$.

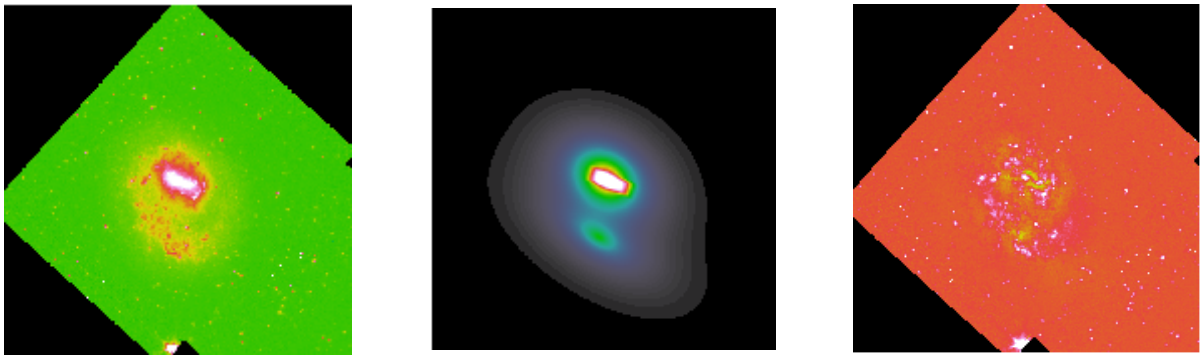

Figure A.30: NGC4618. Left: Galaxy image, middle: The model and right: The residual. The shape parameter value is $C_0 = 9.72$.

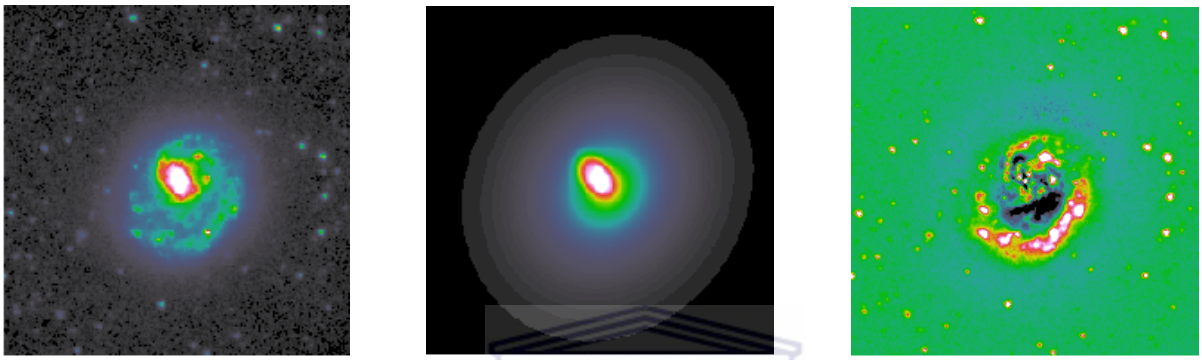

Figure A.31: NGC4625. Left: Galaxy image, middle: The model and right: The residual. The shape parameter value is $C_0 = 1.27$.

Figure A.32: NGC4668. Left: Galaxy image, middle: The model and right: The residual. The shape parameter value is $C_0 = 0.4$.

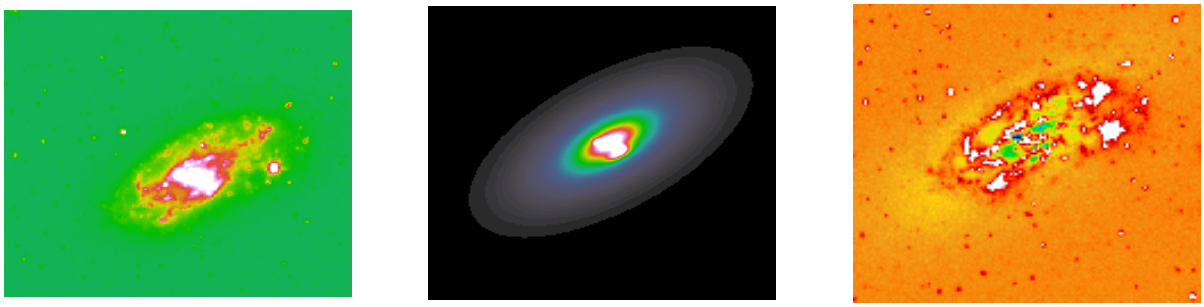

Figure A.33: NGC4781. Left: Galaxy image, middle: The model and right: The residual. The shape parameter value is $C_0 = 0.97$.

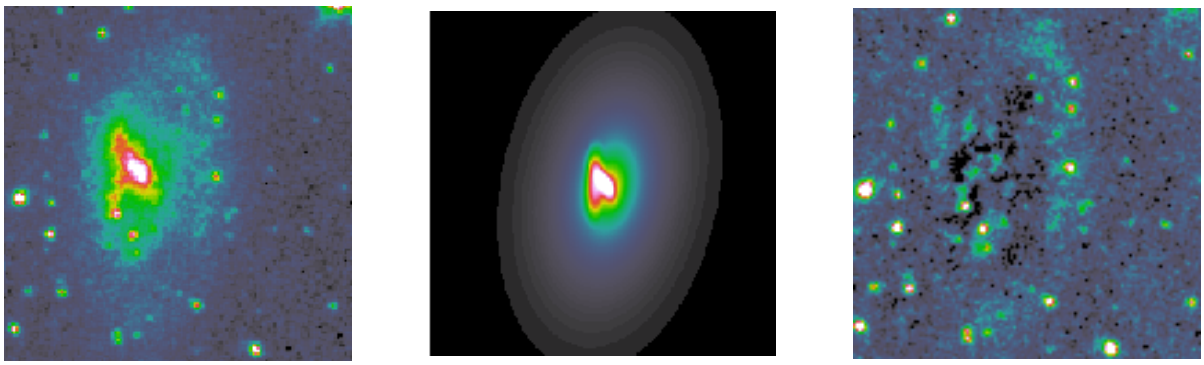

Figure A.34: NGC5002. Left: Galaxy image, middle: The model and right: The residual. The shape parameter value is $C_0 = 0.97$.

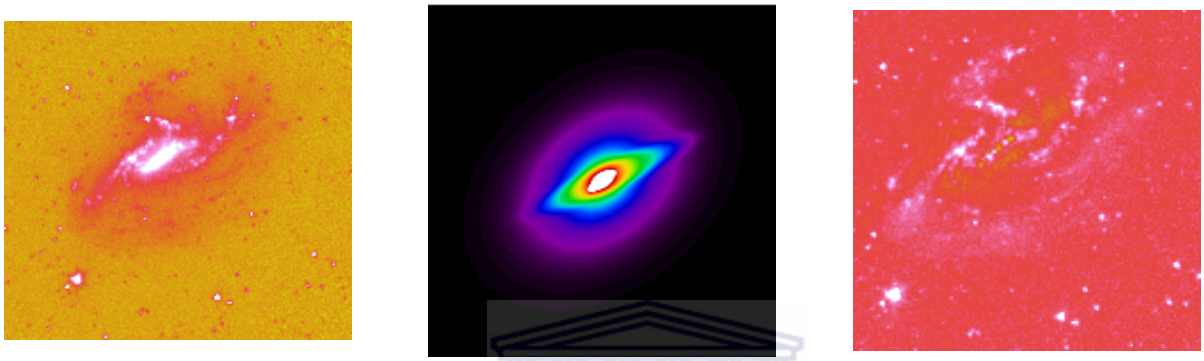

Figure A.35: NGC5112. Left: Galaxy image, middle: The model and right: The residual. The shape parameter value is $C_0 = 2.25$.

Figure A.36: NGC5691. Left: Galaxy image, middle: The model and right: The residual. The shape parameter value is $C_0 = 0.29$.

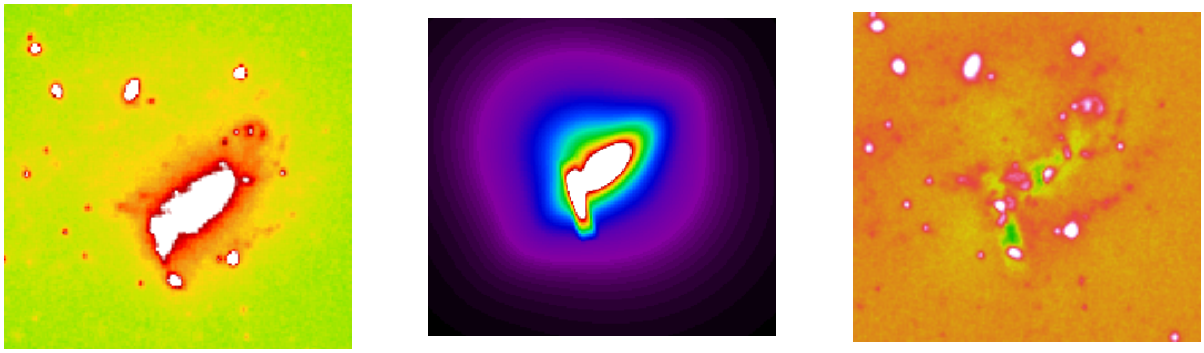

Figure A.37: NGC7154. Left: Galaxy image, middle: The model and right: The residual. The shape parameter value is $C_0 = 0.33$.

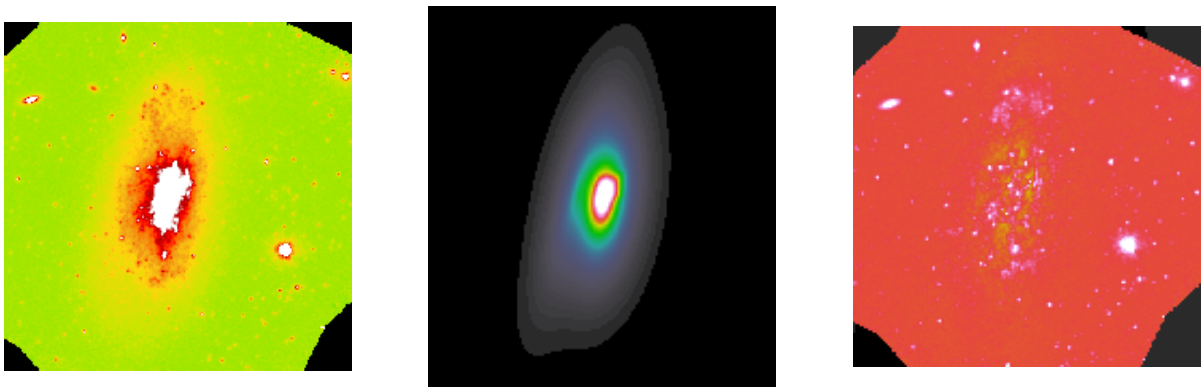

Figure A.38: NGC7713. Left: Galaxy image, middle: The model and right: The residual. The shape parameter value is $C_0 = 0.08$.

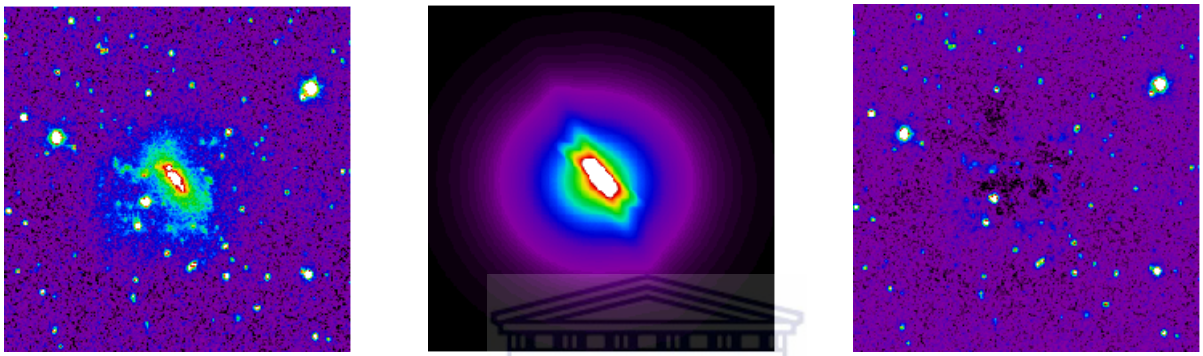

Figure A.39: PGC012068. Left: Galaxy image, middle: The model and right: The residual. The shape parameter value is $C_0 = 0.94$.

Figure A.40: PGC066559. Left: Galaxy image, middle: The model and right: The residual. The shape parameter value is $C_0 = 1.47$.

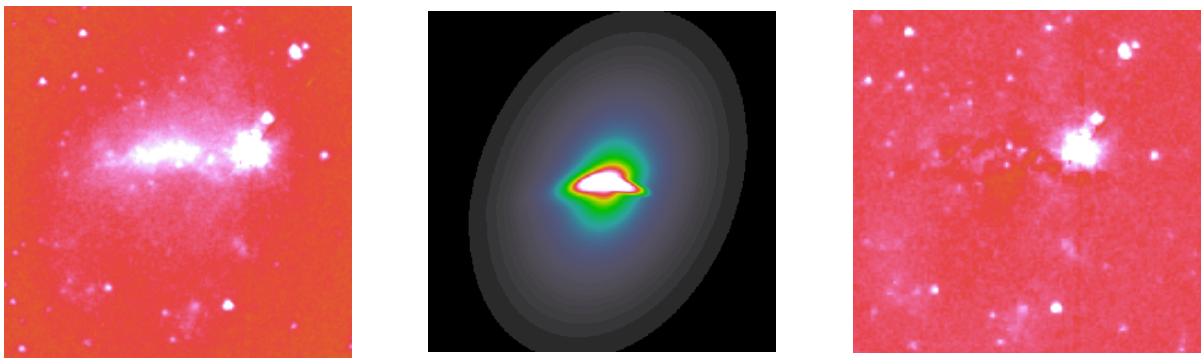

Figure A.41: UGC05612. Left: Galaxy image, middle: The model and right: The residual. The shape parameter value is $C_0 = 3.42$.

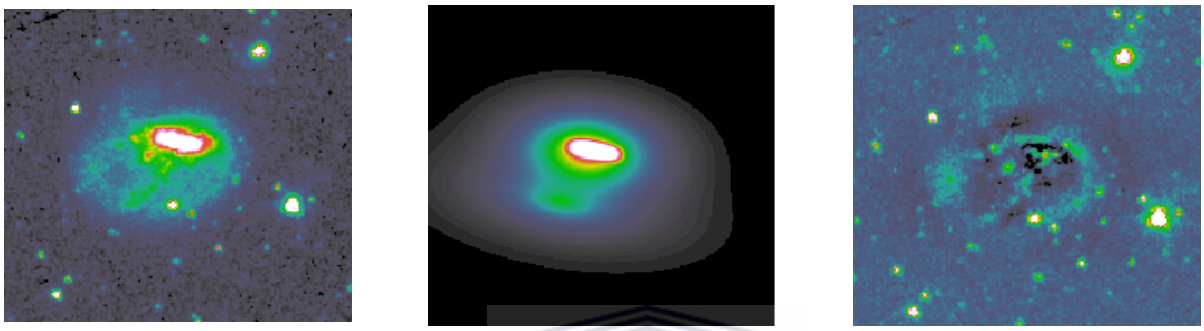

Figure A.42: UGC05832. Left: Galaxy image, middle: The model and right: The residual. The shape parameter value is $C_0 = 1.49$.

Figure A.43: UGC06157. Left: Galaxy image, middle: The model and right: The residual. The shape parameter value is $C_0 = 0.4$.

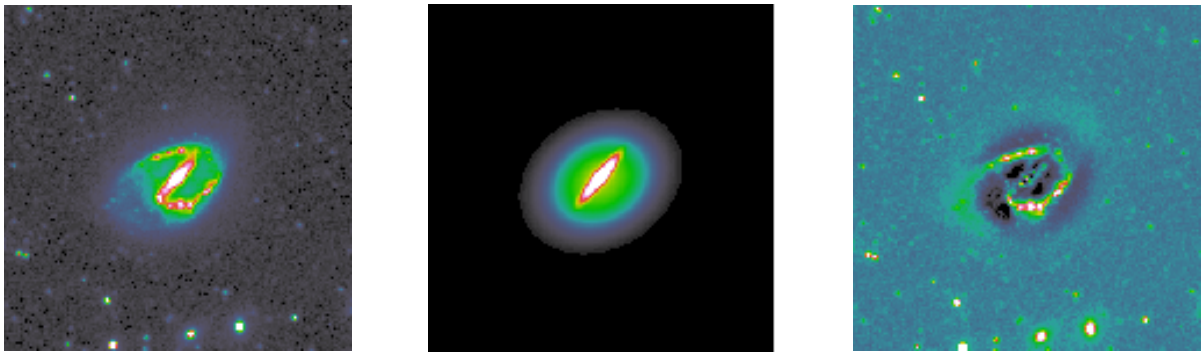

Figure A.44: UGC06309. Left: Galaxy image, middle: The model and right: The residual. The shape parameter value is $C_0 = 0.33$.

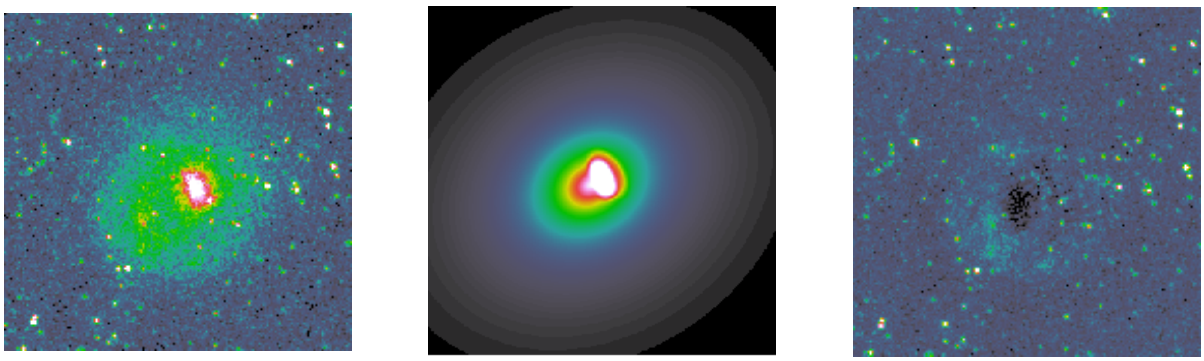

Figure A.45: UGC07239. Left: Galaxy image, middle: The model and right: The residual. The shape parameter value is $C_0 = 0.43$

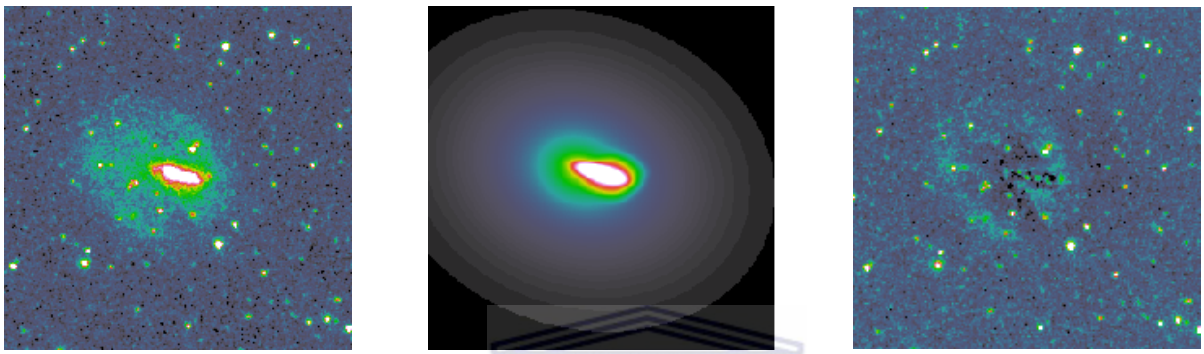

Figure A.46: UGC08084. Left: Galaxy image, middle: The model and right: The residual. The shape parameter value is $C_0 = 4.61$.

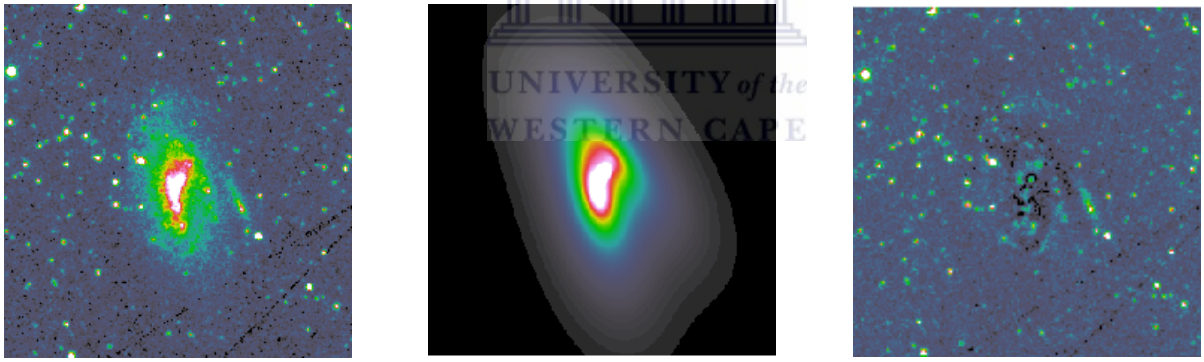

Figure A.47: UGC08733. Left: Galaxy image, middle: The model and right: The residual. The shape parameter value is $C_0 = 1.42$.

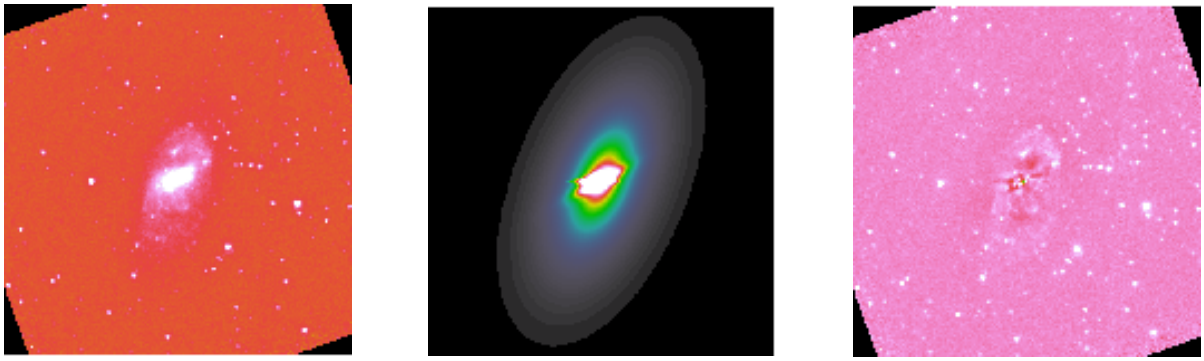

Figure A.48: UGC09215. Left: Galaxy image, middle: The model and right: The residual. The shape parameter value is $C_0 = 3.77$.

Figure A.49: UGC09661. Left: Galaxy image, middle: The model and right: The residual. The shape parameter value is $C_0 = 0.84$.

Bibliography

R. G. Abraham, M. R. Merrifield, R. S. Ellis, N. R. Tanvir, and J. Brinchmann. The evolution of barred spiral galaxies in the Hubble deep fields north and south. *MNRAS*, 308:569–576, 1999. doi: arXiv:astro-ph/9811476. URL http://adsabs.harvard.edu/abs/1999MNRAS.308..569A.

R. G. Abraham et al. A new approach to galaxy morphology. I. Analysis of the Sloan Digital Sky Survey early data release. *The Astrophysical Journal*, 588:218–229, 2003. doi: arXiv:astro-ph/0301239. URL http://adsabs.harvard.edu/abs/2003ApJ...588..218A.

E. Athanassoula. Morphology of bar orbits. *MNRAS*, 259:328–344, 1992a. URL http://adsabs.harvard.edu/abs/1992MNRAS.259..328A.

E. Athanassoula. The existence and shapes of dust lanes in galactic bars. *MNRAS*, 259:345, 1992b. URL http://adsabs.harvard.edu/abs/1992MNRAS.259..345A.

E. Athanassoula. Evolution of bars in isolated and in interaction disk galaxies. *ASP Conf. Ser*, 91: 309, 1996. URL http://adsabs.harvard.edu/abs/1996ASPC...91..309A.

E. Athanassoula. Bar-halo interaction and bar growth. *The Astrophysical Journal*, 569:83–86, 2002. doi: arXiv:astro-ph/0203368. URL http://adsabs.harvard.edu/abs/2002ApJ...569L..83A.

E. Athanassoula. Bars and secular evolution in disk galaxies: Theoretical input. *Cambridge University Press*, page 305, 2013. doi: arXiv:1211.6752. URL http://adsabs.harvard.edu/abs/2013seg..book..305A.

E. Athanassoula et al. The shape of bars in early-type barred galaxies. *MNRAS*, 245:130–139, 1990. URL http://adsabs.harvard.edu/abs/1990MNRAS.245..130A.

J. E. Baldwin et al. Lopsided galaxies. *MNRAS*, 193:313–319, 1980. URL http://adsabs.harvard.edu/abs/1980MNRAS.193..313B.

K. Bekki. Formation of the off-centre bar in the large magellanic cloud: a collision with a dark satellite? *MNRAS*, 393:60–64, 2009. doi: arXiv:0811.3279. URL http://adsabs.harvard.edu/abs/2009MNRAS.393L..60B.

I. Berentzen, E. Athanassoula, C. H. Heller, and K. J. Fricke. Numerical simulations of interacting gas rich barred galaxies: vertical impact of small companions. *MNRAS*, 341:343–360, 2003. doi: arXiv:astro-ph/0301300. URL http://adsabs.harvard.edu/abs/2003MNRAS.341..343B.

C. P. Blackman. UBVRI surface photometry of barred spiral NGC7479. *MNRAS*, 202:379–395, 1983. URL http://adsabs.harvard.edu/abs/1983MNRAS.202..379B.

F. Bournaud et al. Lopsided spiral galaxies: evidence for gas accretion. *Astronomy and Astrophysics*, 438:507–520, 2005. doi: arXiv:astro-ph/0503314. URL http://adsabs.harvard.edu/abs/2005A%26A...438..507B.

F. Combes and Elmegreen B. G. Bars in early- and late-type galaxies. *Astron. Astrophycs*, 271: 391–401, 1993. URL http://adsabs.harvard.edu/abs/1993A%26A...271..391C.

H. Curtis. Description of 762 nebulae and clusters photographed with the crossley reflector. *Publication of the click observatory*, Vol. XIII:Part I, 1918. URL http://adsabs.harvard.edu/abs/1918PLicO..13....9C.

B. de Swardt. The odd offset between the galactic disk and its bar in NGC 3906. *The Astrophysical Journal*, 808:90, 2015. doi: arXiv:1506.05153. URL http://adsabs.harvard.edu/abs/2015ApJ...808...90D.

A. de Vaucouleurs, H. G. Corwin, Jr. Buta, R. J., G. Paturel, and P Fouque. Third Reference Catalogue of Bright Galaxies. *(New York: Springer) (RC3)*, 1991. URL http://adsabs.harvard.edu/abs/1991rc3..book.....D.

G. de Vaucouleurs. Classification and Morphology of External Galaxies. *Handbuch der Physik*, 53: 275, 1959. URL http://adsabs.harvard.edu/abs/1959HDP....53..275D.

G. de Vaucouleurs. Revised classification of 1500 bright galaxies. *The Astrophysical Journal*, 8:31, 1963. URL http://adsabs.harvard.edu/abs/1963ApJS....8...31D.

G. de Vaucouleurs and K. C. Freeman. Structure and dynamics of barred spiral galaxies, in particular of the magellanic type. *Vistas in Astronomy*, 14:163–1994, 1972. URL http://adsabs.harvard.edu/abs/1972VA.....14..163D.

B. G. Elmegreen and D. M. Elmegreen. Properties of barred spiral galaxies. *The Astrophysical Journal*, 288:438–455, 1985. URL http://adsabs.harvard.edu/abs/1985ApJ...288..438E.

P. B. Eskridge et al. The frequency of barred spiral galaxies in the near-infrared. *The Astrophysical Journal*, 119:536–544, 2000. doi: arXiv:astro-ph/9910479. URL http://adsabs.harvard.edu/abs/2000AJ....119..536E.

G. G. Fasio et al. The Infrared Array Camera (IRAC) for the *Spitzer* Space Telescope. *The Astronomical Journal Supplement Series*, 154:10–17, 2004. doi: arXiv:astro-ph/0405616. URL http://adsabs.harvard.edu/abs/2004ApJS..154...10F.

J. V. Feitzinger. Magellanic-type galaxies. *Space Science Reviews*, 27:35–105, 1980. URL http://adsabs.harvard.edu/abs/1980SSRv...27...35F.

A. W. Graham. Evidence for an outer disk in the prototype "compact elliptical" galaxy M32. *The Astrophysical Journal*, 568:L13–L17, 2002. URL http://adsabs.harvard.edu/abs/2002ApJ...568L..13G.

E. Hubble. Extra-galactic nebulae. *The Astrophysical Journal*, 64:321, 1926. URL http://adsabs.harvard.edu/abs/1926ApJ....64..321H.

R. I. Jedrzejewski et al. CCD surface potometry of ellipticals galaxies-I. Observations, redaction and results. *MNRAS*, 226:747–766, 1987. URL http://adsabs.harvard.edu/abs/1987MNRAS.226..747J.

C. J. Jog and F. Combes. Lopsided spiral galaxies. *Physics Reports*, 471:75–111, 2009. doi: arXiv:0811.1101. URL http://adsabs.harvard.edu/abs/2009PhR...471...75J.

W. T. Kim, W. Y. Seo, and Y. Kim. Gaseous structures in barred galaxies: Effects of the bar strength. *The Astrophysical Journal*, 758:14, 2012. doi: arXiv:1208.1821. URL http://adsabs.harvard.edu/abs/2012ApJ...758...14K.

J. Kormendy. A morphological survey of bar, lens, and ring components in galaxies: Secular evolution in galaxy structure. *The Astronomical Journal*, 227:714–728, 1979. URL http://adsabs.harvard.edu/abs/1979ApJ...227..714K.

J. Kormendy and R. C. Kennicutt. Secular evolution and the formation of pseudobulges in disk galaxies. *Annual Review of Astronomy and Astrophysics*, 42:603–683, 2004. doi: arXiv:astro-ph/0407343. URL http://adsabs.harvard.edu/abs/2004ARA%26A..42..603K.

Eija Laurikainen and Heikki Salo. Bar strengths in spiral galaxies estimated from 2MASS images. *Astronomy and Astrophysics*, 337:1118–1138, 2002. doi: arXiv:astro-ph/0209214. URL http://adsabs.harvard.edu/abs/2002MNRAS.337.1118L.

Levine et al. A model for lopsided galactic disks. *The Astrophysical Journal*, 496:13–16, 1998. doi: arXiv:astro-ph/9803146. URL http://adsabs.harvard.edu/abs/1998ApJ...496L..13L.

M. O. Lorenz. Methods of measuring the concentration of wealth. *Publication of American Statistical Association*, 9:70, 1905.

J. M. Lotz, J. Primack, and P. Madau. A new nonparametric approach to galaxy morphological classification. *The Astrophysical Journal*, 128:163–182, 2004. doi: astro-ph/0311352. URL http://adsabs.harvard.edu/abs/2004AJ....128..163L.

K. Menendez-Delmestre, Sheth K., E. Schinnerer, T. H. Jarrett, and N. Z. Scoville. A near-infrared study of 2MASS bars in local galaxies: An anchor for high-redshift studies. *The Astrophysical Journal*, 657:790–804, 2007. doi: arXiv:astro-ph/0611540. URL http://adsabs.harvard.edu/abs/2007ApJ...657..790M.

Edo Noordermeer. The kinematics of lopsided galaxies. *MNRAS*, 328:1064–1080, 2001. doi: arXiv:astro-ph/0112305. URL http://adsabs.harvard.edu/abs/2001MNRAS.328.1064N.

S. C. Odewahn. Properties of the magellanic-type spirals. I - Surface photometry of ngc 4618 and ngc 4625. *The Astrophysical Journal*, 101:829–844, 1991. URL http://adsabs.harvard.edu/abs/1991AJ....101..829O.

S. C. Odewahn. Properties of the magellanic type spirals. 2: The frequency of companion galaxies. *The Astronomical Journal*, 107,n$_o$ 4:1320–1327, 1994. URL http://adsabs.harvard.edu/abs/1994AJ....107.1320O.

S. C. Odewahn. Properties of the magellanic type galaxies. *ASP Conf. Ser*, 91:30, 1996. URL http://adsabs.harvard.edu/abs/1996ASPC...91...30O.

K. Ohta, M. Sasaki, and M. Saito. Co observations of the barred spiral galaxy ngc 5383. *Astronomical Society of Japan, Publications*, 38:677–683, 1986. URL http://adsabs.harvard.edu/abs/1986PASJ...38..677O.

S. C. Pardy et al. Tidally induced offset disks in magellanic spiral galaxies. *The Astrophysical Journal*, 827:149, 2016. URL http://adsabs.harvard.edu/abs/2016ApJ...827..149P.

G. Paturel, C. Petit, Ph. Prugniel, G. Theureau, J. Rousseau, M. Brouty, P. Dubois, and L. Cambresy. Hyperleda I. Identification and designation of galaxies. *Astronomy and Astrophysics*, 412:45–55, 2003. URL http://adsabs.harvard.edu/abs/2003A%26A...412...45P.

W. D. Pence et al. Detailed study of the barred spiral galaxy ngc 4027. II - Internal kinematics. *The Astrophysical Journal*, 326:564–573, 1988. URL http://adsabs.harvard.edu/abs/1988ApJ...326..564P.

C. Y. Peng, C. H. Luis, D. I. Chris, and Rix Hans-Walter. Detailed decomposition of galaxy images. II. Beyond axisymmetric models. *The Astrophysical Journal*, 139:2097–2129, 2010. doi: arXiv:0912.0731. URL http://adsabs.harvard.edu/abs/2010AJ....139.2097P.

M. Pohlen and I. Trujillo. The structure of galactic disks. Studying late-type spiral galaxies using SDSS. *Astronomy and Astrophysics*, 454:759, 2006. doi: arXiv:astro-ph/0603682. URL http://adsabs.harvard.edu/abs/2006A%26A...454..759P.

M. Pohlen, R. J. Dettmar, R. Lutticke, and G. Aronica. Outer edges of face-on spiral galaxies. Deep optical imaging of NGC 5923, UGC 9837 and NGC 5434. *Astronomy and Astrophysics*, 392:807–816, 2002. URL http://adsabs.harvard.edu/abs/2002A%26A...392..807P.

H. W. Rix and D Zaritsky. Nonaxisymmetric structures in the stellar disks of galaxies. *The Astrophysical Journal*, 447:82, 1995. doi: arXiv:astro-ph/9505111. URL http://adsabs.harvard.edu/abs/1995ApJ...447...82R.

A. S. G. Robotham. Galaxy And Mass Assembly (GAMA): in search of Milky Way Magellanic Cloud analogues. *MNRAS*, 424:1448–1453, 2012. doi: arXiv:1208.4293. URL http://adsabs.harvard.edu/abs/2012MNRAS.424.1448R.

A. Sandage. The hubble atlas of galaxies. *Carnegie Inst. of Wash*, Pub. No.:618, 1961. URL http://adsabs.harvard.edu/abs/1961hag..book.....S.

A. Sandage and G. A. Tammann. A Revised Shapley-Ames Catalog of Bright Galaxies. *2nd. ed.; Washington: Carnegie Inst. Washington*, 1987. URL http://adsabs.harvard.edu/abs/1987rsac.book.....S.

R. H. M. Schoenmakers et al. Measuring non-axisymmetry in spiral galaxies. *MNRAS*, 292:349, 1997. doi: arXiv:astro-ph/9707332. URL http://adsabs.harvard.edu/abs/1997MNRAS.292..349S.

M. K. Seidel et al. The BaLROG projet-II. Quantitying the influence of bars on the stellar populations of nearby galaxies. *MNRAS*, 000:1–43, 2016. doi: arXiv:1605.06500. URL http://adsabs.harvard.edu/abs/2016MNRAS.460.3784S.

J. A. Sellwood and A. Wilkinson. Dynamics of barred galaxies. *Reports on Progress in Physics*, 56: 173–256, 1993. doi: arXiv:astro-ph/0608665. URL http://adsabs.harvard.edu/abs/1993RPPh...56..173S.

W. Y. Seo and W. T. Kim. Star formation in nuclear rings of barred galaxies. *The Astrophysical Journal*, 769:100, 2013. doi: arXiv:1304.3899. URL http://adsabs.harvard.edu/abs/2013ApJ...769..100S.

K. Sheth, M. N. Regan, N. Z. Scoville, and L. E. Strubbe. Barred Galaxies at z $>$ 0.7: Nicmos Hubble Deep Field-North Observations. *The Astrophysical Journal*, 592:L13–L16, 2003. doi: arXiv:astro-ph/0305589. URL http://adsabs.harvard.edu/abs/2003ApJ...592L..13S.

K. Sheth et al. Molecular gas, dust, and star formation in the barred spiral NGC 5383. *The Astrophysical Journal*, 532:221–237, 2000. doi: arXiv:astro-ph/9911280. URL http://adsabs.harvard.edu/abs/2000ApJ...532..221S.

K. Sheth et al. Comparing molecular gas and star formation properties in the central regions of barred and unbarred spirals. *Astronomical Society of the Pacific Conference Series*, 275:263–266, 2002. URL http://adsabs.harvard.edu/abs/2002ASPC..275..267S.

K. Sheth et al. The redshift evolution of bulges and disks of spiral galaxies in cosmos. *Astronomical Society of the Pacific Conference Series*, 390:426, 2008a. URL http://adsabs.harvard.edu/abs/2008ASPC..390..426S.

K. Sheth et al. The redshift evolution of bulges and disks of spiral galaxies in cosmos. *ed. Knapen J. H.,Mahoney T. J. and Vazdekis A. (San Francisco: ASP), in press*, 2008b. URL http://adsabs.harvard.edu/abs/2008ASPC..390..426S.

K. Sheth et al. The *Spitzer* Survey of Stellar Structure in Galaxies (S^4G). *The astronomical society of the pacific*, 122:1397–1414, 2010. doi: arXiv:1312.3384. URL http://adsabs.harvard.edu/abs/2010PASP..122.1397S.

K. Sheth et al. Hot disks and delayed bar formation. *The Astrophysical Journal*, 758:136, 2012. doi: arXiv:1208.6304. URL http://adsabs.harvard.edu/abs/2012ApJ...758..136S.

V. Springel. The cosmological simulation code gadget-2. *MNRAS*, 364:1105–1134, 2005. doi: arXiv:astro-ph/0505010. URL http://adsabs.harvard.edu/abs/2005MNRAS.364.1105S.

R. A. Swaters et al. Measuring non-axisymmetry in spiral galaxies. *MNRAS*, 304:330–334, 1999. doi: arXiv:astro-ph/9811424. URL http://adsabs.harvard.edu/abs/1999MNRAS.304..330S.

K. Taehyun et al. Unveiling the structure of barred galaxies at 3.6μm with the *Spitzer* Survey of Stellar Structure in Galaxies (S^{4}G). I. disk breaks. *The Astrophysical Journal*, 782:64, 2014. doi: arXiv:1312.3384. URL http://adsabs.harvard.edu/abs/2014ApJ...782...64K.

Kim Taehyun et al. The mass profile and shape of bars in the *Spitzer* Survey of Stellar Structure in Galaxies (S^{4}G): Search for an age indicator for bars. *The Astrophysical Journal*, 799:99, 2015. doi: arXiv:1411.4650. URL http://adsabs.harvard.edu/abs/2015ApJ...799...99K.

S. van den Bergh, R. G. Abraham, R. S. Ellis, N. R. Tanvir, B. Santiago, and K. G. Glazebrook. A morphological catalog of galaxies in the hubble deep field. *The Astrophysical Journal*, 112:359, 1996. doi: arXiv:astro-ph/9604161. URL http://adsabs.harvard.edu/abs/1996AJ....112..359V.

L. F. Whyte, R. G. Abraham, M. R. Merrifield, P. B. Eskridge, J. A. Frogel, and R. W. Pogge. Morphological classification of the OSU bright spiral galaxy survey. *MNRAS*, 336:1281–1286, 2002. doi: arXiv:astro-ph/0207461. URL http://adsabs.harvard.edu/abs/2002MNRAS.336.1281W.

E. M. Wilcots and M. K. M. Prescott. HI observations of barred magellanic spirals. II. The frequency and impact of companions. *The Astronomical Journal*, 127:1900–1916, 2004. URL http://adsabs.harvard.edu/abs/2004AJ....127.1900W.